

**Cold Regions Research
and Engineering Laboratory**

ERDC/CRREL TR-03-9



**US Army Corps
of Engineers®**
Engineer Research and
Development Center

A State–Space Model for River Ice Forecasting

Steven F. Daly

May 2003

ERDC/CRREL TR-03-9
May 2003

A State–Space Model for Ice Forecasting

Steven F. Daly

*Cold Regions Research and Engineering Laboratory
72 Lyme Road
Hanover, New Hampshire 03755*

Approved for public release; distribution is unlimited

Prepared for OFFICE OF THE CHIEF OF ENGINEERS

ABSTRACT

Each winter, ice forms on rivers, streams, and navigable waterways, causing many problems through its effects on the operation of hydraulic control structures, locks and dams, hydropower plants, and water intakes. Ice covers increase river stages by presenting an additional rough boundary, which increases the channel wetted perimeter, reduces the channel hydraulic radius, and typically increases overall effective channel roughness. The increase in stage can result in flooding, especially during severe ice conditions or in low-lying areas. This situation is particularly critical downstream of hydroelectric power plants because the risk of ice-induced flooding may require operators of such plants to curtail power production and provide more expensive replacement power. This study presents a state-space model for forecasting ice conditions and the resulting stages in rivers. The model incorporates a hydraulic component, a thermal and ice transport component, and an ice-cover progression component. The Kalman filter procedure is used to update the model with observed stages and observed positions of the upstream leading edge of the ice cover. The model thereby arrives at an efficient and optimal estimate of the river ice and hydraulic conditions. The state-space model can also recursively estimate the effective channel roughness using the augmented Kalman filter procedure to account for changes in the channel roughness produced by the river ice cover and other effects. By way of an example the state-space model is applied to the Missouri River downstream of Oahe Dam, located in Pierre, South Dakota, USA. Outflow from the dam, which is used for peaking power production, can vary between 0 and 55,000 cfs in a matter of minutes to meet the demands of the electric power grid it supplies. The system noise covariance of the model was adjusted to produce the optimal results based on least-squares criteria. Forecasts of the downstream stages and river ice conditions are presented. Accuracies of the forecasts obtained with the model are assessed using ice and flow observations from a series of past winters in which ice conditions were severe. The updated model results show substantial improvements in the forecasts compared to a non-updated model.

DISCLAIMER: The contents of this report are not to be used for advertising, publication, or promotional purposes. Citation of trade names does not constitute an official endorsement or approval of the use of such commercial products. All product names and trademarks cited are the property of their respective owners. The findings of this report are not to be construed as an official Department of the Army position unless so designated by other authorized documents.
DESTROY THIS REPORT WHEN IT IS NO LONGER NEEDED. DO NOT RETURN TO THE ORIGINATOR.

CONTENTS

PREFACE	v
1 INTRODUCTION	1
1.1 Background	1
1.2 Objectives	3
1.3 Outline of the model	4
1.4 Synopsis of state-space river ice model development	8
2 RIVER ICE MODEL	10
2.1 Introduction	10
2.2 Hydraulic model component	10
2.3 Thermal and ice transport model component	26
2.4 Simulation of stationary ice cover progression and retreat	38
2.5 Solution procedure for the river ice model	41
3 STATE-SPACE RIVER ICE MODEL	43
3.1 Introduction	43
3.2 Hydraulic state-space model	43
3.3 Thermal and transport state-space model	52
4 APPLICATION TO THE MISSOURI RIVER BELOW OAHE DAM, SOUTH DAKOTA	58
4.1 Introduction	58
4.2 Application of the river ice model	59
4.3 Estimation of filter parameters	71
4.4 Hindcasting	82
4.5 Forecasting	90
4.6 Summary	99
5 CONCLUSIONS AND RECOMMENDATIONS	100
5.1 Summary	100
5.2 Conclusions and recommendations	100
LITERATURE CITED	102

ILLUSTRATIONS

Figure 1. Missouri River downstream of Oahe Dam at Pierre, SD	2
Figure 2. Large ice floes in the Missouri River moving past LaFramboise Island	3
Figure 3. Recorded outflows out of Oahe Dam during June 1998	62
Figure 4. Observed and simulated stages at the four gages	63
Figure 5. Observed and simulated stages during the ice-affected period of January 1994	67
Figure 6. Observed and simulated ice cover extents	69
Figure 7. Overall coefficient of determination of the state-space model as a function of assumed system noise for the stage and discharge	75
Figure 8. Average model flow with the estimated model uncertainty based on the estimated error covariance	77
Figure 9. Average model stage with the model uncertainty based on the estimated error covariance	77
Figure 10. Average discharge and water surface elevation at each model cross section during June 1998	78
Figure 11. Comparison of the model uncertainty and the variance of the un-updated model results	79
Figure 12. Results of data assimilation experiment for 19 December 1996 through 26 January 1997	83
Figure 13. Results of data assimilation experiment for 18 January 1996 through 11 February 1996	86
Figure 14. Results of data assimilation experiment for 7 January 1994 through 3 March 1994	88
Figure 15. Ice floes moving downstream past LaFramboise Island to the leading edge of the ice cover	93
Figure 16. Examples of four-day forecasts of stage for the winter of 1996-97	93
Figure 17. Four-day forecasts of the ice cover extent	95
Figure 18. Error statistics for the forecasts	97

TABLES

Table 1. Data sources available for the Missouri River downstream of Oahe Dam	60
Table 2. Summary of geometric data for the Missouri River	61
Table 3. Calibrated Manning's coefficients	65
Table 4. Summary of data for ice periods	68
Table 5. Coefficient of determination for the June 1998 simulation using various system error covariances	81
Table 6. Coefficient of determination for the June 1998 simulation with updating	81
Table 7. Coefficient of determination for wintertime simulation	86
Table 8. Mean error by day of forecast	96

PREFACE

This report was prepared by Dr. Steven F. Daly, Research Hydraulic Engineer, RS/GIS and Water Resources Branch, Ice Engineering Group, Engineer Research and Development Center, Cold Regions Research and Engineering Laboratory, Hanover, New Hampshire. This report was originally prepared as the author's doctoral dissertation at the University of Iowa. The author thanks Dr. Robert Ettema of the University of Iowa for his encouragement; Dr. Ettema chaired the author's Ph.D. committee. The author also thanks the other members of his committee: Dr. Witold Krajewski, Dr. Wilfred A. Nixon, Dr. L. Chen, and Dr. F.M. Holly. Funding was provided by the Office of the Chief of Engineers, Cold Regions Engineering Program, Work Unit 32980, *River Ice Forecasting*.

This publication reflects the personal views of the authors and does not suggest or reflect the policy, practices, programs, or doctrine of the U.S. Army or Government of the United States. The contents of this report are not to be used for advertising or promotional purposes. Citation of brand names does not constitute an official endorsement or approval of the use of such commercial products.

The Commander and Executive Director of ERDC is COL John W. Morris III, EN. The Director is Dr. James R. Houston.

A State–Space Model for River Ice Forecasting

STEVEN F. DALY

1 INTRODUCTION

1.1 Background

Each winter, ice forms on rivers, streams, and navigable waterways in northern regions, causing many problems through its effects on the operation of hydraulic control structures, locks and dams, hydropower plants, and water intakes. Ice formation delays navigation and has the potential for causing sudden and catastrophic flooding. Reliable river ice forecasts would be a great asset in dealing with these problems. Forecasts would provide time to schedule procedures to mitigate the adverse effects on the operations of diverse river structures, such as hydraulic control structures, locks and dams, and hydropower plants. With adequate warning, the procedures could be implemented in an orderly and effective manner. Additionally, if needed, emergency measures such as evacuation or flood fighting could be instituted in a timely manner.

A river reach where ice forecasting could play an important role, and the one that usefully illustrates the need for this study, is the reach immediately downstream of Oahe Dam on the Missouri River (Fig. 1). The hydroelectric plant at Oahe Dam operates as a peaking plant. Its outflow can be varied between 0 and 55,000 cfs in a matter of minutes to match the demands of the electric power grid. Typically it produces 700 MW at its normal maximum discharge of 55,000 cfs. Oahe Dam, therefore, is a valuable power production asset in the midwestern region of the U.S.

Ninety miles downstream of Oahe Dam, the Big Bend Dam reservoir creates Lake Sharpe, which extends upstream to within 20 miles of Oahe Dam. Each winter, ice forms on Lake Sharpe. During especially cold periods, the leading edge of the stationary ice cover can progress upstream in the Missouri River until it reaches the cities of Pierre and Fort Pierre, South Dakota, situated immediately downstream of Oahe Dam. The presence of river ice locally decreases the hydraulic conveyance of the Missouri River and causes the stage in the river to

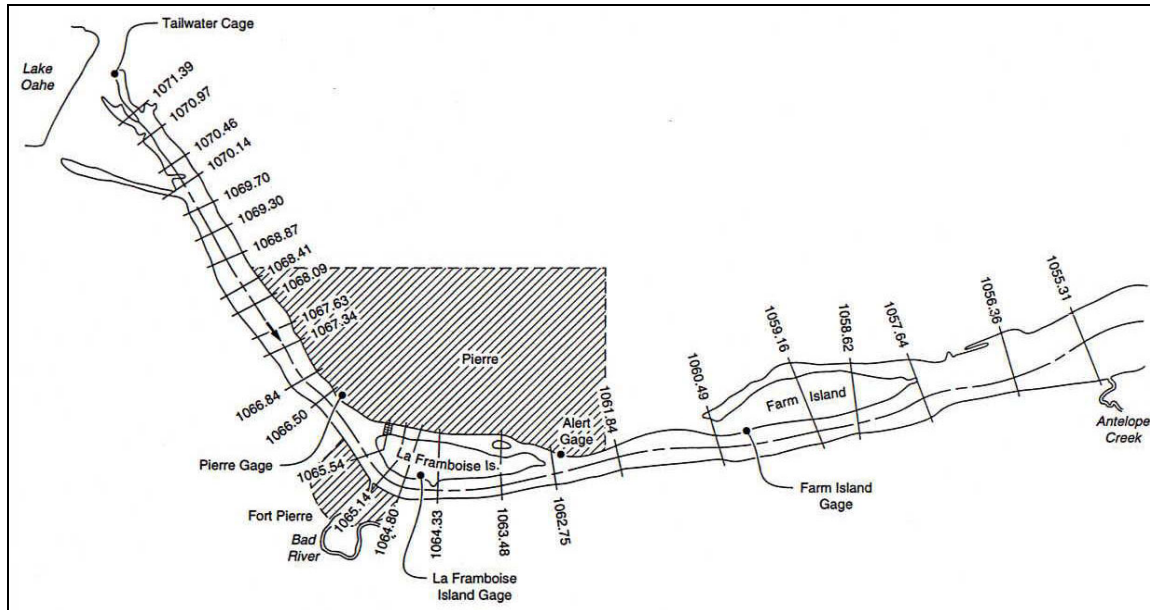


Figure 1. Missouri River downstream of Oahe Dam at Pierre, SD. Shown are the locations of river stage measurement gages and channel cross sections, which are identified by river mile.

rise. If the river ice cover has advanced sufficiently, the increased stages create flooding at Pierre and Fort Pierre. The Reservoir Control Center (RCC) of the Corps of Engineers at Omaha, Nebraska, reduces Oahe releases as stages approach alert levels at any of the four gages downstream of Oahe Dam (Fig. 1). The gages are closely monitored by the Oahe Dam operators and by the RCC staff when weather conditions are conducive to rapid ice formation. The corresponding limits on power generation are immediately coordinated with Western Area Power Administration (WAPA). City officials have alerted project and RCC staff in the past when storm sewers have flooded street intersections in southeast Pierre. However, when the outflow is abruptly reduced, a major component of the power production capacity of the entire Midwest is disrupted unexpectedly. The power distribution agencies must scramble to replace the lost hydropower, often at expensive rates.

Reliable forecasts of the river stages downstream of Oahe Dam, and at similar dams, would be a great advantage in regulating flow levels. Forecasts would provide dam operators time to schedule reductions in flow so that flooding was eliminated entirely. This advance time would also give the power distributors time to seek alternate and economical sources of electric power to replace the capacity of a facility such as Oahe Dam.



Figure 2. Large ice floes in the Missouri River moving past LaFramboise Island.

However, forecasting stages in ice-covered rivers is not a simple proposition, because complex interacting processes of heat transfer, ice production, ice transport, river flow, and ice cover formation mechanics need to be accounted for. The complexity of these processes is further enhanced by the highly unsteady flow releases from the Oahe Dam, the daily cycling of the air temperature, changes in the release water temperature, and the movement of the leading edge of the ice cover itself (Fig. 2). In fact it will be seen that simulation of the ice cover extent is difficult, and the accuracy of the results leaves much to be desired. It is this difficulty in simulation that motivates the search for a means of improving forecasts by using the additional tools provided by the Kalman filter.

1.2 Objectives

The central objective of this report is to assess the usefulness of Kalman filtering for improving forecasts of water surface elevations when river ice is forming. The following tasks were undertaken to attain this objective:

- A state-space river ice model was developed, with the Missouri River downstream of Oahe Dam being used as a case study application. The state-space model uses the Kalman filter to update the model using available observations.

- The Kalman filter parameters were estimated through numerical experiments.
- The accuracy of the forecasts using the Kalman filter was assessed. Practical problems in its application and possible solutions are discussed. The use of a state–space model offers a potentially useful way to obtain reliable forecasts of river ice conditions and their effects on river stages. Accurate stage forecasts during winter are needed to avert ice-induced flooding of flow-regulated rivers and maintain maximum hydropower production.
- The problem of missing and/or inaccurate data from field instrumentation to support the use of the Kalman filter approach was discussed and solution procedures outlined.

1.3 Outline of the model

In this study a numerical model with several components is used to simulate the rapidly changing stage, discharges, and ice conditions that occur in the Missouri River. The components are a hydraulic model, which estimates the water surface elevations and flows in the river system; a thermal and ice transport model, which estimates the river water temperatures, the frazil ice and surface ice concentrations, and the surface ice thickness; and an ice progression model, which estimates the extent and thickness of any stationary ice covers.

The hydraulics model can be thought of as the base of the ensemble; it operates as a stand-alone model or as part of the ensemble. It is a one-dimensional, unsteady flow model. The water surface elevations and flows determined by the hydraulics model are used as input in the thermal and transport model.

The ice transport model is a “free drift model.” This term means that ice is carried by the river flow as a passive tracer. For low to moderately high concentrations of surface ice, and at all physically realizable concentrations of frazil ice, this is a good assumption. In addition, while it is recognized that there are a number of the fluid properties (such as density) and coefficients (such as the hydraulic roughness of the bed) used in the hydraulics model that are theoretically temperature dependent, these properties and coefficients can safely be assumed to be constant over the winter period and their temperature dependence ignored. As a result, there is no feedback from the thermal and ice transport model to the hydraulic model.

The final component model is an ice cover progression model. This model determines the length and thickness of any stationary ice covers in the river system. It requires input from the hydraulics model and the thermal and ice transport

model. In turn, the output of the ice progression model is required as input into the hydraulics model and the thermal and ice transport model. There is strong feedback between the ice cover progression model and the others.

Numerical river ice models, such as the one described above, have become valuable tools for investigating many aspects of river ice, but they have not become a standard means for forecasting river ice conditions, largely for reasons of accuracy and reliability. The accuracy of a numerical river ice model, as with all numerical models of physical systems, reflects the accuracy of the model input, the empirical coefficients (or parameters), and the model structure. The model input includes the description of the channel geometry, the time-varying boundary conditions that drive the model, and the initial conditions from which the model starts. The model structure is composed of the numerical discretization of the underlying mathematical equations that describe the physical processes, and the mathematical equations themselves. In theory, if the input data, the model parameters, and the model structure were highly accurate, the model output should also be highly accurate. In practice, there are always inaccuracies in the model input, the model parameters, the numerical discretization, and the viability of the differential equations. In a numerical river ice model used for forecasting, these inaccuracies compound because the models are used in a continuous manner throughout the winter season to “track” the river ice conditions, as will be seen. Consequently errors, such as discrepancies between the calculated and observed locations of the leading edge of the ice cover, accumulate with time. In addition, the reliability (estimates of model error) of the river ice forecasts produced by deterministic numerical models have not been adequately determined. It is difficult to make practical use of a forecast if there is no understanding of the accuracy of that forecast. Indeed, an estimate of the forecast reliability may be as important as the forecast itself. Given these issues of accuracy and reliability, it is understandable that numerical models for river ice forecasting are, at best, considered experimental.

Given the above discussion, it must be pointed out that there is usually an alternate source of information available on the conditions in the Missouri River and other flow-regulated rivers: direct field observations of the river stages and the location of the leading edge of the ice cover. Stages are typically measured once an hour by automatic gages that transmit the data via geostationary satellites every four hours. The number of recording gages on the Missouri River between Oahe Dam and Big Bend Dam, for instance, has increased over the years, and there are currently six. Observations of the leading edge of the ice cover are made from the shore or small planes. The scheduling of the ice observations depends on the constraints of weather, road conditions, and manpower availability. Typically the observations are made only when the leading edge of the ice

cover approaches Pierre and are made once, or at most twice, a day. Often there are a number of days with no observations. It is interesting to note that there has never been a measurement of the ice thickness in the Missouri River near Pierre because of the rapidly changing and dangerous ice conditions in the river.

In conventional hydraulic modeling practice, these direct field observations would be used only to calibrate the simulation model. During calibration, a set of empirical coefficients required by the model (for example, the Manning's flow-resistance coefficient) are adjusted manually or by other means until the model is able to reproduce the observed measurements to within some specified tolerance. Calibration is a time-consuming task that is typically done once. After calibration is complete, the direct field observations can serve as criteria to judge the model performance. Large discrepancies, if (or when) they occur, alert the user that some part of the simulation model, such as the input data, the empirical coefficients, or the underlying model structure, as discussed above, is in error. Often the response is to recalibrate the model. However, operational time demands and manpower limitations usually preclude the ability of an operator to recalibrate in any meaningful way once the model is in use.

Given the direct field observations that are available, and the difficulties in reaching an accurate numerical model as described above, it is attractive to contemplate forgoing the numerical model altogether and developing a modeling procedure based solely on the statistics of the observations themselves. Of course, given the rapidly changing ice conditions on the Missouri River downstream of Oahe, it would be difficult to use the direct field observations to estimate the river stages between the gages, and it would be impossible to predict the stages at any future time, when obviously no observations are available. It is clear that a deterministic numerical model, as described previously, would be required to estimate the stages in the rivers between the gages and to predict the stages at a future time. What is desired is an approach that would combine the best features of the empirical and deterministic approaches to river stage modeling. Kalman (1960) and Kalman and Bucy (1961) developed such an approach, referred to as the Kalman filter. The Kalman filter is an optimal estimator that is defined as "a computational algorithm that processes measurements to deduce a minimum error (in accordance with some stated criterion of optimality) estimate of the state of a system by utilizing: knowledge of system and measurement dynamics, assumed statistics of system noises and measurement errors and initial condition information" (Gelb 1992). The Kalman filter provides a means of "updating" the model results with new observations as they are received.

To show how the Kalman filter would be used, it is beneficial to describe the steps of the forecasting procedure. Initially the deterministic river ice model is

recast in state-space form, which treats the state variables as random variables described by probability distributions. There are examples of state-space models described in the literature similar to that discussed here. Such models have found extensive use in a wide range of related problems, including hydrology (e.g., Kitanidis and Bras 1980, Georgakakos and Krajewski 1985, Mizumura and Chiu 1985, Assaf and Quick 1991, Lee and Singh 1999) and hydraulics (Chiu and Isu 1978, Budgell 1981, Hsieh 1987, Bravo et al. 1993, Crissman et al. 1993, Fread and Jin 1993). The first step of the forecast is to track the river hydraulic and ice conditions by propagating the state-space river ice model in time, using the observations that serve as the model boundary conditions. The boundary conditions are discussed in more detail in the following chapters, but they consist of an upstream hydraulic boundary condition—the time-varying flow release of Oahe Dam; a downstream hydraulic boundary condition—the time-varying stage at Big Bend Dam; an upstream thermal boundary condition—the release water temperature; and the observed air temperature. At periodic intervals, using the Kalman filter procedure, observations of the stages and leading edge of the ice cover are used to update the state-space river ice model. This procedure provides an optimal estimate of the state-space variables, not only at the gages but also at locations between the gages, and even of variables that are not observed, such as the effective channel roughness, a model parameter.

At this point in the procedure, step one can be repeated, and a cycle of model propagation and updating repeated for the entire winter season. This describes a process of data assimilation that arrives at an optimal estimate of the state variables over the entire winter season. This type of analysis could provide valuable information for a study of the stage frequencies along the river reach, for example. This also describes a process of recursive parameter estimation by making repeated adjustment of the effective channel roughness. The advantage of recursive parameter estimation over a one-time calibration is obvious. A forecast is made by propagating the state-space river ice model into the future, using predictions of the future boundary conditions. Typically the forecast is made immediately after the state-space river ice model is updated. This assures that the initial conditions at the start of the forecast are an optimal estimate of the actual conditions in the river at the time that the forecast is made. After the forecast, step one is repeated and a cycle of model propagation, updating, and forecasting is repeated throughout the winter season.

In summary, this report brings together three areas of study: river ice engineering, numerical modeling of unsteady flow and convection dominated dispersion, and optimal estimation using the Kalman filter. The ice-related problems of flow regulation of Oahe Dam provide a useful case study to jointly apply these areas of study.

A large body of literature covering many aspects of these areas is available and, taken altogether, is much more than a single work such as this can comprehensively describe. However, there are certain works that the interested reader will find indispensable. In the area of ice engineering, Ashton (1986) provides an in-depth overview of the entire field. Beltaos (1995) provides a good description of granular ice jam theory and many other aspects of river ice as well. The many works of Shen (see for example, Shen et al. 1995, Wang et al. 1995, Shen 1996), taken together, provide comprehensive and consistent descriptions of numerical river ice simulations. In the area of numerical modeling of river flow, Cunge et al. (1980) is a good introduction with a number of practical examples. Fischer et al. (1979) describes dispersion in channels and covers theory and modeling. In applying the Kalman filter, the works by Gelb (1992) and Grewal and Andrews (1993) are excellent basic texts, and the compilation by Sorenson (1985) contains many practical applications as well as theory. Descriptions of practical applications with relevance to hydraulics and river flow problems can be found in the conference proceedings edited by Chiu (1978).

1.4 Synopsis of state-space river ice model development

Chapter 2 describes the development of the deterministic river ice model and its numerical solution. Each component of the river ice model is based on equations that describe the mechanics of physical process that the component simulates. The equations are solved numerically by schematizing the river system in a consistent manner in both space and time. Each component is one dimensional and uses appropriate averages of all variables at each channel cross section. The models also solve for the variables at one time step based on the values of those variables at the time step immediately preceding the solution time and the imposed boundary conditions. As a result only the values of variables at two consecutive time steps, t^{n+1} and t^n , are required at any one time. This situation can be represented as

$$f(a^{n+1}, b^n, t^{n+1}, t^n, \bar{U}^n) = 0 \quad (1)$$

where a^{n+1} = column vector of variables of interest at time $n+1$

b^n = column vector of the variables at time n

\bar{U}^n = column vector containing the appropriate boundary conditions.

Both b^n and \bar{U}^n are known; a^{n+1} is the vector of unknown values that is found by solving the system of algebraic equations represented by f . In general the series of equations represented by f will be nonlinear and will require an iterative solution procedure.

Chapter 3 recasts the numerical model into a state–space model in which the model variables are replaced by state variables. In addition, f is augmented by additional equations that propagate the values of additional state variables representing model parameters. These additional equations propagate the values of the coefficients in time with no change. This is not surprising, as the value of model parameters cannot, by definition, be determined by the model. Only through the update process can the value of these coefficients change. To develop the state–space model, the series of equations represented by f are recast in a suitable form. It is shown that, to first order, the equations represented by f can be written as

$$\mathbf{X}^{n+1} = \Phi^n \mathbf{X}^n + \Lambda^n \mathbf{U}^n + \mathbf{N}^n + \mathbf{w} \quad (2)$$

where \mathbf{X}^{n+1} = column vector of the state variables at time $n+1$

\mathbf{X}^n = column vector of the state variables at time n

Φ^n = state transition matrix

Λ^n = input coupling matrix

\mathbf{N} = matrix containing elements unaffected by the expectation operator

\mathbf{w} = zero mean additive model error term, which is uncorrelated (or “white”) in time.

This form is entirely suitable for use with state–space models and the Kalman filter. Once the equations have been recast in this form, the development of the state–space model follows directly based on the Kalman filter procedure.

In Chapter 4 the deterministic river ice model is applied to the case of the Missouri River downstream of Oahe Dam at Pierre, South Dakota, and the results are reviewed. Next, the parameters required by the Kalman filter procedure are estimated based on numerical experiments. The state–space model is then used to hindcast the stages and ice covers in the Missouri River over three winter periods using the estimated statistical parameters. Procedures for dealing with missing and bad data are developed and applied. Finally, the state–space model is applied to forecast stages and ice cover extents for the Missouri River downstream of Oahe Dam. The accuracy of the forecast is assessed based on the actual conditions recorded in the river during two winters in which ice played an important role.

Finally, Chapter 5 presents the principal conclusions of this study, along with suggestions for further study.

2 RIVER ICE MODEL

2.1 Introduction

This chapter describes the development of the river ice model, which has three components: a *hydraulic component*, for estimating the water surface elevations and flows in the river system; a *thermal and ice transport component*, for estimating the river water temperatures, the frazil ice and surface ice concentrations, and the surface ice thickness; and an *ice progression component*, for estimating the extent and thickness of any stationary ice covers. The physical processes, the governing equations, and the numerical solution of each component are also discussed in this chapter.

The hydraulic component is a one-dimensional, unsteady flow model that closely follows the development provided by Barkau (Corps of Engineers 1997). It uses the actual river geometry provided by the user in a form compatible with the program HEC-2 (Corps of Engineers 1990). The thermal and ice model follows closely the development of Lal and Shen (1993). Water temperature, frazil ice concentration, and surface ice concentration are each calculated simultaneously, along with the deposited frazil ice and stationary ice thickness at each time step. The advected properties are all estimated using a one-dimensional Holly–Preissman scheme (Holly 1984, Sauvaget 1984). The ice progression model determines the length and thickness of any stationary ice covers in the river system. This algorithm follows closely that proposed by Lal and Shen (1993).

The forms that ice can take in rivers range widely. No attempt was made in this study to produce a comprehensive ice model that could simulate the river ice conditions in all channels and all flow conditions. Rather, the emphasis is on the type of ice conditions that can form in large rivers with relatively mild gradients, such as prevail for the Missouri River downstream of Oahe Dam. The present combination of a one-dimensional unsteady flow model, a thermal and ice transport model, and an ice cover progression model has been shown to be able to simulate winter ice conditions on large rivers such as the Ohio (Shen et al. 1991) and the St. Lawrence (Lal and Shen 1993). The following sections of this chapter describe the various components of the river ice model.

2.2 Hydraulic model component

2.2.1 Background

This chapter describes the development of a hydraulic model for estimating the flow stages and discharges for a channel whose ice cover changes dynamically. The basic continuity and momentum equations describing one-dimensional,

unsteady flow in channels with a floodplain are presented for both open-water and ice-covered flow. The four-point, finite-difference forms of the equations are derived following the development given by Barkau (Corps of Engineers 1997). As is usual, the channel geometric properties are described at only a finite number of discrete cross sections (Cunge et al. 1980) that segments the river into a series of subreaches. The continuity and momentum equations are solved for each subreach. This approach solves for the change in discharge (ΔQ) and the change in stage (ΔZ), from time n to $n + 1$, at each cross section. If there are j number of cross sections, this approach results in $2j$ unknowns and $2(j - 1)$ equations. Two additional boundary condition equations are required so that the number of equations equals the number of unknowns and a unique solution exists. The final result is a quasi-linear set of equations that can be solved using the Newton-Raphson iterative approach.

A pre-processor program (Corps of Engineers 1997) analyzes each cross section and prepares a “look-up” table of the geometric properties of each cross section as a function of the water surface elevation. The geometry of each cross section can be unique. The look-up table approach provides an efficient means of estimating the geometric values required for each continuity and momentum equation. As is shown in this chapter, the presence of a floating, stationary ice cover modifies the effective channel geometry by reducing the channel flow area, increasing the channel wetted perimeter, and modifying the effective hydraulic roughness of the channel. The combined result of these changes is largely to reduce the conveyance of the channel compared to the open-water conveyance at an equivalent water depth. To account for the presence of ice, the look-up table results must be modified heuristically for each time step at sections where an ice cover exists.

An additional problem is presented by the fact that the ice cover extent along the channel may be continuously increasing or decreasing with time. A conflict arises with the description of the river channel using discrete cross sections that cause abrupt changes in the results each time the ice cover extent passes through a cross section. To overcome this conflict, a means of interpolating the channel properties between the ice-covered and open-water geometries was developed to smooth the changes as the ice cover advances or retreats past a cross section. This interpolation requires two new variables per cross section: Σu_{s_j} , which describes the ice cover extent immediately upstream of cross section number j , and Σd_{s_j} , which describes the ice cover extent immediately downstream of j . The rate of ice cover progression is calculated using the straightforward approach originally presented by Lal and Shen (1993). In this method the rate of ice cover progression is proportional to the ice volume arriving at the leading edge of the ice cover and inversely proportional to the thickness of the advancing ice edge.

The method of estimating the ice volume arriving at the leading edge is described in the next chapter. The rate of ice cover retreat is a more problematic quantity to determine. In essence, melting of the ice cover reduces the thickness until a minimum allowable thickness is reached. At that point the ice cover is considered no longer stable and is removed by the simulation.

In Chapter 3 the state–space form of the hydraulic model is formed by linearizing the finite-difference system of equations around the state vector. In this chapter it is demonstrated that the solution of the finite-difference representation of the governing equations is found by linearizing the finite-difference equations around a solution estimate and iteratively solving the linearized equations using the Newton–Raphson method. The parallel between these two requirements can be exploited to minimize the number of numerical computations, as shown in the next chapter.

2.2.2 Governing equations

The basic equations governing flow in channels are the continuity and momentum equations. They are presented first without making any distinction between ice-covered and open-water conditions.

2.2.2.1 *Continuity.* In the present approach, separate equations are written for the main channel and the floodplain. The continuity equation for the channel is

$$\frac{\partial A_c}{\partial t} + \frac{\partial Q_c}{\partial x_c} = q_f . \quad (3)$$

The continuity equation for the floodplain is

$$\frac{\partial A_f}{\partial t} + \frac{\partial Q_f}{\partial x_f} = q_c + q_l \quad (4)$$

where t = time
 x = longitudinal distance
 A = flow area
 Q = discharge
 q_f = lateral inflow from the floodplain to the channel
 q_c = lateral inflow from the channel into the floodplain
 q_l = lateral inflow into the floodplain.

The subscript c refers to the channel while the subscript f refers to the floodplain.

2.2.2.2 *Momentum.* The momentum equation for the channel is

$$\frac{\partial Q_c}{\partial t} + \frac{\partial V_c Q_c}{\partial x_c} + g A_c \left(\frac{\partial Z}{\partial x_c} + S_{fc} \right) = M_f. \quad (5)$$

The corresponding equation for flow in the floodplain is

$$\frac{\partial Q_f}{\partial t} + \frac{\partial V_f Q_f}{\partial x_c} + g A_f \left(\frac{\partial Z}{\partial x_f} + S_{ff} \right) = M_c \quad (6)$$

where g = gravity
 V = flow velocity
 Z = water surface elevation
 S_f = energy gradient
 M_f = momentum transfer into the channel from the floodplain
 M_c = momentum transferred from the floodplain from the channel.

At any section, S_f can be estimated as

$$S_f = \frac{Q^2}{K^2} \quad (7)$$

where K is the conveyance of the channel. Based on Manning's equation the conveyance is

$$K = \frac{1}{n} AR^{2/3} \quad (8)$$

where n is Manning's flow-resistance coefficient and R is the hydraulic radius.

2.2.3 Effects of an ice cover

The presence of a stationary, floating ice cover changes the effective geometry of the channel. Accordingly, changes occur to the flow area, the hydraulic radius, and the effective hydraulic roughness of the channel. These changes can have a significant effect on the channel conveyance, K , and as a result the friction slope, S_f .

Let the subscript o stand for open-water, and i ice-covered, conditions. Then the flow area under an ice cover, A_i , is

$$A_i = A_o - \frac{\rho'}{\rho} \eta B \quad (9)$$

where η = mean ice thickness
 B = channel width
 ρ' = ice density
 ρ = water density.

The hydraulic radius, R_i , in a channel with an ice cover can be estimated as

$$R_i = \frac{A_i}{Wp_o + B} \quad (10)$$

where Wp_o is the open-water wetted perimeter of the channel. Notice that the hydraulic radius for ice-covered channels is significantly less than that for open-water channels ($R_o = A_o/Wp_o$), depending on the relative width-to-depth ratio of the channel. As most large channels are usually much wider than they are deep and are roughly rectangular in shape, the hydraulic radius of open-water channels is approximately equal to the mean depth of the channel. The hydraulic radius of ice-covered channels, however, is usually about half of the open-water hydraulic radius, or half the mean depth of the channel. The hydraulic roughness of the channel can be estimated using the composite Manning's roughness coefficient, n_c . It can be estimated approximately as

$$n_c = \left(\frac{n_b^{3/2} + n_i^{3/2}}{2} \right)^{2/3} \quad (11)$$

where n_b is the Manning's roughness coefficient for the bed and n_i is the corresponding value of the Manning's roughness coefficient for the ice cover. The channel conveyance for ice-covered channels is then

$$K_i = \frac{1}{n_c} A_i R_i^{2/3} \quad (12)$$

Finally, the energy gradient, S_f , can be estimated as

$$S_f = \frac{Q^2}{K_i^2} \quad (13)$$

2.2.4 Finite-difference scheme

The continuity and momentum equations are solved using the four-point, implicit finite-difference scheme. There are many methods available for numeri-

cally solving finite-difference equations. The method used here has been widely adopted for solving channel flow problems because it is robust and accurate and has well-described numerical properties. In this scheme the channel geometry is described at a finite number of cross sections. In theory the cross sections can be an arbitrary distance apart, with the maximum separation distance consistent with numerical accuracy and an accurate description of the channel. Solutions are advanced from one time step to the next based on the values at the initial time step at each cross section and the imposed boundary conditions. Solutions for the flow equations are found only at the intersections of the channel cross sections and time lines, which together can be visualized to form a grid in time and space. A separate continuity and momentum equation is written for each subreach. (A subreach is defined by the river length bounded by an upstream and downstream cross section. If there are j cross sections, there are $j - 1$ subreaches.) All the equations are solved simultaneously, which allows information from the entire river to influence the solution at any single point.

2.2.4.1 Four-point difference representation. The discretization scheme is based on representing the values of the dependent variables and functions of the variables between the computational grid points in terms of the values at the grid points. Note that subscripts denote the x -location along the river while superscripts denote time level. A derivative of any function F with respect to time is now

$$\frac{\partial F}{\partial t} = \frac{0.5}{\Delta t} [F_{i+1}^{n+1} - F_{i+1}^n] + \frac{0.5}{\Delta t} [F_i^{n+1} - F_i^n]. \quad (14)$$

A derivative with respect to distance can be represented in finite-difference form as

$$\frac{\partial F}{\partial x} = \frac{\theta}{\Delta x} [F_{i+1}^{n+1} - F_i^{n+1}] + \frac{(1-\theta)}{\Delta x} [F_{i+1}^n - F_i^n] \quad (15)$$

where θ is a weighting factor. The value of θ has a significant impact on the numerical properties of the solution scheme (Fread 1974.) In general, if $\theta > 0.5$, the solution is unconditionally stable. The value of any function can be represented as

$$\bar{F} = \frac{\theta}{2} [F_{i+1}^{n+1} + F_i^{n+1}] + \frac{(1-\theta)}{2} [F_{i+1}^n + F_i^n]. \quad (16)$$

For any variable F ,

$$\Delta F_i = F_i^{n+1} - F_i^n. \quad (17)$$

The above three equations can be restated in this form as

$$\frac{\partial F}{\partial t} = \frac{1}{2\Delta t} [\Delta F_{i+1} + \Delta F_i] \quad (18)$$

$$\frac{\partial F}{\partial x} = \frac{1}{\Delta x} [F_{i+1}^n - F_i^n] + \frac{\theta}{\Delta x} [\Delta F_{i+1} - \Delta F_i] \quad (19)$$

$$\bar{F} = \frac{1}{2} [F_{i+1}^n + F_i^n] + \frac{\theta}{2} [\Delta F_{i+1} + \Delta F_i]. \quad (20)$$

2.2.4.2 Finite-difference form of the governing equations. The finite-difference form of the continuity equation can now be written for the channel and the floodplain by rewriting eq 5 and 6 in the form of eq 18, 19, and 20:

$$\frac{1}{\Delta x_c} (Q_{ci+1}^n - Q_{ci}^n) + \frac{\theta}{\Delta x_c} (\Delta Q_{ci+1} - \Delta Q_{ci}) + \frac{1}{2\Delta t} (\Delta A_{ci+1} + \Delta A_{ci}) - q_1 = 0 \quad (21)$$

$$\frac{1}{\Delta x_e} (Q_{fi+1}^n - Q_{fi}^n) + \frac{\theta}{\Delta x_e} (\Delta Q_{fi+1} - \Delta Q_{fi}) + \frac{1}{2\Delta t} (\Delta A_{fi+1} + \Delta A_{fi}) - q_c - q_1 = 0. \quad (22)$$

The momentum equation for the channel and floodplain can be written in a similar fashion:

$$\begin{aligned} & \frac{1}{2\Delta t} [\Delta Q_{ci+1} + \Delta Q_{ci}] - \frac{1}{\Delta x_c} [(VQ)_{ci+1}^n - (VQ)_{ci}^n] + \\ & \frac{\theta}{\Delta x_c} [\Delta (VQ)_{ci+1} - \Delta (VQ)_{ci}] + g \left[\frac{1}{2} (A_{ci+1}^n + A_{ci}^n) + \frac{\theta}{2} (\Delta A_{ci+1} + \Delta A_{ci}) \right] \end{aligned} \quad (23)$$

$$\left[\frac{Z_{ci+1} - Z_{ci}}{\Delta x_c} + \frac{\theta}{\Delta x_c} (\Delta Z_{ci+1} - \Delta Z_{ci}) + \frac{1}{2} (S_{fci+1}^n + S_{fci}^n) + \frac{\theta}{2} (\Delta S_{fci+1} + \Delta S_{fci}) \right]$$

$$= M_f$$

$$\begin{aligned}
& \frac{1}{2\Delta t} [\Delta Q_{fi+1} + \Delta Q_{fi}] - \frac{1}{\Delta x_f} [(VQ)_{fi+1}^n - (VQ)_{fi}^n] + \\
& \frac{\theta}{\Delta x_f} [\Delta (VQ)_{fi+1} - \Delta (VQ)_{fi}] + g \left[\frac{1}{2} (A_{fi+1}^n + A_{fi}^n) + \frac{\theta}{2} (\Delta A_{fi+1} + \Delta A_{fi}) \right] \\
& \left[\frac{Z_{ci+1} - Z_{ci}}{\Delta x_f} + \frac{\theta}{\Delta x_f} (\Delta Z_{fi+1} - \Delta Z_{fi}) + \frac{1}{2} (S_{fi+1}^n + S_{fi}^n) + \frac{\theta}{2} (\Delta S_{fi+1} + \Delta S_{fi}) \right] \\
& = M_c
\end{aligned} \tag{24}$$

At this point the continuity equations for the channel and the floodplain need to be summed into one equation, as do the momentum equations for the channel and floodplain. These can be done by first determining an effective length, $-x_e$, for any subreach i , as

$$\Delta x_{ei} = \frac{(A_{ci} + A_{ci+1})_i \Delta x_{ci} + (A_{fi} + A_{fi+1})_i \Delta x_{fi}}{A_{fi} + A_{fi+1} + A_{ci} + A_{ci+1}} \tag{25}$$

and the equivalent channel energy slope as

$$S_f = \frac{S_{fc} A_c \Delta x_c + S_{ff} A_f \Delta x_f}{A \Delta x_e} \tag{26}$$

Next the flow weighting factor, ϕ , is defined, for any cross section i , as

$$\phi_i = \frac{Q_{ci}}{Q_{ci} + Q_{fi}} \tag{27}$$

If it is assumed that the flow distribution is given by the ratio of the conveyances, then

$$\phi_i = \frac{K_{ci}}{K_{ci} + K_{fi}} \tag{28}$$

A velocity distribution factor, β_i , for any cross section i , can be defined as

$$\beta_i = \frac{(V_c Q_c)_i + (V_f Q_f)_i}{V_i Q_i} \quad (29)$$

Finally, it is assumed that the Δ function of the following variables can be expanded as

$$\Delta A_i = \left(\theta \frac{dA^{n+1}}{dZ_i} + (1-\theta) \frac{dA^n}{dZ_i} \right) \Delta Z_i = \frac{dA}{dZ} \Big|_{Z_i=Z_i^n + \theta \Delta Z_i} \Delta Z \quad (30)$$

and

$$\Delta S_{fi} = \frac{-2S_{fi}}{K_i} \frac{dK}{dZ} \Big|_{Z_i=Z_i^n + \theta \Delta Z_i} \Delta Z_i + \frac{2S_{fi}}{Q_i} \Delta Q_i \quad (31)$$

The evaluation of the derivative of A with respect to Z is described next.

2.2.5 Representing geometric properties

As mentioned earlier, a pre-processor program analyzes each river section and prepares a look-up table of the geometric properties of each section as a function of a finite number of discrete water surface elevations. The pre-processor program estimates the channel and river valley area, the channel and valley conveyance, and other variables at a preset number of equally spaced elevations. These elevations must span the distance from the minimum to maximum expected water levels in the simulations. All the geometric properties are assumed to be piece-wise linear between the selected water surface elevations. In this section the linear interpolation are described for the open-water variables as well as the adjustments that are made to account for the presence of the ice cover.

This method of estimating channel geometry properties can be used to reduce the computational requirements of the four-point finite-difference scheme. It can be seen by formalizing the geometric function at any section. Recall that any function can be estimated using the formula

$$\bar{F} = \frac{1}{2} [F_{i+1}^n + F_i^n] + \frac{\theta}{2} [\Delta F_{i+1} + \Delta F_i] \quad (32)$$

which can be restated as

$$\bar{F} = \frac{1}{2} \left[\left(F_{i+1}^n + \theta \Delta F_{i+1} \right) + \left(F_i^n + \theta \Delta F_i \right) \right]. \quad (33)$$

As F is a function of the water surface elevation, Z , at each section, it can be written as

$$F_{i+1}^n = F_{i+1} \left(Z_{i+1}^n \right) \quad (34)$$

because the form of function F_{i+1} is constant with time but not with Z . ΔF_{i+1} can be written as

$$\Delta F_{i+1} = F_{i+1} \left(Z_{i+1}^{n+1} \right) - F_{i+1} \left(Z_{i+1}^n \right). \quad (35)$$

Therefore, as F is piece-wise linear with respect to Z , to first-order accuracy,

$$F_{i+1}^n + \theta \Delta F_{i+1} = F_{i+1} \left(Z_{i+1}^n + \theta \Delta Z_{i+1} \right). \quad (36)$$

Consequently the function F can be represented as

$$\bar{F} = \frac{1}{2} \left[F_{i+1} \left(Z_{i+1}^n + \theta \Delta Z_{i+1} \right) + F_i \left(Z_i^n + \theta \Delta Z_i \right) \right]. \quad (37)$$

This formulation reduces the number of times the geometric properties needed to be estimated from four to two. The finite-difference representation of the derivative with respect to x , eq 19, can also be written in this manner.

2.2.5.1 Open-water geometric properties. Herein, Z_0 is the water surface elevation of interest. Let Z_1 be the elevation of the first point in the look-up table that is less than or equal to Z_0 and Z_2 be the elevation of the first point in the look-up table that is greater than Z_0 . The open-water flow area at a water surface elevation of Z_0 , $A(Z_0)$, and the conveyance at a water surface elevation of Z_0 , $K(Z_0)$, are estimated as shown in the following equations. For convenience the distinction between the channel and the floodplain is not made here. However, both the channel and floodplain values are found in a similar manner as below:

$$A(Z_0) = A(Z_1) + \frac{A(Z_2) - A(Z_1)}{Z_2 - Z_1} (Z_0 - Z_1) \quad (38)$$

$$\frac{dA}{dZ}(Z_o) = \frac{A(Z_2) - A(Z_1)}{Z_2 - Z_1} \quad (39)$$

$$K(Z_o) = K(Z_1) + \frac{K(Z_2) - K(Z_1)}{Z_2 - Z_1}(Z_o - Z_1) \quad (40)$$

$$\frac{dK}{dZ}(Z_o) = \frac{K(Z_2) - K(Z_1)}{Z_2 - Z_1}. \quad (41)$$

2.2.5.2 *Ice cover influence on flow geometry.* In sections where an ice cover exists, a new elevation, Z_i , can be defined:

$$Z_i = Z_o - \frac{\rho'}{\rho} \eta. \quad (42)$$

This elevation is the bottom of the ice cover. The flow area variables affected by ice can then be estimated as

$$A_{ice}(Z_o) = A_o(Z_i) \quad (43)$$

and

$$\frac{dA_{ice}(Z_o)}{dZ} = \frac{dA_o(Z_i)}{dZ} \quad (44)$$

where A_o is the open-water flow area. The ice-affected conveyance variables are found as

$$K_{ice}(Z_o) = \frac{A_o^{5/3}(Z_i)}{n_c [Wp(Z_i) + B(Z_i)]^{2/3}} \quad (45)$$

and

$$\frac{dK_{ice}(Z_o)}{dZ} = K_{ice}(Z_1) + \frac{K_{ice}(Z_2) - K_{ice}(Z_1)}{Z_2 - Z_1}(Z_i - Z_1). \quad (46)$$

2.2.5.3 Dynamic ice cover representation. The finite-difference scheme discussed above requires that the geometrical properties of each river cross section (except for the extreme upstream and downstream sections) be used twice in the computations: once for estimating the hydraulic properties of the downstream subreach, and once for estimating the hydraulic properties of the upstream subreach. The presence of an ice cover complicates these calculations because its length may vary with time on the upstream side of a section, the downstream side, or both. In open water the geometric properties of each cross section need only be determined once, then used for both the upstream and downstream subreach calculations. In the ice-covered case the geometric properties need only be determined once but may need to be modified separately for downstream or upstream subreach calculations. This is done as follows.

Let Δx_{icei} be the distance that the ice cover extends upstream of cross section I . Then the following two variables associated with each cross section can be defined:

$$\Sigma us_i = \frac{\Delta x_{icei}}{\Delta x_{ci}} \quad \text{if } 0 \leq \frac{\Delta x_{icei}}{\Delta x_{ci}} \leq 0.5 \quad (47)$$

and

$$\Sigma us_i = 0.5 \quad \text{if } 1 \geq \frac{\Delta x_{icei}}{\Delta x_{ci}} > 0.5 . \quad (48)$$

The following relationship is found because cross-section numbering increases in the downstream direction:

$$\Sigma ds_i = 0 \quad \text{if } 0 \leq \frac{\Delta x_{icei+1}}{\Delta x_{ci+1}} \leq 0.5 \quad (49)$$

and

$$\Sigma ds_i = \frac{\Delta x_{icei+1}}{\Delta x_{ci+1}} - 0.5 \quad \text{if } 1 \geq \frac{\Delta x_{icei+1}}{\Delta x_{ci+1}} > 0.5 . \quad (50)$$

Let R_i be any geometric variable at section i determined though the use of the look-up table. Then let \bar{R}_i be the value of the variable weighted for the ice cover presence. The value of \bar{R}_i for use in determining the hydraulic properties of the flow reach defined by sections i and $i + 1$ can be estimated as

$$\bar{R}_i = 2 \left[(0.5 - \sum ds_i) R_{oi} + \sum ds_i R_{ii} \right] \quad (51)$$

where R_{oi} is the open-water value of R_i , and R_{ii} is the ice-covered value. The value of \bar{R}_i for use in determining the hydraulic properties of the flow reach defined by section $i - 1$ and i can be estimated as

$$\bar{R}_i = 2 \left[(0.5 - \sum us_i) R_{oi} + \sum us_i R_{ii} \right]. \quad (52)$$

2.2.5.4 Time-varying channel conveyance. The effective channel conveyance at a section may vary with time because of changes in the cross-sectional area or through changes in the effective hydraulic roughness of the channel bed or the river ice cover. For example, sediment transport may both change the cross-sectional area and alter the effective roughness of a section. In this study the concern is with changes in the effective roughness of the ice cover with time (Ashton 1986, Shen and Yapa 1986). The most direct approach would seem to be to allow the Manning's roughness coefficient of the ice cover or the channel or both to vary with time. However, the use of geometric tables that include conveyance greatly complicate this direct approach. The use of geometric tables is implicitly based on the assumption that the cross-sectional properties are constant with time, an assumption that is not true if the ice cover roughness is varying with time. In this study a conveyance factor, C_v , is proposed that is applied to the effective channel conveyance as shown in the following equation:

$$\bar{K}_i = C_v 2 \left[(0.5 - \sum us_i) K_{oi} + \sum us_i K_{ii} \right] \quad (53)$$

where K_{oi} and K_{ii} are the open-water and ice-cover channel conveyances, respectively. C_v can also be regarded as the inverse of the hydraulic roughness factor that modifies the composite Manning's roughness coefficient of a section. As the effective channel roughness decreases, for example through smoothing of the river ice cover, C_v increases. In the remaining portion of this chapter, C_v will be regarded as constant and equal to one. In the following chapter on the state-space model, C_v will be discussed in more detail.

2.2.6 Summary of finite-difference representation

At this point the combined continuity and momentum equations for the channel and floodplain can be found by summing the channel and the floodplain version of each equation (the variables affected by the presence of the ice cover are indicated by the overbar):

$$\begin{aligned} & \frac{1}{\Delta x_{ei}} (Q_{i+1}^n - Q_i^n) + \frac{\theta}{\Delta x_{ei}} (\Delta Q_{i+1} - \Delta Q_i) + \\ & \frac{1}{2\Delta t \Delta x_{ei}} \left(\Delta x_{ci} \frac{d\bar{A}_{ci+1}}{dZ} \Delta Z_{i+1} + \Delta x_{fi} \frac{d\bar{A}_{fi+1}}{dZ} \Delta Z_{i+1} \right) + \end{aligned} \quad (54)$$

$$\frac{1}{2\Delta t \Delta x_{ei}} \left(\Delta x_{ci} \frac{d\bar{A}_{ci}}{dZ} \Delta Z_i + \Delta x_{fi} \frac{d\bar{A}_{fi}}{dZ} \Delta Z_i \right) - \frac{Q_i}{\Delta x_{ei}} = 0$$

$$\begin{aligned} & \frac{1}{2\Delta t \Delta x_{ei}} \left[\phi_{i+1} \Delta Q_{i+1} + \phi_i \Delta Q_i \right] \Delta x_{ci} + \\ & \frac{1}{2\Delta t \Delta x_{ei}} \left[(1 - \phi_{i+1}) \Delta Q_{i+1} + (1 - \phi_i) \Delta Q_i \right] \Delta x_{fi} + \\ & \frac{1}{\Delta x_{ei}} \left[(\beta V Q)_{i+1}^n - (\beta V Q)_i^n \right] + \frac{\theta}{\Delta x_{ei}} \left[(\beta V)_{i+1}^n \Delta Q_{i+1} - (\beta V)_i^n \Delta Q_i \right] + \\ & 0.5g \left(\bar{A}_{i+1}^n + \bar{A}_i^n \right) \left(\frac{Z_{i+1} - Z_i}{\Delta x_{ei}} + \frac{\theta}{\Delta x_{ei}} (\Delta Z_{i+1} - \Delta Z_i) \right) + \\ & 0.5g\theta \left(\frac{d\bar{A}_{i+1}}{dZ} \Delta Z_{i+1} + \frac{d\bar{A}_i}{dZ} \Delta Z_i \right) \left(\frac{Z_{ci+1} - Z_{ci}}{\Delta x_{ei}} \right) + \\ & 0.5g \left(\bar{A}_{i+1}^n + \bar{A}_i^n \right) 0.5 \left(\bar{S}_{fi+1}^n + \bar{S}_{fi}^n \right) + \\ & 0.5g \left(\bar{A}_{i+1}^n + \bar{A}_i^n \right) \theta \left[\begin{aligned} & \frac{-2\bar{S}_{fi+1}}{\bar{K}_{i+1}} \frac{d\bar{K}_{i+1}}{dZ} \Delta Z_{i+1} + \frac{2\bar{S}_{fi+1}}{Q_{i+1}} \Delta Q_{i+1} \\ & + \frac{-2\bar{S}_{fi}}{\bar{K}_i} \frac{d\bar{K}_i}{dZ} \Delta Z_i + \frac{2\bar{S}_{fi}}{Q_i} \Delta Q_i \end{aligned} \right] + \\ & 0.5g \left(\bar{S}_{fi+1}^n + \bar{S}_{fi}^n \right) \left[\frac{d\bar{A}_{i+1}}{dZ} \Delta Z_{i+1} + \frac{d\bar{A}_i}{dZ} \Delta Z_i \right] = 0 \end{aligned} \quad (55)$$

The foregoing assumes that $\Delta F \Delta F \approx 0$ and that ϕ_j , β_j , Δx_{ej} , and V are constant over a time step.

A system of quasi-linear equations results:

$$\begin{bmatrix} BC(\Delta Q_1, \Delta Z_1) \\ C(\Delta Q_1, \Delta Z_1, \Delta Q_2, \Delta Z_2, Q_1^n, Z_1^n, Q_2^n, Z_2^n) \\ M(\Delta Q_1, \Delta Z_1, \Delta Q_2, \Delta Z_2, Q_1^n, Z_1^n, Q_2^n, Z_2^n) \\ C(\Delta Q_2, \Delta Z_2, \Delta Q_3, \Delta Z_3, Q_2^n, Z_2^n, Q_3^n, Z_3^n) \\ M(\Delta Q_2, \Delta Z_2, \Delta Q_3, \Delta Z_3, Q_2^n, Z_2^n, Q_3^n, Z_3^n) \\ \vdots \\ C(\Delta Q_{j-1}, \Delta Z_{j-1}, \Delta Q_j, \Delta Z_j, Q_{j-1}^n, Z_{j-1}^n, Q_j^n, Z_j^n) \\ M(\Delta Q_{j-1}, \Delta Z_{j-1}, \Delta Q_j, \Delta Z_j, Q_{j-1}^n, Z_{j-1}^n, Q_j^n, Z_j^n) \\ BC(\Delta Q_j, \Delta Z_j) \end{bmatrix} = 0 \quad (56)$$

where the BC s are the additional equations describing the conditions at the upstream and downstream boundaries of the river. The equations are quasi-linear because the coefficients of the unknowns ($\Delta Q_1, \Delta Z_1, \dots, \Delta Q_j, \Delta Z_j$) depend in part on the value of the unknowns.

It is convenient in further discussions to use a shorthand notation to refer to the above series of equations. This can be done by referring to the equations using the following functional form:

$$f(\bar{a}, \bar{b}^n, t, t + \Delta t, \bar{U}^{n+1}) = 0 \quad (57)$$

where \bar{a} and \bar{b} are column vectors defined as

$$\begin{aligned} \bar{a} &= [\Delta Q_1, \Delta H_1, \dots, \Delta Q_j, \Delta H_j]^T \\ \bar{b}^n &= [Q_1^n, H_1^n, \dots, Q_j^n, H_j^n]^T \end{aligned} \quad (58)$$

Note that the relationship between \bar{a} and \bar{b} can be simply stated as

$$\bar{a} = \bar{b}^{n+1} - \bar{b}^n. \quad (59)$$

The input data entered in the model include the hydraulic boundary conditions and the calculated ice cover extents. These variables are combined in the column vector \bar{U}^{n+1} :

$$\bar{U}^{n+1} = \left[Q_0^{n+1}, H_0^{n+1}, \Sigma ds_1^{n+1} \dots \Sigma us_j^{n+1} \right]^T. \quad (60)$$

2.2.7 Solution of the finite-difference equations

It is assumed that all values are known except for those included in \bar{a} . The above equations are quasi-linear with respect to \bar{a} as described above. As a result the unknowns in \bar{a} cannot be solved for directly. The Newton–Raphson procedure has been shown to be an effective procedure for iteratively estimating \bar{a} . This procedure can be described in the following manner. Let \tilde{a} be an estimate of \bar{a} . Then the equations included in f above can be expanded in a Taylor's series about \tilde{a} :

$$0 = f\left(\tilde{a}, \bar{b}^n, t, t + \Delta t, \bar{U}^{n+1}\right) + \left. \frac{\partial f}{\partial \bar{a}} \right|_{\bar{a}=\tilde{a}} (\bar{a} - \tilde{a}^n) \quad (61)$$

or more simply,

$$\mathbf{F}_a \delta_a = -f \quad (62)$$

where

$$\begin{aligned} f &= f\left(\tilde{a}, \bar{b}^n, t, t + \Delta t, \bar{U}^{n+1}\right) \\ \delta_a &= (\bar{a} - \tilde{a}) \\ \mathbf{F}_a &= \left. \frac{\partial f}{\partial \bar{a}} \right|_{\bar{a}=\tilde{a}} \end{aligned} \quad (63)$$

\mathbf{F}_a is a $2I$ by $2I$ square, banded matrix; δ_a and f are vectors. δ_a is found by inverting \mathbf{F}_a and multiplying both sides of the above equation. Consequently

$$\delta_a = \mathbf{F}_a^{-1} (-f). \quad (64)$$

Once δ_a is found, a new estimate for \tilde{a} is produced:

$$\tilde{a}_{\text{new}} = \tilde{a}_{\text{old}} + \delta_a. \quad (65)$$

This solution procedure is repeated until δ_a is smaller than some predetermined tolerance or a maximum number of iterations has taken place.

2.3 Thermal and ice transport model component

2.3.1 Background

It has been shown that in large, well-mixed rivers the longitudinal (along the channel) distribution of temperature and passive tracers (materials that do not modify the flow field of the channel) can be well described using the one-dimensional advection–diffusion equation (Fischer et al. 1979). In the present study the longitudinal temperature distribution of the channel is estimated along with two passive tracers: the concentration of suspended frazil ice and the area concentration of transported surface ice. Transported frazil ice and surface ice can be considered passive tracers because, under most circumstances, they do not influence river flow. Concentrations of frazil ice in rivers are quite low, usually several orders of magnitude less than 1% by volume (Daly 1994). Concentrations of surface ice may become large enough that some portion of the drag imparted on the floating ice by the flow is resisted by the riverbanks. In the case of the Missouri River downstream of Oahe Dam, there is apparently not enough travel time for the surface concentration of floating ice to become great enough for interaction with the banks to become important. In other locations this may not be the case. Therefore, the “free drift” approximation will be used in this study.

It is clear from the physics of ice growth that the water temperature, frazil ice concentration, and surface ice concentration are mutually dependent. Consequently the transport equation for each ice form must be solved simultaneously (Lal and Shen 1993). The transport equations must also handle either open-water or ice-covered conditions; a means for doing this is presented.

A solution procedure is presented that solves the transport equations at each cross section in turn, starting from upstream and progressing downstream. The channel geometric properties are described at the same number of discrete cross sections as the hydraulic model.

An important challenge that the solution procedure must handle is the abrupt transition from open-water to ice-covered conditions that occurs at the leading upstream edge of the ice cover. This transition represents a “shock” at which the

properties of the equations change abruptly. It would be difficult to integrate the governing equations through this transition in any accurate way. By interpolating a cross section at the leading edge of the ice cover, this transition can be dealt with and the accuracy of the solution maintained. The transport equations are successively solved for the open-water subreach upstream of the leading edge, then for the ice-covered subreach downstream of the leading edge. As with the overall solution procedure described for the hydraulic model, this solution procedure anticipates the state–space model form. The parallel between the solution procedure described here and the requirements of the state–space form can be exploited to minimize the number of numerical computations, as are shown in the next chapter.

2.3.2 Governing equations

The one-dimensional transport of heat in a river can be written as (Shen 1996)

$$\begin{aligned} \frac{\partial T}{\partial t} + U \frac{\partial T}{\partial x} = & \\ \frac{\partial}{\partial x} \left(\psi \frac{\partial T}{\partial x} \right) + (1 - \Omega) \frac{B h_{wa} (T_a - T)(1 - C_a)}{\rho C_p A} + & \quad (66) \\ \frac{\rho_i L_i}{\rho C_p} \frac{DC_f}{Dt} + \Omega \frac{B h_{wi} (T_m - T)}{\rho C_p A} & \end{aligned}$$

where T = cross-sectional water temperature
 C_a = surface concentration of floating ice
 C_f = concentration of suspended frazil ice
 U = mean flow velocity
 ψ = longitudinal heat diffusion coefficient
 C_p = heat capacity of the water
 B = width of the open-water surface
 h_{wa} = water-to-air heat transfer coefficient
 h_{wi} = water-to-ice heat transfer coefficient
 T_a = air temperature
 Ω = ice cover index.

If an ice cover is present, $\Omega = 1$; otherwise $\Omega = 0$. The terms on the right-hand side of the equation represent the diffusion due to the longitudinal temperature

gradient, the heat transfer exchange with the atmosphere, the latent heat transfer from melting or growing suspended frazil ice, and the heat transfer exchange with the ice cover, respectively. In this study the heat transport in the longitudinal direction is assumed to be dominated by convection; diffusion can be ignored and ψ set as 0. Heat transfer from the water surface is assumed to be a linear function of the difference between water temperature and air temperature, or if the channel is ice covered, it is assumed that the heat transfer is a linear function of the difference between water temperature and ice/water equilibrium temperature, T_m . In both cases the heat transfer coefficient must be defined.

Surface ice is assumed to be transported in the form of ice floes that form from frazil slush, although how floes form from frazil ice is probably one of the least well described processes in the evolution of frazil ice (Daly 1994). Observations and recent work suggest that the floe size may be determined by the structure of the surface turbulence of the channel (Matousek 1984, Andreasson et al. 1998). A quantitative means of estimating the surface ice concentration that avoids estimating the floe diameter, but rather focuses on the surface concentration, was developed by Lal and Shen (1993). They describe the surface concentration of ice in terms of a conservation equation:

$$\frac{\partial C_a}{\partial t} + U \frac{\partial C_a}{\partial x} = (1 - \Omega) \left(\frac{C_f \Theta V_b (1 - C_a)}{h_i + (1 - e_f) h_f} - C_a \frac{\partial U}{\partial x} - \frac{C_a}{B} \frac{DB}{Dt} \right) \quad (67)$$

where V_b = rise velocity of the suspended frazil ice crystals
 Ω = probability of the frazil crystals remaining at the underside of surface pans after they have contacted them
 h_i = thickness of frazil pans
 h_f = thickness of frazil ice deposited under pans
 e_f = porosity of the deposited frazil.

The terms on the right-hand side of the equation represent the increase in surface concentration due to the arrival of frazil ice at the water surface and its incorporation into pans, and the last two terms represent the changes in surface ice concentration due to changes in the flow velocity and channel width. To apply this formula it is required that a minimum allowable floe thickness be specified at the start of the simulation.

To implement the foregoing equations, it is necessary to review what is known about the initial formation of frazil ice and how it can be simulated. Frazil ice initially appears in natural water bodies as distinct, separate ice crystals suspended in turbulent flow. The initial crystals form through secondary nucleation,

which starts when seed crystals are introduced into turbulent, supercooled water. While the details of secondary nucleation are not known, it is known that millions of frazil ice crystals can result from a few seed crystals (Daly 1984). There are two approaches to simulating the development of frazil ice in natural water bodies. The first, termed “frazil ice dynamics,” attempts to simulate the size distribution function of the frazil crystals (Daly 1984, Hammar and Shen 1995) based on estimations of the heat transfer rate from the suspended crystals, the secondary nucleation rate, and the seeding rate. In practice, while physically rigorous, this approach requires extensive computational effort, and there have been few data available for validation. The second approach simulates the concentration of frazil and assumes that the frazil particles can be described by a mean diameter, which remains constant with time. This approach has found success in modeling frazil ice in the oceans (described by Omstedt in Daly 1994) and is the approach adopted by Lal and Shen (1993):

$$\frac{\partial C_f}{\partial t} + U \frac{\partial C_f}{\partial x} = -\frac{C_f \Theta V_b B}{A} + \frac{1}{\rho_i L_i} \frac{N_u k_w}{d_f} a_o N_f (T_m - T) + S(1 - \Omega) \quad (68)$$

where N_u = frazil crystal Nusselt number (a non-dimensional heat transfer coefficient)
 k_w = thermal conductivity of water
 d_f = length scale associated with a frazil ice particle
 a_o = mean area of a frazil ice particle
 N_f = number of frazil ice particles per unit volume
 S = seeding rate of new particles.

The seeding rate describes the number of frazil ice particles that are introduced through the water surface per unit time. The seed crystals are produced by the freezing of water droplets in the air. The droplets are produced through a variety of mechanisms (Daly 1994). The separate terms on the right-hand side of the equation represent the sink of crystals at the water surface as they are incorporated into ice floes, the growth or melting of the ice crystals through heat transfer with the water, and the entrance of new crystals through seeding.

In addition to the three transport equations described above, two auxiliary equations are required in order to estimate the thickness of the floating ice floes through thermal growth and the thickness of the deposited frazil beneath the pans. The thermal growth is estimated by assuming that the heat transfer through the floe is quasi-steady: the floe surface is at the air temperature, the floe’s horizontal interface with the water is at the ice/water equilibrium temperature, and the temperature gradient between is linear. In addition, accelerated ice growth is

possible if frazil ice deposits against the underside of the floe. The requisite equation is

$$\frac{D h_i}{D t} = \frac{1}{e_f \rho_i L_i} \frac{(T_m - T_a)}{\left(\frac{1}{H_{ia}} + \frac{h_i}{k_i} \right)} \quad (69)$$

where H_{ia} is the ice–air heat transfer coefficient and k_i is the thermal conductivity of ice. The thickness of deposited frazil ice is estimated as

$$\frac{D h_f}{D t} = \frac{\Theta V_b C_v}{(1 - e_f)} - \frac{D h_i}{D t} \quad (70)$$

where the terms on the right-hand side of the equation represent the thickness of frazil deposition minus the thickness lost due to thermal thickening of the ice floe into the deposited frazil ice.

2.3.3 One-dimensional Holly–Preissman representation

The thermal transport is solved by using the method of characteristics, which consists of replacing the partial differential equation with two ordinary differential equations:

$$\frac{d T}{d t} = (1 - \Omega) \frac{B h_{wa} (T_a - T)(1 - C_a)}{\rho C_p A} + \frac{\rho_i L_i}{\rho C_p} \frac{D C_f}{D t} + \Omega \frac{B h_{wi} (T_m - T)}{\rho C_p A} \quad (71)$$

$$\frac{d C_a}{d t} = (1 - \Omega) \left(\frac{C_f \Theta V_b (1 - C_a)}{h_i + (1 - e_f) h_f} - C_a \frac{\partial U}{\partial x} - \frac{C_a}{B} \frac{D B}{D t} \right) \quad (72)$$

$$\frac{d C_f}{d t} = - \frac{C_f \Theta V_b B}{A} + \frac{1}{\rho_i L_i} \frac{N_u k_w}{d_f} a_o N_f (T_m - T) + S(1 - \Omega) \quad (73)$$

$$\frac{d x}{d t} = \bar{U} . \quad (74)$$

The above equations are next translated into the finite-difference form presented earlier. The finite-difference form is written along the flow characteristic:

$$\begin{aligned}
\frac{1}{\Delta t} (T_i^{n+1} - T_\xi) &= \frac{\theta B_i^{n+1}}{\rho C_p A_i^{n+1}} (1 - \Omega_i) h_{wa} (T_a - T_i^{n+1}) (1 - C_{ai}^{n+1}) \\
&+ \frac{(1 - \theta) B_\xi^{n+1}}{\rho C_p A_\xi^{n+1}} (1 - \Omega_\xi) h_{wa} (T_a - T_\xi^n) (1 - C_{a\xi}^n) + \\
\frac{\rho_i L_i}{\rho_i C_p} Y_f & \left[\theta C_{vi}^{n+1} (T_m - T_i^{n+1}) + (1 - \theta) C_{v\xi}^n (T_m - T_\xi^n) \right] + \\
\frac{\theta B_i^{n+1}}{\rho C_p A_i^{n+1}} \Omega_i h_{wi} (T_m - T_i^{n+1})_i &+ \frac{(1 - \theta) B_\xi^{n+1}}{\rho C_p A_\xi^{n+1}} \Omega_\xi h_{wi} (T_m - T_\xi^n)
\end{aligned} \tag{75}$$

$$\begin{aligned}
\frac{1}{\Delta t} (C_{ai}^{n+1} - C_{a\xi}) &= \theta (1 - \Omega_i) \frac{\Theta V_b C_{fi}^{n+1}}{(h_{ii}^{n+1} + (1 - e_f) h_{fi}^{n+1})} (1 - C_{ai}^{n+1}) \\
&+ (1 - \theta) (1 - \Omega_i) \frac{\Theta V_b C_{f\xi}^n}{(h_{i\xi}^n + (1 - e_f) h_{f\xi}^n)} (1 - C_{a\xi}^n)
\end{aligned} \tag{76}$$

$$\begin{aligned}
\frac{1}{\Delta t} (C_{fi}^{n+1} - C_{f\xi}) &= \theta Y_f (T_m - T_i^{n+1}) + (1 - \theta) Y_f (T_m - T_\xi^n) + \\
\theta \frac{\Theta V_b C_{fi}^{n+1} B_i^{n+1}}{A_i^{n+1}} &+ (1 - \theta) \frac{\Theta V_b C_{f\xi}^n B_\xi^n}{A_\xi^n} + S \left[\theta (1 - \Omega_i) + (1 - \theta) (1 - \Omega_\xi) \right]
\end{aligned} \tag{77}$$

$$\frac{1}{\Delta t} (h_{ii}^{n+1} - h_{i\xi}) = \theta \frac{1}{e_f \rho_i L_i} \frac{(T_m - T_a)}{\left(\frac{1}{h_{ia}} + \frac{h_{ii}^{n+1}}{k_i} \right)} + (1 - \theta) \frac{1}{e_f \rho_i L_i} \frac{(T_m - T_a)}{\left(\frac{1}{h_{ia}} + \frac{h_{i\xi}^n}{k_i} \right)} \tag{78}$$

$$\begin{aligned} \frac{1}{\Delta t} (h_{fi}^{n+1} - h_{f\xi}) = & -\theta \frac{1}{e_f \rho_i L_i} \frac{(T_m - T_a)}{\left(\frac{1}{h_{ia}} + \frac{h_{fi}^{n+1}}{k_i} \right)} - (1-\theta) \frac{1}{e_f \rho_i L_i} \frac{(T_m - T_a)}{\left(\frac{1}{h_{ia}} + \frac{h_{f\xi}^n}{k_i} \right)} \\ & + \theta \frac{\Theta V_b C_{fi}^{n+1}}{e_f} + (1-\theta) \frac{\Theta V_b C_{f\xi}^n}{e_f} \end{aligned} \quad (79)$$

where

$$Y_f = \frac{1}{\rho_i L_i} \frac{N_u k_w}{d_f} a_o N_f. \quad (80)$$

Variables with the subscript ξ indicate values at the foot of the characteristic arriving at x_i at time $n + 1$. In the present formulation the foot must be on the boundary of the space–time grid cell defined by x_i and x_{i-1} and t^n and t^{n+1} . The general problem is to interpolate the values of the variables at ξ . Linear interpolation has been shown to introduce substantial inaccuracies into the calculations. In the present formulation the “two-point higher order” scheme of Holly and Preissman is used (Sauvaget 1984). In this scheme the value of any variable can be interpolated at ξ through knowing the value of the variable and its derivative at the grid cells points x_i and x_{i-1} at time t^n and at x_{i-1} at time t^{n+1} . The implicit assumption is that the flow is in the downstream direction only. In this case the transported properties at ξ are

$$T_\xi = c_1 T_{i-1}^n + c_2 T_i^n + c_3 TX_{i-1}^n + c_4 TX_i^n + c_5 T_{i-1}^{n+1} + c_6 TX_{i-1}^{n+1} \quad (81)$$

$$C_{a\xi} = c_1 C_{ai-1}^n + c_2 C_{ai}^n + c_3 CX_{ai-1}^n + c_4 CX_{ai}^n + c_5 C_{ai-1}^{n+1} + c_6 CX_{ai-1}^{n+1} \quad (82)$$

$$C_{f\xi} = c_1 C_{fi-1}^n + c_2 C_{fi}^n + c_3 CX_{fi-1}^n + c_4 CX_{fi}^n + c_5 C_{fi-1}^{n+1} + c_6 CX_{fi-1}^{n+1} \quad (83)$$

where TX , CX_a , and CX_f are the respective derivatives of temperature, surface ice concentration, and frazil ice concentration with respect to the longitudinal distance along the river. In this scheme it is necessary to also determine the value of the derivatives at time t^{n+1} . They are

$$TX_i^{n+1} = \left(d_1 T_{i-1}^n + d_2 T_i^n + d_3 TX_{i-1}^n + d_4 TX_i^n + d_5 T_{i-1}^{n+1} + d_6 TX_{i-1}^{n+1} \right) \left(\frac{1 - \frac{\Delta t}{2} \frac{du}{dx}}{1 + \frac{\Delta t}{2} \frac{du}{dx}} \right) \quad (84)$$

$$CX_{ai}^{n+1} = \left(d_1 C_{ai-1}^n + d_2 C_{ai}^n + d_3 CX_{ai-1}^n + d_4 CX_{ai}^n + d_5 C_{ai-1}^{n+1} + d_6 CX_{ai-1}^{n+1} \right) \left(\frac{1 - \frac{\Delta t}{2} \frac{du}{dx}}{1 + \frac{\Delta t}{2} \frac{du}{dx}} \right) \quad (85)$$

$$CX_{fi}^{n+1} = \left(d_1 C_{fi-1}^n + d_2 C_{fi}^n + d_3 CX_{fi-1}^n + d_4 CX_{fi}^n + d_5 C_{fi-1}^{n+1} + d_6 CX_{fi-1}^{n+1} \right) \left(\frac{1 - \frac{\Delta t}{2} \frac{du}{dx}}{1 + \frac{\Delta t}{2} \frac{du}{dx}} \right) \quad (86)$$

If the Courant Number, C_r , defined as $\bar{U} \Delta t / \Delta x$, is in the range $1 \geq C_r \geq 0$, then

$$\alpha = \frac{x_i - \xi_i}{x_i - x_{i-1}} = \frac{\bar{U} \Delta t}{x_i - x_{i-1}} \quad (87)$$

and

$$\begin{aligned} c_1 &= \alpha^2 (3 - 2\alpha) \\ c_2 &= 1 - c_1 \\ c_3 &= \alpha^2 (1 - \alpha)(x_i - x_{i-1}) \\ c_4 &= -\alpha(1 - \alpha)^2 (x_i - x_{i-1}) \\ c_5 &= 0 \\ c_6 &= 0 \end{aligned} \quad (88)$$

$$\begin{aligned}
d_1 &= 6\alpha(1-\alpha)/(x_i - x_{i-1}) \\
d_2 &= -d_1 \\
d_3 &= \alpha(3\alpha - 2) \\
d_4 &= (\alpha - 1)(3\alpha - 1) \\
d_5 &= 0 \\
d_6 &= 0
\end{aligned} \tag{89}$$

If $C_r > 1$, then

$$\beta = \frac{t^{n+1} - t_\xi}{t^{n+1} - t^n} = \frac{1}{\alpha} \tag{90}$$

and

$$\begin{aligned}
c_1 &= \beta^2(3 - 2\beta) \\
c_2 &= 0 \\
c_3 &= -\beta^2(1 - \beta)U_{i-1}^n \Delta t \\
c_4 &= 0 \\
c_5 &= 1 - c_1 \\
c_6 &= \beta(1 - \beta)^2 U_{i-1}^{n+1} \Delta t
\end{aligned} \tag{91}$$

$$\begin{aligned}
d_1 &= 6\beta(\beta - 1)/\Delta t \\
d_2 &= 0 \\
d_3 &= \beta(2 - 3\beta)U_{i-1}^n \\
d_4 &= 0 \\
d_5 &= 6\beta(1 - \beta)/\Delta t \\
d_6 &= (1 - \beta)(3\beta - 1)U_{i-1}^{n+1}
\end{aligned} \tag{92}$$

It is assumed in the above formulation that reverse flow does not occur; that is, C_r cannot be less than 0. However, the equations could be modified to handle this case.

2.3.4 Solution of the governing equations

At this point the five transport equations at each section have been developed along with their Holly–Preissman representation. As the flow model and the transport model are effectively decoupled, the hydraulic model can be solved independently. Therefore, the flow variables and the channel geometric variables are known at each section at the time of solution of the transport equations. By inspection it can be seen that the transport equations at any section at time t^{n+1} depend only on the information at time t^n , and not on information at time t^{n+1} , if the Courant number at that section is less than one. If the Courant number is greater than one, then the solution depends on information at time t^n and information at the next upstream section at time t^{n+1} . This relationship suggests a solution procedure that starts at the upstream end of the channel and progresses downstream, simultaneously solving the five transport equations at each section in turn. The requirement for this solution procedure is that the Courant number everywhere exceeds zero. In physical terms this means that there cannot be reverse (upstream) flow anywhere in the channel. Reverse flow is not considered in this study.

The progressive solution procedure is now described in a series of steps:

1. At the upstream section the boundary conditions of water temperature, surface ice concentration, frazil ice concentration, floe thickness, and deposited frazil thickness are set as

$$\begin{aligned}
 T_1^{n+1} &= T_o^{n+1} \\
 C_{al}^{n+1} &= 0 \\
 C_{vl}^{n+1} &= 0 \\
 h_{f1}^{n+1} &= 0 \\
 h_{i1}^{n+1} &= 0
 \end{aligned} \tag{93}$$

It is assumed that ice is not available at the upstream end of the channel. This assumption is reasonable for the reach of river below Oahe Dam, as virtually all the flow is released through hydropower turbines, and it is not physically possible for ice to be present in the released flow. The derivatives of the transported properties are therefore set as

$$TX_1^{n+1} \approx -\frac{(T_o^{n+1} - T_o^n)}{\bar{U}\Delta t} \tag{94}$$

$$\begin{aligned} CX_{al}^{n+1} &= 0 \\ CX_{fl}^{n+1} &= 0 \end{aligned}$$

2. The thermal and transport equations are solved at the next downstream section. There are three possible cases: a) no ice cover exists between the present section and the next, in which case the ice cover index, Ω , is set equal to zero; b) a continuous ice cover exists between the present section and the next, in which case Ω is set equal to one; and c) the leading edge of the ice cover is found between the present section and the next. In this last case a section is interpolated between the present section and the next and the hydraulic and geometric properties of the sections are estimated. Ω is set equal to zero because the subreach from the present section to the leading edge of the ice cover is not ice covered. The next iteration starts from the interpolated cross section and proceeds to the next downstream section. As that subreach is ice covered, Ω is set to one.

3. The Courant number is found for the next section, α and β calculated, and the coefficients of the Holly–Preissman scheme determined. The transport variables at the foot of the characteristic, T_ξ , $C_{a\xi}$, $C_{v\xi}$, $h_{f\xi}$, and $h_{i\xi}$, are determined.

4. The simultaneous solution of the five transport equations at a particular section is now described. At any section, x_{i+1} , at time t^{n+1} , the five transport equations are dependent only on the five transport variables T_{i+1}^{n+1} , C_{ai+1}^{n+1} , C_{vi+1}^{n+1} , h_{fi+1}^{n+1} , and h_{ii+1}^{n+1} ; the variables at the foot of the characteristic that intersects x_{i+1} at t^{n+1} , T_ξ , $C_{a\xi}$, $C_{v\xi}$, $h_{f\xi}$, and $h_{i\xi}$, which can be calculated immediately using information from the previous time step and the next upstream section; various known geometric and flow variables; and the air temperature. Let the five equations at section x_{i+1} at time t^{n+1} be represented as

$$f_{i+1}^{n+1}(\bar{a}_{i+1}^{n+1}, \bar{a}_\xi^n, t, t + \Delta t, \bar{U}^{n+1}) = 0 \quad (95)$$

where \bar{a}_{i+1}^{n+1} and \bar{a}_ξ^n are column vectors defined as

$$\bar{a}_{i+1}^{n+1} = [T_{i+1}^{n+1}, C_{ai+1}^{n+1}, C_{vi+1}^{n+1}, h_{fi+1}^{n+1}, h_{ii+1}^{n+1}] \quad (96)$$

and

$$\bar{a}_\xi^n = [T_\xi^n, C_{a\xi}^n, C_{v\xi}^n, h_{f\xi}^n, h_{i\xi}^n]. \quad (97)$$

It is assumed that all values are known except for those included in \bar{a}_{i+1}^{n+1} . The above equations are nonlinear with respect to \bar{a}_{i+1}^{n+1} . Consequently the unknowns in \bar{a}_{i+1}^{n+1} cannot be solved for directly. As done in the previous section the Newton–Raphson procedure is used for iteratively estimating \bar{a}_{i+1}^{n+1} . Let \tilde{a}_{i+1}^{n+1} be an estimate of \bar{a}_{i+1}^{n+1} . Then the equations included in f_{i+1}^{n+1} above can be expanded in a Taylor’s series about \tilde{a}_{i+1}^{n+1} :

$$0 = f_{i+1}^{n+1} \left(\tilde{a}_{i+1}^{n+1}, \bar{a}_{\xi}^n, t, t + \Delta t, \bar{U}^{n+1} \right) + \left. \frac{\partial f_{i+1}^{n+1}}{\partial \bar{a}_{i+1}^{n+1}} \right|_{\bar{a}_{i+1}^{n+1} = \tilde{a}_{i+1}^{n+1}} \left(\bar{a}_{i+1}^{n+1} - \tilde{a}_{i+1}^{n+1} \right) \quad (98)$$

or more simply,

$$\mathbf{F}_{i+1}^{n+1} \delta_{i+1}^{n+1} = -f_{i+1}^{n+1} \quad (99)$$

where

$$\begin{aligned} f_{i+1}^{n+1} &= f_{i+1}^{n+1} \left(\tilde{a}_{i+1}^{n+1}, \bar{a}_{\xi}^n, t, t + \Delta t, \bar{U}^{n+1} \right) \\ \delta_{i+1}^{n+1} &= \left(\bar{a}_{i+1}^{n+1} - \tilde{a}_{i+1}^{n+1} \right) \\ \mathbf{F}_{i+1}^{n+1} &= \left. \frac{\partial f_{i+1}^{n+1}}{\partial \bar{a}_{i+1}^{n+1}} \right|_{\bar{a}_{i+1}^{n+1} = \tilde{a}_{i+1}^{n+1}} \end{aligned} \quad (100)$$

\mathbf{F}_{i+1}^{n+1} is a five-by-five square matrix; and δ_{i+1}^{n+1} and f_{i+1}^{n+1} are vectors. δ_{i+1}^{n+1} is found by inverting \mathbf{F}_{i+1}^{n+1} and multiplying both sides of the above equation:

$$\delta_{i+1}^{n+1} = \mathbf{F}_{i+1}^{n+1-1} \left(-f_{i+1}^{n+1} \right). \quad (101)$$

Once δ_{i+1}^{n+1} is found, a new estimate for \bar{a}_{i+1}^{n+1} is produced:

$$\tilde{a}_{i+1\text{new}}^{n+1} = \tilde{a}_{i+1\text{old}}^{n+1} + \delta_{i+1}^{n+1}. \quad (102)$$

This procedure is repeated until δ_{i+1}^{n+1} is smaller than some predetermined tolerance or until a maximum number of iterations has taken place.

5. The derivatives of the transported properties are then found using eq 84 through 86 described above.

6. At this point the solution procedure returns to step 2 and the sequence is repeated. The solution procedure continues until the end of the channel is reached.

2.4 Simulation of stationary ice cover progression and retreat

2.4.1 Background

In rivers with any significant flow, stationary ice covers progress upstream from an initiation point as ice is brought to the leading upstream edge of the ice cover by the flow of the river. Many separate processes may occur at the leading edge, depending on the hydraulic flow conditions and the form of the arriving ice:

1. *Bridging*. At very low flow velocities and relatively high concentrations of surface ice, it is possible for the ice cover to spontaneously arch across the open width of a channel and stop moving. In the Missouri River downstream of Oahe Dam, a stationary ice cover appears spontaneously in the backwater of Big Bend Dam where the flow velocity is very low.

2. *Juxtaposition*. At relatively low flow velocities, ice floes arriving at the leading edge may simply come to a stop and assemble as a single layer of juxtaposed floes. In this way the ice cover progresses upstream by juxtaposition. The maximum flow velocity at which juxtaposition occurs depends on floe geometry and channel depth. The ice cover progression in the Missouri River occurs largely through juxtaposition of frazil floes.

3. *Underturning of floes*. At higher flow velocities, arriving floes may not assemble as a stable layer but may instead overturn. If flow velocity is not too high, the overturned floes remain as a jumbled accumulation at the leading edge of the ice cover.

4. *Ice cover shoving*. Shoving in an ice cover can happen over a wide range of flow velocities. The cover collapses in the downstream direction and becomes thicker if the forces acting on it exceed its ability to withstand those forces. The strength of an ice cover formed from many separate pieces of ice increases with its thickness, so that when shoving takes place, cover strength increases. An ice cover may repeatedly shove and thicken as it progresses upstream. If an ice cover is treated as a “granular” material, its strength characteristics and its final thickness can be estimated.

5. *Under-ice transport of floes*. At relatively high flow velocities, ice floes arriving at the leading edge of an ice cover may be overturned and transported under the ice cover for considerable distances. At this point, further upstream

progression may be halted until the deposition of the floes somewhere downstream of the leading edge reduces the channel conveyance sufficiently to cause the upstream water levels to rise and the flow velocities at the leading edge to be reduced.

6. *No ice cover progression.* An ice cover stops progressing upstream if flow velocities at the cover's leading edge remain too high. In this case, open water remains upstream of the leading edge throughout the winter season.

Simulation of ice cover retreat is more problematic than simulation of ice cover progression. In general, ice cover retreat is referred to as breakup. River ice cover breakup is bracketed by two ideal forms: thermal meltout and mechanical breakup. Thermal meltout results when an ice cover deteriorates through heat transfer from warm water (here, the definition of warm merely implies water with a temperature greater than 0°C) and/or absorption of solar radiation and melts in place, with little or no ice movement. Mechanical breakup requires no deterioration of an ice cover but rather results from the increase of stresses in the ice cover caused by increases in the flow rate. The stresses cause cracks and the ultimate fragmentation of the ice cover into pieces that are carried by the channel flow. In the case of the Missouri River downstream of Oahe Dam, the primary means of ice cover retreat is most likely a thermal meltout resulting from warm water released by Oahe Dam contacting the stationary ice cover. This occurs when the heat transfer from the open-water reach upstream of the leading edge is reduced because of mild weather conditions and the water released by the dam is not cooled to 0°C before reaching the leading edge. The present study proposes a criterion establishing the required amount of melting (actually ice cover weakening and thinning) to effectively remove the ice cover.

2.4.2 Governing equations for ice cover progression

The progression rate of the stationary ice cover, V_{cp} , can be estimated by conserving the arriving mass of ice at the leading edge of the cover (Lal and Shen 1993). If all the arriving ice is incorporated into the ice cover,

$$V_{cp}t_i B(1 - e_i) = (V_{cp} + \bar{U})\bar{h}_i B \bar{C}_a \quad (103)$$

where t_i = thickness of the progressing ice cover
 B = width of the channel
 e_i = porosity of the ice cover
 \bar{U} = mean flow velocity
 \bar{h}_i = mean thickness of the arriving ice floes
 \bar{C}_a = mean surface concentration of the surface ice.

The rate at which an ice cover progresses is then

$$V_{cp} = \frac{\bar{U}\bar{h}_i\bar{C}_a}{t_i(1-e_i) - \bar{h}_i\bar{C}_a}. \quad (104)$$

This equation is adequate to describe the progression of the ice cover as long as

$$\bar{C}_a \ll \frac{t_i(1-e_i)}{\bar{h}_i}. \quad (105)$$

This condition generally prevails because the progressing ice cover is thicker than the arriving ice floes, and \bar{C}_a always is less than one. At very high concentrations of surface ice, it is possible that the stationary ice cover advances upstream in the form of a shock wave that halts the moving surface ice. The velocity of the propagating shock is determined by the concentration and material properties of the arriving surface ice (Lal and Shen 1992). In the case of the Missouri River immediately downstream of Oahe Dam, observations show that surface ice concentrations are low enough that the above equations suffice.

2.4.3 Solution of the governing equations for ice cover progression

Mean values of \bar{U} , \bar{h}_i , and \bar{C}_a are estimated in the subreach upstream of the ice cover. As the cross section information is interpolated at the location of the leading edge of the ice cover, information is available at this location and can be used to estimate \bar{U} , \bar{h}_i , and \bar{C}_a using a four-point finite-difference representation:

$$\bar{U} = \frac{\theta}{2}(V_{us}^{n+1} + V_{le}^{n+1}) + \frac{(1-\theta)}{2}(V_{us}^n + V_{le}^n) \quad (106)$$

$$\begin{aligned} \bar{h}_i = & \frac{\theta}{2} \left[h_{fus}^{n+1} + (1-e_f)h_{fus}^{n+1} + h_{ile}^{n+1} + (1-e_f)h_{ile}^{n+1} \right] \\ & + \frac{(1-\theta)}{2} \left[h_{fus}^n + (1-e_f)h_{fus}^n + h_{ile}^n + (1-e_f)h_{ile}^n \right] \end{aligned} \quad (107)$$

$$\bar{C}_a = \frac{\theta}{2}(C_{a\ us}^{n+1} + C_{a\ le}^{n+1}) + \frac{(1-\theta)}{2}(C_{a\ us}^n + C_{a\ le}^n) \quad (108)$$

where V is the flow velocity. The subscript *le* implies the value at the leading edge of the ice cover, and the subscript *us* represents the variables at the cross

section immediately upstream of the leading edge of the ice cover. The extent of the progression of the ice cover in one time step, dl , can be estimated as

$$dl = \frac{\Delta t \overline{U} \overline{h}_i \overline{C}_a}{t_i (1 - e_i) - \overline{h} \overline{C}_a}. \quad (109)$$

2.4.4 Estimation of ice cover retreat

The overall heat balance for the stationary ice cover is

$$\frac{Dt_i}{Dt} = \frac{1}{e_f \rho_i L_i} \frac{(T_m - T_a)}{\left(\frac{1}{H_{ia}} + \frac{h_i}{k_i}\right)} + \frac{H_{iw}}{\rho_i L_i} (T_m - T_w) \quad (110)$$

where t_i is the thickness of the ice cover, and H_{iw} is the effective heat transfer coefficient between the ice cover and the water following beneath. Note that the effective heat transfer coefficient is set to zero as long as there is frazil deposited beneath the ice cover. In short, the water beneath the ice cover cannot melt the ice cover until any deposited frazil has been melted. Equation 110 can be solved using the finite-difference scheme proposed earlier:

$$\begin{aligned} \frac{1}{\Delta t} (t_{ii}^{n+1} - t_{ii}^n) = & \theta \frac{1}{e_f \rho_i L_i} \frac{(T_m - T_a)}{\left(\frac{1}{h_{ia}} + \frac{h_{ii}^{n+1}}{k_i}\right)} + (1 - \theta) \frac{1}{e_f \rho_i L_i} \frac{(T_m - T_a)}{\left(\frac{1}{h_{ia}} + \frac{h_{i\xi}^n}{k_i}\right)} + \\ & + \theta \frac{H_{iwi}^{n+1}}{\rho_i L_i} (T_m - T_i^{n+1}) + (1 - \theta) \frac{H_{i\xi}}{\rho_i L_i} (T_m - T_\xi) \end{aligned} \quad (111)$$

The ice cover can thin if the water beneath the cover is warmer than T_m . It is assumed that the ice cover is melted out if the ice cover thickness is reduced by a preset fraction.

2.5 Solution procedure for river ice model

Before presenting the procedure details, it is useful to provide a brief summary of the overall solution procedure.

1. The channel reach to be simulated is selected and schematized into cross sections. The geometry of each cross section is surveyed and entered into a format that lists the elevation and station of each surveyed point [the particular for-

mat is typically referred to as the HEC-2 format (Corps of Engineers 1990)]. In addition, the distances between cross sections also are determined.

2. The pre-processor program (Corps of Engineers 1997) analyzes each river section and prepares a look-up table of the geometric properties of each section as a function of a finite number of discrete water surface elevations. It estimates the geometric variables at a preset number of equally spaced elevations as described earlier. At this point, no ice information is required.

3. A second separate pre-processor program (Corps of Engineers 1997) prepares the time-varying boundary conditions data. For the case considered in this study, the following data are needed: the time-varying flow release of Oahe Dam, the time-varying stage at Big Bend Dam, the Oahe Dam release water temperature, and the observed air temperature. Typically this information would be in a HEC-DSS database (Corps of Engineers 1995).

4. The river ice simulation model proceeds through each time step of the simulation period. For each time step the following sequence is followed:

a) The hydraulic model simulates the flow based on the initial conditions at the start of the time step, the boundary conditions prescribed during the time step, and the extent and properties of the river ice cover.

b) The thermal and ice transport model determines the water temperature and ice concentrations at each cross section based on the flow conditions determined by the hydraulic model and the extent and properties of the river ice cover. A cross section is interpolated at the leading edge of the ice cover and the water temperature and ice concentration estimated at this location.

c) Ice cover progression and retreat is simulated based on the calculated flow conditions and the calculated thermal and surface ice concentrations. The thermal and transported ice concentrations at the leading edge of the ice cover are re-estimated if the leading edge of the ice cover changes position.

d) The river ice model returns to step a above. This sequence is repeated until the river ice conditions are simulated for the entire simulation period.

5. After the simulation is completed, a separate post-processor program (Corps of Engineers 1997) writes the simulation model output to a HEC-DSS database. The following information is written to the database for each cross section: the stage, the discharge, the water temperature, the frazil ice concentration, the surface ice concentration, the floe thickness, the deposited frazil ice thickness, the stationary ice cover thickness, and the frazil ice thickness deposited under the stationary ice cover. In addition, the position of the leading edge of the ice cover is written to the database in river miles.

3 STATE-SPACE RIVER ICE MODEL

3.1 Introduction

The previous chapter presents the river ice model with its three components: a river hydraulic component, a thermal and ice transport component, and an ice cover progression component. In applying such a model to actual water bodies, discrepancies often arise between the model results and the actual observed field conditions. The reasons for such discrepancies are discussed in the first chapter and may be grouped into three categories: model error, input error, and errors in the empirical coefficients used in the model. A state-space model incorporates, or assimilates, observations into the model to reduce the model error to a minimum. This chapter presents a state-space model based on the river ice model described in Chapter 2. The state-space river ice model potentially incorporates two state-space components: a hydraulic state-space model and a thermal and ice transport state-space model.

In actual application to the Missouri River, there are no accurate observations available for any of the state variables used for the model. As a result, only the hydraulic state-space model is used in this study. The thermal and ice transport state-space model is not employed. However, its development is described, and the field observations needed to implement it are discussed. The intent is that the U.S. Army Corps of Engineers, and other agencies, will set up the field instrumentation needed for improved forecasting and monitoring of ice conditions.

3.2 Hydraulic state-space model

3.2.1 State variables

As described by Kailath (1980), knowledge of the state vector at a time, t_0 , specifies the *state* or *condition* of the system at that time. The values of the state vector allow responses to future inputs to be determined without reference to inputs that occurred before time t_0 . In this way the state vector is a sufficient statistic; it contains just enough information, no more and no less, to enable the calculations of future responses without reference to the old history of inputs and responses. In the case of an open channel in which the geometry and hydraulic roughness are fixed, the flows and stages at each cross section would be sufficient for the state vector. In the case of a channel in which the ice cover is varying with time, the extent of the ice cover and the ice roughness must also be a component of the state vector. The concentration of floating surface ice and the concentration of suspended frazil ice do not influence the flows and stages, as this a *free drift* model in which those components are considered to move at the flow velocity and provide no hydraulic resistance.

Ice cover thickness could also be considered as a possible component of the state vector. However, ice thickness was also not included, for several reasons. First, observations of ice thickness are rarely available, and there is little to no opportunity to update the model estimation of the ice thickness. Second, in large channels, which are the intended subjects of this model, ice cover thickness has little influence on the stages and flows. In large channels the ice extent and roughness play a much greater role. Last, there is a practical consideration with regard to the size of the state vector. The number of elements of the error covariance matrix, \mathbf{P} , and the state transformation matrix, Φ , are equal to the square of the number of components of the state vector. The number of operations required to create and propagate these matrices in time is proportional to the square (and even the cube) of the number of elements. There is a trade-off required between the comprehensiveness of the state vector and the efficiency and computational run time of the simulation. In this case, not including the ice thickness is the necessary result.

The state vector at time $n + 1$ is \mathbf{X}^{n+1} . It contains flows, stages, ice extents, and conveyance factors as follows:

$$\mathbf{X}^{n+1} = \left[Q_1^{n+1}, H_1^{n+1}, \dots, Q_j^{n+1}, H_j^{n+1}, \Sigma ds_1^{n+1} \dots \Sigma us_j^{n+1}, C_{v1}^{n+1} \dots C_{vk}^{n+1} \right]^T. \quad (112)$$

The following discussion takes advantage of the fact that \mathbf{X}^{n+1} can be naturally partitioned in two parts, one part containing the flows and stages and a second containing the ice cover extents:

$$\begin{aligned} \mathbf{X}^{n+1} &= \left[Q_1^{n+1}, H_1^{n+1}, \dots, Q_j^{n+1}, H_j^{n+1}, \Sigma ds_1^{n+1} \dots \Sigma us_j^{n+1}, C_{v1}^{n+1} \dots C_{vk}^{n+1} \right]^T = \\ &\left[\bar{b}^{n+1} \mid \Sigma^{n+1} \mid \mathbf{C}^{n+1} \right]^T \end{aligned} \quad (113)$$

The sub-vector \bar{b}^{n+1} is identical to that of the previous section. The state vector at time n can be written in a similar manner:

$$\begin{aligned} \mathbf{X}^n &= \left[Q_1^n, H_1^n, \dots, Q_j^n, H_j^n, \Sigma ds_1^n \dots \Sigma us_j^n, C_{v1}^n \dots C_{vk}^n \right]^T = \\ &\left[\bar{b}^n \mid \Sigma^n \mid \mathbf{C}^n \right]^T \end{aligned} \quad (114)$$

The elements of \mathbf{X} are variables, and from this point forward they should be considered as *random variables* with an associated Gaussian probability distribution

function. The number of elements in \mathbf{X} is determined by the number of cross sections used in the simulation. There are separate elements representing the stage, the discharge, the downstream ice extent, the upstream ice extent, and the conveyance factors for each section. At the extreme upstream and downstream sections only one ice extent is required. These two sections have elements representing the stage and discharge but the upstream section has only a downstream ice extent and the downstream section only an upstream ice extent. Altogether there are $4n - 2$ elements in \mathbf{X} , where n is the total number of sections.

3.2.2 System model

The system model is the one derived above, but at this point, in keeping with the designation of the elements of the state vector as random variables, the concept of uncertainty is required to enter the derivation. It can be done in the following manner:

$$f(\bar{a}, \bar{b}^n, t, t + \Delta t, \bar{U}^{n+1}) = \mathbf{w}^n \quad (115)$$

where the equations represented by f have been described in section 2.2 above. The elements of \mathbf{w}^n describe the uncertainties associated with each equation in f . The uncertainties are assumed to be Gaussian white noise with a known variance, \mathbf{Q} . The non-diagonal elements of \mathbf{Q} are all zero, because the individual components of \mathbf{Q} are assumed to be uncorrelated. In principle the uncertainty can vary with time and position. Equation 115 is written in the most general form that allows for both. In a subsequent chapter the distribution of uncertainty along the channel is explored. Equation 115 is extended by additional equations describing ice extent at each time:

$$\begin{aligned} \sum ds_1^{n+1} - \sum ds_1^n &= w_1^n \\ \vdots & \\ \sum us_j^{n+1} - \sum us_j^n &= w_j^n \\ C_{vj+1}^{n+1} - C_{vj+1}^n &= w_{j+1}^n \\ \vdots & \\ C_{vk}^{n+1} - C_{vk}^n &= w_k^n \end{aligned} \quad (116)$$

The extent of the ice cover is assumed to be constant over the time interval of the calculation. In shorthand notation the entire set of equations expressed using eq 115 can be stated as

$$f_s \begin{bmatrix} f(\bar{a}, \bar{b}^n, t, t + \Delta t, \bar{U}^{n+1}) \\ \Sigma(\Sigma^{n+1}) \\ \mathbf{C}(C_v^{n+1}) \end{bmatrix} = f_s(\mathbf{X}^{n+1}, \mathbf{X}^n, \bar{U}^{n+1}) = \Gamma^n \mathbf{w}^n. \quad (117)$$

All the elements of \mathbf{X}^{n+1} , \mathbf{X}^n , and \mathbf{U}^{n+1} are random functions. $\hat{\mathbf{X}}^{n+1}$, $\hat{\mathbf{X}}^n$, and $\hat{\mathbf{U}}^{n+1}$ are the best estimates of \mathbf{X}^{n+1} , \mathbf{X}^n , and \mathbf{U}^{n+1} , defined by the expectation operator, E , as

$$\begin{aligned} \hat{\mathbf{X}}^{n+1} &= E\langle \mathbf{X}^{n+1} \rangle \\ \hat{\mathbf{X}}^n &= E\langle \mathbf{X}^n \rangle \\ \hat{\mathbf{U}}^n &= E\langle \mathbf{U}^n \rangle \end{aligned} \quad (118)$$

Γ^n in eq 117 is required to specify a system noise value for each equation. They are discussed further in Chapter 4. For now, it can be mentioned that, by its size and form, Γ^n allows any number of separate system noises to be specified. For example, each equation could have its own noise specified, in which case Γ^n would be the identity matrix. Similarly all the continuity equations could have one noise and all the momentum equations could have another, in which case Γ^n would be have j rows and two columns, with elements alternating ones and zeros. (Of course, the number of elements in the vector \mathbf{w}^{n+1} would have to change commensurately.) The system equation can be expanded in a Taylor's series as

$$\begin{aligned} f_s(\mathbf{X}^{n+1}, \mathbf{X}^n, \mathbf{U}^{n+1}) &= \Gamma^n \mathbf{w}^n = f_s(\hat{\mathbf{X}}^{n+1}, \hat{\mathbf{X}}^n, \hat{\mathbf{U}}^{n+1}) + \\ &(\mathbf{X}^{n+1} - \hat{\mathbf{X}}^{n+1}) \left. \frac{\partial f_s}{\partial \mathbf{X}} \right|_{\mathbf{X}=\hat{\mathbf{X}}^{n+1}} + \\ &(\mathbf{X}^n - \hat{\mathbf{X}}^n) \left. \frac{\partial f_s}{\partial \mathbf{X}} \right|_{\mathbf{X}=\hat{\mathbf{X}}^n} + (\mathbf{U}^{n+1} - \hat{\mathbf{U}}^{n+1}) \left. \frac{\partial f_s}{\partial \mathbf{U}} \right|_{\mathbf{U}=\hat{\mathbf{U}}^{n+1}} \end{aligned} \quad (119)$$

This equation can be restated as

$$\mathbf{X}^{n+1} = -\mathbf{F}^{-1} \mathbf{G} \mathbf{X}^n - \mathbf{F}^{-1} \mathbf{K} \mathbf{U}^{n+1} - \mathbf{F}^{-1} \mathbf{N}^n + -\mathbf{F}^{-1} \Gamma^n \mathbf{w}^n \quad (120)$$

where

$$\begin{aligned}
\mathbf{F} &= \left. \frac{\partial f_s}{\partial \mathbf{X}} \right|_{\mathbf{X}=\hat{\mathbf{X}}^{n+1}} \\
\mathbf{G} &= \left. \frac{\partial f_s}{\partial \mathbf{X}} \right|_{\mathbf{X}=\hat{\mathbf{X}}^n} \\
\mathbf{K} &= \left. \frac{\partial f_s}{\partial \mathbf{U}} \right|_{\mathbf{U}=\hat{\mathbf{U}}^{n+1}} \\
\mathbf{N}^n &= f_s(\hat{\mathbf{X}}^{n+1}, \hat{\mathbf{X}}^n, \hat{\mathbf{U}}^{n+1}) + \mathbf{F}\hat{\mathbf{X}}^{n+1} - \hat{\mathbf{X}}^n \left. \frac{\partial f_s}{\partial \mathbf{X}} \right|_{\mathbf{X}=\hat{\mathbf{X}}^n} - \hat{\mathbf{U}}^n \left. \frac{\partial f_s}{\partial \mathbf{U}} \right|_{\mathbf{U}=\hat{\mathbf{U}}^{n+1}}
\end{aligned} \tag{121}$$

\mathbf{N} is unaffected by the expectation operator. Equation 120 can be restated in state–space model form as

$$\mathbf{X}^{n+1} = \Phi^n \mathbf{X}^n + \Lambda^n \mathbf{U}^{n+1} + \mathbf{N}^n + \Gamma^n \mathbf{w}^n \tag{122}$$

where

$$\begin{aligned}
\Phi^n &= -\mathbf{F}^{-1}\mathbf{G} \\
\Lambda^n &= -\mathbf{F}^{-1}\mathbf{K} \\
\mathbf{N}^n &= -\mathbf{F}^{-1}\mathbf{N}^n \\
\Gamma^n &= -\mathbf{F}^{-1}\Gamma^n
\end{aligned} \tag{123}$$

The elements of the state vector are random elements with Gaussian probability distribution functions (pdf's). To completely describe a Gaussian pdf, two quantities are required: the mean or expected value of the distribution and the variance of the distribution. The best estimate or expected value of the state vector at time n is defined as $\hat{\mathbf{X}}^n$. $\hat{\mathbf{X}}^n = E\langle \mathbf{X}^n \rangle$ where E is the expectation operator. The evolution of the mean of the distribution can be found, to first-order accuracy, as

$$E\langle f_s(\mathbf{X}^{n+1}, \mathbf{X}^n, \bar{U}^{n+1}) \rangle = f_s(\hat{\mathbf{X}}^{n+1}, \hat{\mathbf{X}}^n, \hat{U}^{n+1}) = 0. \tag{124}$$

Solving the set of equations f_s for the unknown variables in $\hat{\mathbf{X}}^{n+1}$ provides an estimate of the mean of the pdf's of the random elements of \mathbf{X}^{n+1} . The equations included in f are solved using the Newton–Raphson procedure as described the previous chapter.

3.2.3 Error covariance propagation

The covariance of the state variables at time $n + 1$ is defined as

$$\mathbf{P}^{n+1} = E \left\langle \left[\mathbf{X}^{n+1} - E \langle \mathbf{X}^{n+1} \rangle \right] \left[\mathbf{X}^{n+1} - E \langle \mathbf{X}^{n+1} \rangle \right]^T \right\rangle. \quad (125)$$

Substituting the state equations for \mathbf{X}^{n+1} , the covariance becomes

$$\begin{aligned} \mathbf{P}^{n+1} = E \left\langle \left[\Phi^n \left[\mathbf{X}^n - E \langle \mathbf{X}^n \rangle \right] + \Lambda^n \left[\mathbf{U}^n - E \langle \mathbf{U}^n \rangle \right] + \Gamma^n \mathbf{w} \right] \right. \\ \left. \left[\Phi^n \left[\mathbf{X}^n - E \langle \mathbf{X}^n \rangle \right] + \Lambda^n \left[\mathbf{U}^n - E \langle \mathbf{U}^n \rangle \right] + \Gamma^n \mathbf{w} \right]^T \right\rangle \end{aligned} \quad (126)$$

Finally

$$\mathbf{P}^{n+1} = \Phi^n \mathbf{P}^n \Phi^{nT} + \Lambda^n \mathbf{P}_U \Lambda^{nT} + \Gamma^n \mathbf{Q} \Gamma^{nT} \quad (127)$$

where \mathbf{P}_U is the covariance matrix associated with the input vector \mathbf{U} . The model input is assumed to be corrupted by white noise with zero mean. It is necessary to estimate the variance of the pdf's of \mathbf{X}^{n+1} as they propagate in time. It is appropriate at this time to discuss the practical details of creating the Φ^n matrixes.

Λ^n and Γ^n are transition matrices that can be specified once and do not need to be computed. Λ^n is required to relate the imposed boundary conditions to the proper equations.

As shown above, Φ^n is the product of the \mathbf{F}^{-1} and \mathbf{G} matrixes. \mathbf{F} is the Jacobian matrix formed by the derivatives of f_s with respect to $\hat{\mathbf{X}}^{n+1}$, and \mathbf{G} is the Jacobian matrix formed by the derivatives of f_s with respect to $\hat{\mathbf{X}}^n$. \mathbf{F} can be represented as a partitioned matrix:

$$\mathbf{F} = \frac{\partial f_s}{\partial \mathbf{X}} \Big|_{\mathbf{X}=\hat{\mathbf{X}}^{n+1}} = \begin{bmatrix} \frac{\partial f}{\partial \mathbf{X}} \Big|_{\mathbf{X}=[\hat{b}^{n+1}|0|0]} & \frac{\partial f}{\partial \mathbf{X}} \Big|_{\mathbf{X}=[0|\hat{\Sigma}^{n+1}|0]} & \frac{\partial f}{\partial \mathbf{X}} \Big|_{\mathbf{X}=[0|0|\mathbf{C}^{n+1}]} \\ \frac{\partial \Sigma}{\partial \mathbf{X}} \Big|_{\mathbf{X}=[\hat{b}^{n+1}|0|0]} & \frac{\partial \Sigma}{\partial \mathbf{X}} \Big|_{\mathbf{X}=[0|\hat{\Sigma}^{n+1}|0]} & \frac{\partial \Sigma}{\partial \mathbf{X}} \Big|_{\mathbf{X}=[0|0|\mathbf{C}^{n+1}]} \\ \frac{\partial \mathbf{C}}{\partial \mathbf{X}} \Big|_{\mathbf{X}=[\hat{b}^{n+1}|0|0]} & \frac{\partial \mathbf{C}}{\partial \mathbf{X}} \Big|_{\mathbf{X}=[0|\hat{\Sigma}^{n+1}|0]} & \frac{\partial \mathbf{C}}{\partial \mathbf{X}} \Big|_{\mathbf{X}=[0|0|\mathbf{C}^{n+1}]} \end{bmatrix} \quad (128)$$

The advantage of expanding \mathbf{F} in this manner is that the computation required to invert \mathbf{F} is greatly reduced, as is shown next. The first term (the partition in the upper left corner) can be expanded as

$$\begin{aligned} \frac{\partial f}{\partial \mathbf{X}} \Big|_{\mathbf{X}=\left[\hat{b}^{n+1}|0|0\right]} &= \left[\frac{\partial \hat{a}}{\partial \mathbf{X}} \Big|_{\mathbf{X}=\left[\hat{b}^{n+1}|0|0\right]} \right] \left[\frac{\partial f}{\partial \hat{a}} \Big|_{\hat{a}=\left[\hat{a}\right]} \right] = \\ [\mathbf{I}] \left[\frac{\partial f}{\partial \hat{a}} \Big|_{\hat{a}=\left[\hat{a}\right]} \right] &= \mathbf{F}_a \end{aligned} \quad (129)$$

which is the same matrix that was determined during the solution of the hydraulic model as described above. The following matrixes can be readily resolved:

$$\begin{aligned} \frac{\partial \Sigma}{\partial \mathbf{X}} \Big|_{\mathbf{X}=\left[\hat{b}^{n+1}|0|0\right]} &= [0] \\ \frac{\partial \mathbf{C}}{\partial \mathbf{X}} \Big|_{\mathbf{X}=\left[\hat{b}^{n+1}|0|0\right]} &= [0] \\ \frac{\partial \mathbf{C}}{\partial \mathbf{X}} \Big|_{\mathbf{X}=\left[0|\hat{\Sigma}^{n+1}|0\right]} &= [0] \\ \frac{\partial \Sigma}{\partial \mathbf{X}} \Big|_{\mathbf{X}=\left[0|0|\mathbf{C}^{n+1}\right]} &= [0] \end{aligned} \quad (130)$$

and are all the null matrix (all the elements are zero). The upper partition on the right side of the matrix contains the derivatives of the continuity and momentum equations. These derivatives must be estimated. The lower partitions on the right are the identity matrix:

$$\begin{aligned} \frac{\partial \Sigma}{\partial \mathbf{X}} \Big|_{\mathbf{X}=\left[0|\hat{\Sigma}^{n+1}|0\right]} &= [\mathbf{I}] \\ \frac{\partial \mathbf{C}}{\partial \mathbf{X}} \Big|_{\mathbf{X}=\left[0|0|\mathbf{C}^{n+1}\right]} &= [\mathbf{I}] \end{aligned} \quad (131)$$

Now \mathbf{F} can be written as a partition matrix in the form

$$\mathbf{F} = \begin{bmatrix} \mathbf{F}_a & \left. \frac{\partial f}{\partial \mathbf{X}} \right|_{\mathbf{x}=[0|\Sigma^{n+1}|0]} & \left. \frac{\partial f}{\partial \mathbf{X}} \right|_{\mathbf{x}=[0|0|\mathbf{C}^{n+1}]} \\ 0 & \mathbf{I} & 0 \\ 0 & 0 & \mathbf{I} \end{bmatrix} \quad (132)$$

where \mathbf{I} is the identity matrix. One advantage of this approach is that \mathbf{F}_a is found as a step in the state estimate propagation and does not need to be recalculated. Recall also that \mathbf{F}_a was inverted as a step in the solution of the hydraulic model. As a result, \mathbf{F}_a^{-1} is known and \mathbf{F}^{-1} can be calculated as

$$\mathbf{F}^{-1} = \left[\begin{array}{c|c} \mathbf{F}_a^{-1} & -\mathbf{F}_a^{-1} \left(\left. \frac{\partial f}{\partial \mathbf{X}} \right|_{\mathbf{x}=[0|\Sigma^{n+1}|0]} \quad \left. \frac{\partial f}{\partial \mathbf{X}} \right|_{\mathbf{x}=[0|0|\mathbf{C}^{n+1}]} \right) \\ \hline 0 & \mathbf{I} \end{array} \right]. \quad (133)$$

Next the matrix \mathbf{G} is

$$\mathbf{G} = \left. \frac{\partial fs}{\partial \mathbf{X}} \right|_{\mathbf{x}=\hat{\mathbf{x}}^n} = \begin{bmatrix} \left. \frac{\partial f}{\partial \mathbf{X}} \right|_{\mathbf{x}=[\hat{b}^n|0|0]} & \left. \frac{\partial f}{\partial \mathbf{X}} \right|_{\mathbf{x}=[0|\Sigma^n|0]} & \left. \frac{\partial f}{\partial \mathbf{X}} \right|_{\mathbf{x}=[0|0|\mathbf{C}^n]} \\ \left. \frac{\partial \Sigma}{\partial \mathbf{X}} \right|_{\mathbf{x}=[\hat{b}^n|0|0]} & \left. \frac{\partial \Sigma}{\partial \mathbf{X}} \right|_{\mathbf{x}=[0|\Sigma^n|0]} & \left. \frac{\partial \Sigma}{\partial \mathbf{X}} \right|_{\mathbf{x}=[0|0|\mathbf{C}^n]} \\ \left. \frac{\partial \mathbf{C}}{\partial \mathbf{X}} \right|_{\mathbf{x}=[\hat{b}^n|0|0]} & \left. \frac{\partial \mathbf{C}}{\partial \mathbf{X}} \right|_{\mathbf{x}=[0|\Sigma^n|0]} & \left. \frac{\partial \mathbf{C}}{\partial \mathbf{X}} \right|_{\mathbf{x}=[0|0|\mathbf{C}^n]} \end{bmatrix} \quad (134)$$

where

$$\left. \frac{\partial \Sigma}{\partial \mathbf{X}} \right|_{\bar{\mathbf{x}} = [\hat{b}^n | 0 | 0]} = [0] \quad (135)$$

$$\left. \frac{\partial \mathbf{C}}{\partial \mathbf{X}} \right|_{\bar{\mathbf{x}} = [\hat{b}^n | 0 | 0]} = [0]$$

$$\left. \frac{\partial \mathbf{C}}{\partial \mathbf{X}} \right|_{\bar{\mathbf{x}} = [0 | \hat{\Sigma}^n | 0]} = [0]$$

$$\left. \frac{\partial \Sigma}{\partial \mathbf{X}} \right|_{\bar{\mathbf{x}} = [0 | 0 | \mathbf{C}^n]} = [0]$$

$$\left. \frac{\partial \Sigma}{\partial \mathbf{X}} \right|_{\mathbf{x} = [0 | \hat{\Sigma}^n | 0]} = [-\mathbf{I}] \quad (136)$$

$$\left. \frac{\partial \mathbf{C}}{\partial \mathbf{X}} \right|_{\mathbf{x} = [0 | 0 | \mathbf{C}^n]} = [-\mathbf{I}]$$

and $-\mathbf{I}$ is the negative identity matrix. Therefore, Φ , the product of the \mathbf{F}^{-1} and \mathbf{G} matrices, is

$$\Phi^n = \begin{bmatrix} \mathbf{F}_a^{-1} \left. \frac{\partial f}{\partial \mathbf{X}} \right|_{\mathbf{x} = [\hat{b}^n | 0 | 0]} & \mathbf{F}_a^{-1} [G] \\ 0 & -\mathbf{I} \end{bmatrix} \quad (137)$$

where

$$G = \left. \frac{\partial f}{\partial \mathbf{X}} \right|_{\mathbf{x} = [0 | \hat{\Sigma}^{n+1} | 0]} \left. \frac{\partial f}{\partial \mathbf{X}} \right|_{\mathbf{x} = [0 | 0 | \mathbf{C}^{n+1}]} + \left. \frac{\partial f}{\partial \mathbf{X}} \right|_{\mathbf{x} = [0 | \hat{\Sigma}^n | 0]} \left. \frac{\partial f}{\partial \mathbf{X}} \right|_{\mathbf{x} = [0 | 0 | \mathbf{C}^n]} \quad (138)$$

3.2.4 Observation equation

The relationship between the observations and the state variables can be expressed as

$$\mathbf{z}^{n+1} = \mathbf{H}^{n+1} \mathbf{X}^{n+1} + \mathbf{v}^{n+1} \quad (139)$$

where \mathbf{z}^{n+1} contains the observations made at time n , \mathbf{H}^{n+1} is the observation matrix that relates the observations to the state variables, and v is the measurement noise vector. It is assumed that $E[v] = 0$ and that $\text{cov}[v_j, v_k] = E[v_j v_k^T] = \mathbf{R}_n \delta_{ij}$, where δ_{ij} is the Kronecker operator. The types and frequencies of observations that are available for the case considered in this study (the Missouri River downstream of Oahe Dam) are discussed in Chapter 4. Typically there are several observations of stage and an observation of the ice cover extent. The observation of the leading edge of the ice cover must be converted into observations of the upstream and downstream ice extent at each section. This produces $2n - 2$ ice observations. Let J be the number of stage observations. \mathbf{z} is then a vector $J + 2n - 2$ elements in length. The matrix \mathbf{H} is $J + 2n - 2$ by $4n - 2$ in size and is composed of elements that are either ones or zeros.

3.2.5 Updating procedure

There are two means of estimating the state variables: through the solution of the system equation or through observation. The Kalman gain is the procedure by which these two methods of estimation are reconciled. Let $\hat{\mathbf{X}}^{n+1}(-)$ be the *a priori* (prior to the observation) system estimate and $\mathbf{P}^{n+1}(-)$ be the *a priori* covariance estimate. Following the discussion of Grewal and Andrews (1993) an updated estimate $\hat{\mathbf{X}}^{n+1}(+)$ is sought that is a linear function of the *a priori* estimate, $\hat{\mathbf{X}}^{n+1}(-)$, and the observation, \mathbf{z}^{n+1} . In the present case the Kalman gain, \mathbf{K}^{n+1} , is

$$\mathbf{K}^{n+1} = \mathbf{P}^{n+1}(-) \mathbf{H}^T [\mathbf{H} \mathbf{P}^{n+1}(-) \mathbf{H}^T + \mathbf{R}]^{-1}. \quad (140)$$

The system estimate update and covariance update are

$$\hat{\mathbf{X}}^{n+1}(+) = \hat{\mathbf{X}}^{n+1}(-) + \mathbf{K}^{n+1} [\mathbf{z}^{n+1} - \mathbf{H}^{n+1} \hat{\mathbf{X}}^{n+1}(-)] \quad (141)$$

$$\mathbf{P}^{n+1}(+) = [\mathbf{I} - \mathbf{K}^{n+1} \mathbf{H}^{n+1}] \mathbf{P}^{n+1}(-). \quad (142)$$

3.3 Thermal and transport state-space model

3.3.1 State variables

The state vector of the thermal and ice transport state-space model at time $n + 1$, \mathbf{T}^{n+1} , contains the water temperature, the longitudinal temperature deriva-

tive, the surface ice concentration, the longitudinal surface ice concentration derivative, the suspended frazil ice concentration, and the longitudinal frazil ice concentration derivative for each cross section used in the simulation:

$$\mathbf{T}^{n+1} = \begin{bmatrix} T_1^{n+1}, TX_1^{n+1}, C_{a1}^{n+1}, CX_{a1}^{n+1}, C_{f1}^{n+1}, CX_{f1}^{n+1} \dots T_j^{n+1}, \\ TX_j^{n+1}, C_{aj}^{n+1}, CX_{aj}^{n+1}, C_{fj}^{n+1}, CX_{fj}^{n+1} \end{bmatrix}^T \quad (143)$$

The state vector at time n is formed similarly:

$$\mathbf{T}^n = \begin{bmatrix} T_1^n, TX_1^n, C_{a1}^n, CX_{a1}^n, C_{f1}^n, CX_{f1}^n \dots \\ T_j^n, TX_j^n, C_{aj}^n, CX_{aj}^n, C_{fj}^n, CX_{fj}^n \end{bmatrix}^T \quad (144)$$

The elements of \mathbf{T} are variables, and from this point forward they are considered as random variables with associated Gaussian probability distribution functions.

3.3.2 System model

The system model is based on the equations presented in the previous chapter as part of the development of the thermal and ice transport model. There are six equations for each cross section included in the simulation. The equations are repeated here for convenience of referral:

$$\begin{aligned} \frac{1}{\Delta t} (T_i^{n+1} - T_\xi) &= \frac{\theta B_i^{n+1}}{\rho C_p A_i^{n+1}} (1 - \Omega_i) h_{wa} (T_a - T_i^{n+1}) (1 - C_{ai}^{n+1}) \\ &+ \frac{(1 - \theta) B_\xi^{n+1}}{\rho C_p A_\xi^{n+1}} (1 - \Omega_\xi) h_{wa} (T_a - T_\xi^n) (1 - C_{a\xi}^n) + \\ &\frac{\rho_i L_i}{\rho_i C_p} Y_f \left[\theta C_{vi}^{n+1} (T_m - T_i^{n+1}) + (1 - \theta) C_{v\xi}^n (T_m - T_\xi^n) \right] + \\ &\frac{\theta B_i^{n+1}}{\rho C_p A_i^{n+1}} \Omega_i h_{wi} (T_m - T_i^{n+1})_i + \frac{(1 - \theta) B_\xi^{n+1}}{\rho C_p A_\xi^{n+1}} \Omega_\xi h_{wi} (T_m - T_\xi^n) \end{aligned} \quad (145)$$

$$\begin{aligned}
TX_i^{n+1} = & \\
& (d_1 T_{i-1}^n + d_2 T_i^n + d_3 TX_{i-1}^n + d_4 TX_i^n + d_5 T_{i-1}^{n+1} + d_6 TX_{i-1}^{n+1}) \\
& \left(\frac{1 - \frac{\Delta t}{2} \frac{du}{dx}}{1 + \frac{\Delta t}{2} \frac{du}{dx}} \right)
\end{aligned} \tag{146}$$

$$\begin{aligned}
\frac{1}{\Delta t} (C_{ai}^{n+1} - C_{a\xi}) = & \theta (1 - \Omega_i) \frac{\Theta V_b C_{fi}^{n+1}}{(h_{ii}^{n+1} + (1 - e_f) h_{fi}^{n+1})} (1 - C_{ai}^{n+1}) \\
& + (1 - \theta) (1 - \Omega_i) \frac{\Theta V_b C_{f\xi}^n}{(h_{i\xi}^n + (1 - e_f) h_{f\xi}^n)} (1 - C_{a\xi}^n)
\end{aligned} \tag{147}$$

$$\begin{aligned}
CX_{ai}^{n+1} = & \\
& (d_1 C_{ai-1}^n + d_2 C_{ai}^n + d_3 CX_{ai-1}^n + d_4 CX_{ai}^n + d_5 C_{ai-1}^{n+1} + d_6 CX_{ai-1}^{n+1}) \\
& \left(\frac{1 - \frac{\Delta t}{2} \frac{du}{dx}}{1 + \frac{\Delta t}{2} \frac{du}{dx}} \right)
\end{aligned} \tag{148}$$

$$\begin{aligned}
\frac{1}{\Delta t} (C_{fi}^{n+1} - C_{f\xi}) = & \theta Y_f (T_m - T_i^{n+1}) + (1 - \theta) Y_f (T_m - T_\xi^n) + \\
& \theta \frac{\Theta V_b C_{fi}^{n+1} B_i^{n+1}}{A_i^{n+1}} + (1 - \theta) \frac{\Theta V_b C_{f\xi}^n B_\xi^n}{A_\xi^n} \\
& + S [\theta (1 - \Omega_i) + (1 - \theta) (1 - \Omega_\xi)]
\end{aligned} \tag{149}$$

$$\begin{aligned}
CX_{fi}^{n+1} = & \\
& \left(d_1 C_{fi-1}^n + d_2 C_{fi}^n + d_3 CX_{fi-1}^n + d_4 CX_{fi}^n + d_5 C_{fi-1}^{n+1} + d_6 CX_{fi-1}^{n+1} \right) \\
& \left(\frac{1 - \frac{\Delta t}{2} \frac{du}{dx}}{1 + \frac{\Delta t}{2} \frac{du}{dx}} \right)
\end{aligned} \tag{150}$$

In addition to the six equations at each section, there are three auxiliary equations describing the values of the water temperature, surface ice concentration, and frazil ice concentration at the foot of the characteristic:

$$T_\xi = c_1 T_{i-1}^n + c_2 T_i^n + c_3 TX_{i-1}^n + c_4 TX_i^n + c_5 T_{i-1}^{n+1} + c_6 TX_{i-1}^{n+1} \tag{151}$$

$$C_{a\xi} = c_1 C_{ai-1}^n + c_2 C_{ai}^n + c_3 CX_{ai-1}^n + c_4 CX_{ai}^n + c_5 C_{ai-1}^{n+1} + c_6 CX_{ai-1}^{n+1} \tag{152}$$

$$C_{f\xi} = c_1 C_{fi-1}^n + c_2 C_{fi}^n + c_3 CX_{fi-1}^n + c_4 CX_{fi}^n + c_5 C_{fi-1}^{n+1} + c_6 CX_{fi-1}^{n+1} . \tag{153}$$

The above system of equations can be represented compactly in the form

$$f_T \left(\mathbf{T}^{n+1}, \mathbf{T}^n, \mathbf{U}_T^{n+1} \right) = \mathbf{w}^n . \tag{154}$$

The elements of \mathbf{w} describe the uncertainties associated with each equation in f_T . The uncertainties are assumed to be Gaussian white noise with a known variance. The distribution in space and time and the relative magnitudes of the uncertainties are explored in the next chapter. All the elements of \mathbf{T}^{n+1} , \mathbf{T}^n , and \mathbf{U}_T^{n+1} are random functions. $\hat{\mathbf{T}}^{n+1}$, $\hat{\mathbf{T}}^n$, and $\hat{\mathbf{U}}_T^{n+1}$ are the best estimates of \mathbf{T}^{n+1} , \mathbf{T}^n , and \mathbf{U}_T^{n+1} , defined by the expectation operator, E , as

$$\begin{aligned}
\hat{\mathbf{T}}^{n+1} &= E \left\langle \mathbf{T}^{n+1} \right\rangle \\
\hat{\mathbf{T}}^n &= E \left\langle \mathbf{T}^n \right\rangle \\
\hat{\mathbf{U}}_T^n &= E \left\langle \mathbf{U}_T^n \right\rangle
\end{aligned} \tag{155}$$

The system equation can be expanded in a Taylor's series, using the best estimates, as

$$\begin{aligned}
 f_s(\mathbf{T}^{n+1}, \mathbf{T}^n, \mathbf{U}_T^{n+1}) = [\mathbf{w}] = f_s(\hat{\mathbf{T}}^{n+1}, \hat{\mathbf{T}}^n, \hat{\mathbf{U}}_T^{n+1}) + \\
 (\mathbf{T}^{n+1} - \hat{\mathbf{T}}^{n+1}) \left. \frac{\partial f_s}{\partial \mathbf{T}} \right|_{\mathbf{T}=\hat{\mathbf{T}}^{n+1}} + \\
 (\mathbf{T}^n - \hat{\mathbf{T}}^n) \left. \frac{\partial f_s}{\partial \mathbf{T}} \right|_{\mathbf{T}=\hat{\mathbf{T}}^n} + (\mathbf{U}_T^{n+1} - \hat{\mathbf{U}}_T^{n+1}) \left. \frac{\partial f_s}{\partial \mathbf{U}_T} \right|_{\mathbf{U}_T=\hat{\mathbf{U}}_T^{n+1}}
 \end{aligned} \tag{156}$$

This equation can be restated compactly as

$$\mathbf{T}^{n+1} = -\mathbf{F}_T^{-1} \mathbf{G}_T \mathbf{T}^n - \mathbf{F}_T^{-1} \mathbf{K}_T \mathbf{U}_T^{n+1} - \mathbf{F}_T^{-1} \mathbf{N}_T^n + -\mathbf{F}_T^{-1} \mathbf{w}_T^{n+1} \tag{157}$$

where

$$\begin{aligned}
 \mathbf{F}_T &= \left. \frac{\partial f_s}{\partial \mathbf{T}} \right|_{\mathbf{T}=\hat{\mathbf{T}}^{n+1}} \\
 \mathbf{G}_T &= \left. \frac{\partial f_s}{\partial \mathbf{T}} \right|_{\mathbf{T}=\hat{\mathbf{T}}^n} \\
 \mathbf{K}_T &= \left. \frac{\partial f_s}{\partial \mathbf{U}_T} \right|_{\mathbf{U}_T=\hat{\mathbf{U}}_T^{n+1}} \\
 \mathbf{N}_T^n &= f_s(\hat{\mathbf{T}}^{n+1}, \hat{\mathbf{T}}^n, \mathbf{U}_T^{n+1}) + \mathbf{F}_T \hat{\mathbf{T}}^{n+1} - \hat{\mathbf{T}}^n \left. \frac{\partial f_s}{\partial \mathbf{T}} \right|_{\mathbf{T}=\hat{\mathbf{T}}^n} - \\
 &\quad \hat{\mathbf{U}}_T^n \left. \frac{\partial f_s}{\partial \mathbf{U}_T} \right|_{\mathbf{U}_T=\hat{\mathbf{U}}_T^{n+1}}
 \end{aligned} \tag{158}$$

\mathbf{N}_T is unaffected by the expectation operator. This equation can be restated in state-space model form as

$$\mathbf{T}^{n+1} = \Phi_T^n \mathbf{T}^n + \Lambda_T^n \mathbf{U}_T^{n+1} + \mathbf{N}_T^n + \Gamma_T^n \mathbf{w}^n \tag{159}$$

where

$$\begin{aligned}
\Phi_T^n &= -\mathbf{F}_T^{-1} \mathbf{G}_T \\
\Lambda_T^n &= -\mathbf{F}_T^{-1} \mathbf{K}_T \\
\mathbf{N}_T^n &= -\mathbf{F}_T^{-1} \mathbf{N}_T^n
\end{aligned} \tag{160}$$

3.3.3 Covariance propagation

The covariance propagation can be described as being analogous to that undertaken in the previous section. The error covariance is

$$\mathbf{P}_T^{n+1} = \Phi_T^n \mathbf{P}_T^n \Phi_T^{nT} + \Lambda_T^n \mathbf{P}_{U_T}^n \Lambda_T^{nT} + \mathbf{Q}_T. \tag{161}$$

3.3.4 Observation equation

The relationship between the observations and the state variables can be expressed as

$$\mathbf{z}_T^{n+1} = \mathbf{H}_T^{n+1} \mathbf{T}_T^{n+1} + v_T^{n+1} \tag{162}$$

where \mathbf{z}^{n+1} contains the observations made at time n , \mathbf{H}^{n+1} is the observation matrix that relates the observations to the state variables, and v is the measurement noise vector. It is assumed that $E[v] = 0$ and that $\text{cov}[v_j, v_k] = E[v_j v_k^T] = \mathbf{R}_n \delta_{ij}$, where δ_{ij} is the Kronecker operator. The types and frequencies of observations that are available for the case considered in this study (the Missouri River downstream of Oahe Dam) are discussed in Chapter 4. Unfortunately there were no observations of water temperature that could be used for the present study, nor were there any of the transported ice quantities or the ice cover thickness.

3.3.5 Updating procedure

As described earlier, the Kalman gain is found as

$$\mathbf{K}_T^n = \mathbf{P}_T^n(-) \mathbf{H}_T^{nT} \left[\mathbf{H}_T^n \mathbf{P}_T^n(-) \mathbf{H}_T^{nT} + \mathbf{R}_T \right]^{-1} \tag{163}$$

and the system estimate update and the covariance update are, respectively,

$$\hat{\mathbf{T}}(+)=\hat{\mathbf{T}}(-)+\mathbf{K}_T^n\left[\mathbf{z}_T^n-\mathbf{H}_T^n\hat{\mathbf{T}}(-)\right] \tag{164}$$

and

$$\mathbf{P}_T^n(+)=\left[\mathbf{I}-\mathbf{K}_T^n\mathbf{H}_T^n\right]\mathbf{P}_T^n(-). \tag{165}$$

4 APPLICATION TO THE MISSOURI RIVER BELOW OAHE DAM, SOUTH DAKOTA

4.1 Introduction

The Missouri River is a major river in North America. Its watershed encompasses portions of at least 12 states, and it reaches into Canada. There are six reservoirs on the Missouri that serve a variety of uses: flood control, irrigation, hydropower production, and recreation. Oahe Dam is located on the Missouri River at Pierre, South Dakota, and forms Oahe Reservoir (Fig. 1). The flows in the Missouri River downstream of Oahe Dam are completely controlled by Oahe Dam, with the exception of the Bad River and other smaller tributaries. The overall movement of water from Oahe Dam is a function of the flow conditions of the reservoir system along the Missouri River.

The Corps of Engineers' Reservoir Control Center (RCC) in Omaha, Nebraska, schedules daily releases that must take into account the multipurpose uses of the reservoir system. Within this framework the hourly releases out of Oahe Dam are usually determined by the requirements for hydroelectric power production as determined by the Western Area Power Administration (WAPA). Consequently the flows in the Missouri River can change on an hourly basis. In fact, the flow out of Oahe Dam is rarely constant over a 24-hour period. It can change from a minimum of 0 cfs to a maximum of about 55,000 cfs. As described in Chapter 1, the presence of river ice decreases the hydraulic conveyance of the Missouri River and causes the stage in the river to rise. If the river ice cover has advanced into the Pierre area, the increased stages can potentially cause flooding at Pierre and Fort Pierre. The RCC reduces Oahe releases as river stages approach alert levels at any of the four gages downstream of Oahe Dam. The ability to forecast ice cover extent and river stages is potentially a valuable tool for the operators of the dam.

In this chapter the reach of the Missouri River downstream of Oahe Dam is simulated using the state-space model derived in the previous chapters. The goal is to employ the state-space model to forecast river stages when ice is present. The several steps required to reach this goal are described here. First, the steps necessary to apply the deterministic river ice model derived in Chapter 2 are described. It is shown that the deterministic model can simulate the flows when ice is not present with quite good results. Simulation of the flows and the river ice conditions for three winters in which river ice played a major role are then presented. The results, although encouraging, highlight the difficulties in modeling river ice for a reach of highly varying flow. The possible causes of the inaccuracies are discussed. Next, to apply the state-space model the Kalman filter parameters are estimated through numerical experiment. The three winter seasons

are subsequently simulated (or hindcast) using the available stage and ice cover observations to update the state-space model. The problems incurred with missing and bad data are discussed. A particular severe problem for this reach of the Missouri River, though a common problem for most rivers, is the huge number of stage observations compared to the number of ice observations. A procedure for dealing with this imbalance is suggested. Finally, the state-space model is used to provide simulated forecasts during two winter periods. The results are then compared to those obtained from the deterministic model.

4.2 Application of the river ice model

There are ample data available for the Oahe Dam reach of the Missouri River (Table 1); the Pierre, LaFramboise, and Farm Island gages have collected data since the mid-1980s. Stages are typically measured once an hour by automatic gages that transmit the data via geostationary satellites every four hours. The information from these gages is available in computerized form as indicated by the notation DSS in the table. As shown later in this study, on occasion, each of these gages can go off-line due to freezing in the winter, mechanical failure, or a problem with the data stream. In the 1990s, computerized information became available at the Oahe Dam tailwater and at the Big Bend Dam reservoir. Big Bend Dam is located approximately 90 miles downstream of Oahe Dam.

In addition to flow stage, there is also information available on water temperature, air temperature, and ice cover extent downstream of Oahe Dam. Air temperature data are available as daily maximums and minimums at Oahe Dam. In addition, some hourly air temperature information is collected at the Pierre gage, although these data have large gaps. The water temperature data are especially weak, as only one measurement per day is available for the water temperature outflow of Oahe Dam. The water temperature measurements at the Pierre gage are of very low quality, especially after about 1990.

The information available on ice cover formation is generally in the form of observer reports. It is summarized elsewhere (Corps of Engineers 1995). Observations of the leading edge of the ice cover are made from the river's banks or from small planes. The scheduling of the ice observations depends on the constraints of weather, road conditions, and manpower availability. Typically the observations are made only when the leading edge of the ice cover approaches Pierre and are made once, or at most twice, a day. Often there are a number of days with no observations. It is interesting to note that there has never been a single direct measurement of the ice thickness in the Missouri River near Pierre. The rapidly changing and dangerous ice conditions in the river have prevented such measurements.

Table 1. Data sources available for the Missouri River downstream of Oahe Dam.				
Data	Time interval	Form	Period of record	
			Start	End
Flow				
Oahe Dam release	1 day	DSS*	1958	1 July 94
	1 hour	DSS	1984	Present
	1 hour	Paper	1968	1984
Water temperature				
Oahe Dam release	1 day	Paper and DSS	1968	Present
	1 hour	HP data logger	1987	1989
	Irregular	Fluke thermistor	1986	1986
Missouri River at Pierre gage	1 hour	DCP**	1988	Present
	Irregular	Fluke thermistor	1986	1986
Air temperature				
Oahe Dam daily maximum	1 day	CD-ROM	1962	Present
Oahe Dam daily minimum	1 day	CD-ROM	1962	Present
Stages				
Big Bend Dam	1 day	DSS	1963	Present
Farm Island gage	1 hour	DSS	1985	Present
LaFramboise gage	1 hour	DSS	1985	Present
Pierre gage	1 hour	DSS	1982	Present
Oahe tailwater	1 hour	DSS	1994	Present
River ice cover				
	Irregular	Observations	1988	Present

*DSS: Data Storage System—a computerized database developed by the Corps of Engineers.

**DCP: Data Collection Platform—a device for collecting and transmitting data using geostationary satellites.

Information was available describing the geometry of the channel at a number of cross sections. The Corps of Engineers (1995) describes this information in detail. A summary of the geometric data is given in Table 2. The cross-sectional areas and top widths cited in the table were determined for a steady flow of 20,000 cfs. Examination of the table indicates that the channel top width and cross-sectional area increase in the downstream direction. Big Bend Dam controls the stage at the downstream end of the channel; the reservoir created by that dam is responsible for the large top widths and cross-sectional areas.

Table 2. Summary of geometric data for the Missouri River.

River mile	Min. channel elev. (ft)	Cross-sect area (ft ²)	Top width (ft)
1,071.92	1,403.50	15,900.37	772.86
1,071.39	1,403.50	15,897.92	772.85
1,070.97	1,406.20	18,902.27	1,061.49
1,070.46	1,408.80	25,170.54	1,552.22
1,070.14	1,408.60	20,487.88	1,452.00
1,069.7	1,411.00	25,159.09	2,050.53
1,069.30	1,411.10	28,440.05	2,219.08
1,068.87	1,412.30	20,887.21	1,627.00
1,068.41	1,409.90	18,780.97	1,248.87
1,068.09	1,408.40	20,283.44	1,436.50
1,067.63	1,409.50	28,482.31	2,177.13
1,067.34	1,408.30	30,161.29	2,423.68
1,066.84	1,406.70	27,866.77	2,167.73
1,066.52	1,400.30	26,093.57	1,630.35
1,066.50	1,400.30	25,883.46	1,629.61
1,066.32	1,400.30	25,614.98	1,628.66
1,066.29	1,400.30	25,402.32	1,627.91
1,065.97	1,399.20	22,470.73	1,794.08
1,065.54	1,399.20	21,928.05	1,791.15
1,065.11	1,405.60	16,152.22	1,498.25
1,064.82	1,405.00	16,836.53	1,397.61
1,064.27	1,404.90	18,020.16	1,562.91
1,063.52	1,399.20	16,827.29	1,450.18
1,062.78	1,402.80	20,154.77	2,035.91
1,061.69	1,403.10	21,423.64	2,186.29
1,060.58	1,399.60	21,405.55	2,041.65
1,059.49	1,406.70	23,776.54	2,280.49
1,058.62	1,405.30	24,057.19	2,232.24
1,057.64	1,397.70	25,250.77	2,827.00
1,056.36	1,408.00	35,360.91	4,695.00
1,055.31	1,405.70	42,634.86	5,967.96
1,053.02	1,410.60	41,353.67	5,406.90
1,051.37	1,405.00	41,563.24	4,885.27
1,049.30	1,409.70	41,606.06	4,659.24
1,046.52	1,402.20	36,549.80	3,203.48
1,043.86	1,403.90	49,671.56	5,038.47
1,040.94	1,402.20	54,396.74	5,386.30
1,037.30	1,396.70	55,109.22	4,366.97
1,033.30	1,391.00	89,550.06	4,216.43
1,025.32	1,375.00	150,551.83	4,687.01
1,018.73	1,366.80	176,144.78	4,912.13
1,014.86	1,357.30	218,995.92	8,431.96
1,010.60	1,361.40	197,997.52	7,328.58
1,005.90	1,359.00	348,054.94	11,543.77
1,000.50	1,349.80	227,341.95	5,792.19
996.60	1,342.80	287,998.22	7,361.57
995.26	1,344.40	466,425.94	9,320.00
993.78	1,343.40	503,528.50	11,675.34
992.31	1,344.70	388,249.91	10,248.16
990.92	1,344.00	488,879.91	10,295.34
989.74	1,346.90	383,738.41	6,837.44
988.62	1,344.50	324,166.63	5,946.20

The geometry data describing each cross section were available in a form suitable for the program HEC-2 (Corps of Engineers 1990). The channel geometry includes a description of each river cross section, the channel roughness as characterized using the Manning's roughness coefficient, the spacing between cross sections, and other pertinent information. A pre-processor program (Corps of Engineers 1997) analyzed each cross section to produce a look-up table of the geometric properties as a function of water surface elevations. Typically, 12 water surface elevations, spaced at 2-ft intervals were used to generate the look-up table. The information in the table includes the channel area, conveyance (eq 8), top width, and wetted perimeter. The calibration process entailed adjusting the Manning's roughness coefficient until the model reproduced the observed stages along the channel to within a predetermined tolerance.

The hydraulic component of the model was calibrated to match the record of observed open-water peak stages during the period of 1–30 June 1998 by adjusting the channel Manning's roughness coefficient. Figure 3 displays the outflow from Oahe Dam during this period. The flow was highly unsteady, and the outlet discharge was zero during some period in almost each day of the simulation period. Figure 4 compares observed and simulated stage hydrographs at the Oahe Dam tailwater, Pierre, La Framboise Island, and Farm Island gages. Table 3a lists

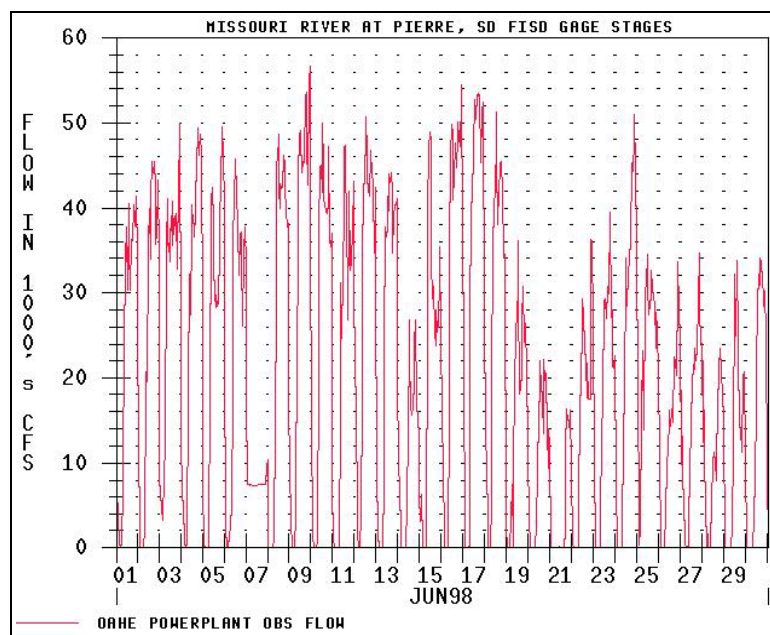
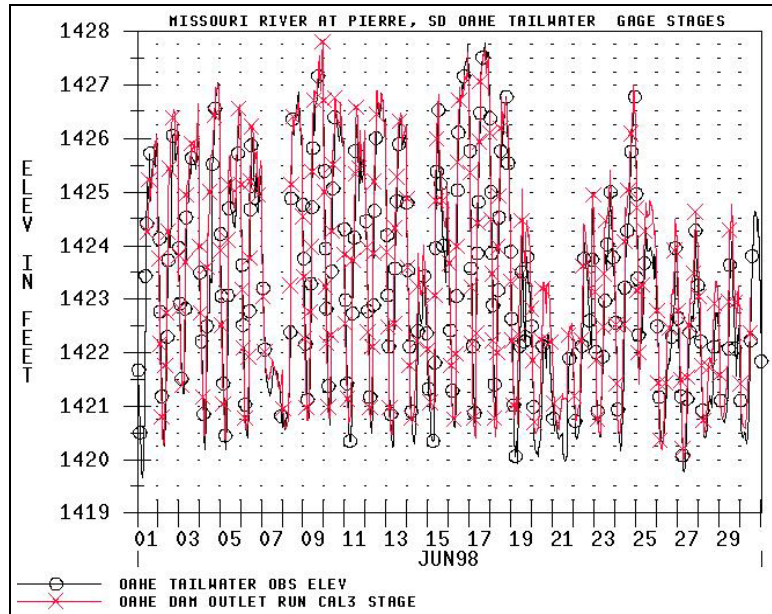
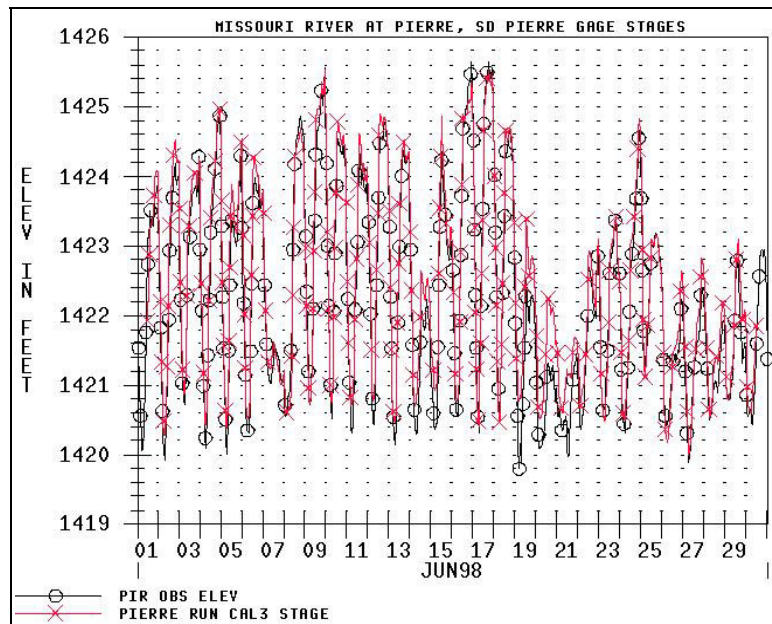


Figure 3. Recorded outflows out of Oahe Dam during June 1998 in thousands of cfs.

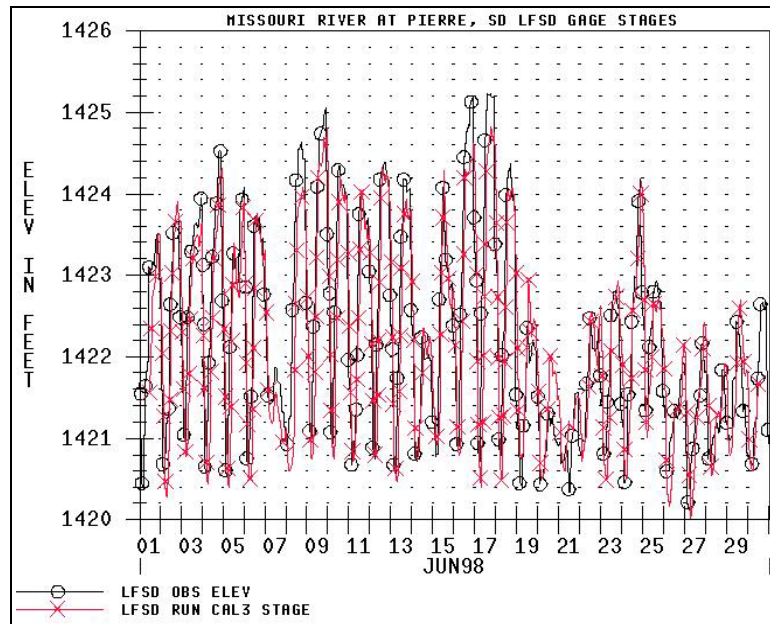


a. Oahe tailwater gage.

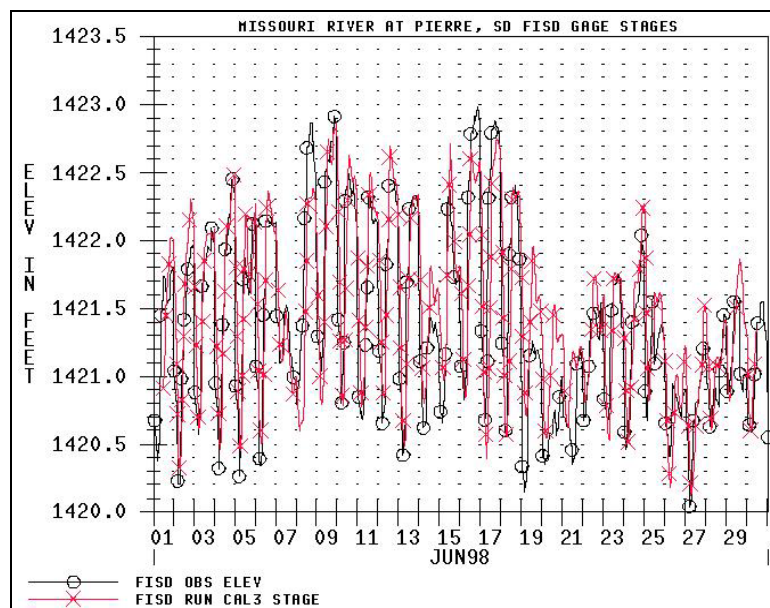


b. Pierre gage.

Figure 4. Observed and simulated stages at the four gages.



c. LaFramboise gage.



d. Farm Island gage.

Figure 4 (cont.). Observed and simulated stages at the four gages.

Table 3. Calibrated Manning's coefficients.

a. Open water	
River mile	Channel Manning's roughness coefficient
1071.92	0.022
1066.32	0.025
1065.11	0.018
1064.82	0.022
1064.27	0.022
1061.69	0.022
1059.49	0.024
1058.62	0.021
1057.64	0.021
1055.31	0.0225
1053.02	0.015
988.62	

b. Ice cover		
Reach	Ice thickness (ft)	Ice roughness coefficient
Big Bend Dam to Farm Island (RM 1059.5)	1.5	0.020
Farm Island to RM 1062.8	1.0	0.042
RM 1062.8 to LaFramboise Island Gage (RM 1064.8)	0.5	0.035
La Framboise Island Gage to Oahe Dam	0.5	0.070

estimated values of Manning's roughness coefficient. The simulation model was able to accurately simulate both the peak stages and the timing of the peak stages at all the gage locations. Only the values of Manning's roughness coefficient for the channel were determined during the calibration as there was no flow in the channel overbanks.

The 14–26 January 1994 period was selected for calibration of the ice cover Manning's roughness coefficient. The ice cover roughness coefficients were calibrated by fixing the ice cover thickness and extent and adjusting its hydraulic roughness to match the maximum observed stages. The extent was determined from available observations. It was expected that the Manning's roughness coefficient associated with the ice cover would vary with location and time. In this calibration procedure a conservative, upper-bound estimate of the Manning's coefficient for the ice cover was sought. The 20–21 January period was selected as the ice cover was at its maximum extent at river mile 1064.5. Figure 5 shows Oahe Dam outflow and ice cover progression for 14–26 January 1994, as well as the observed and simulated stages at the Pierre, La Framboise Island, and Farm Island Gages. During the 19–21 January period the observed and simulated stages compare well. Before 19 January the model overestimates stage because the leading edge of the observed ice cover had not yet reached its maximum extent. The resulting estimates of Manning's coefficients for the ice cover are listed in Table 3b.

Three wintertime periods were selected to simulate the discharges, the stages, and the advance and retreat of the river ice cover in the Missouri River downstream of Oahe Dam. They are 15 December 1996 through January 1997, 18 January 1996 through 11 February 1996, and 7 January 1994 through 3 March 1994. The information available for these periods is listed in Table 4. There are essentially no data available on the water temperature downstream of Oahe Dam for any of these periods. The water temperature measurements at the Pierre Gage are either missing or of such bad quality as to be unusable. The channel Manning's coefficients determined during the June 1998 period were used in the wintertime simulation, as were the Manning's coefficients found during the January 1994 period.

The following additional parameters were estimated prior to simulating ice cover progression. Values assigned to the parameters were estimated based on previous studies, physical insight, and extensive numerical experimentation:

1. *Water-to-air heat transfer coefficient.* This parameter controls the heat transfer rate from the water to the atmosphere. It was set at a value of $24 \text{ W m}^{-2}\text{C}^{-1}$. This value was found in previous study of the Missouri River (Corps of Engineers 1995).

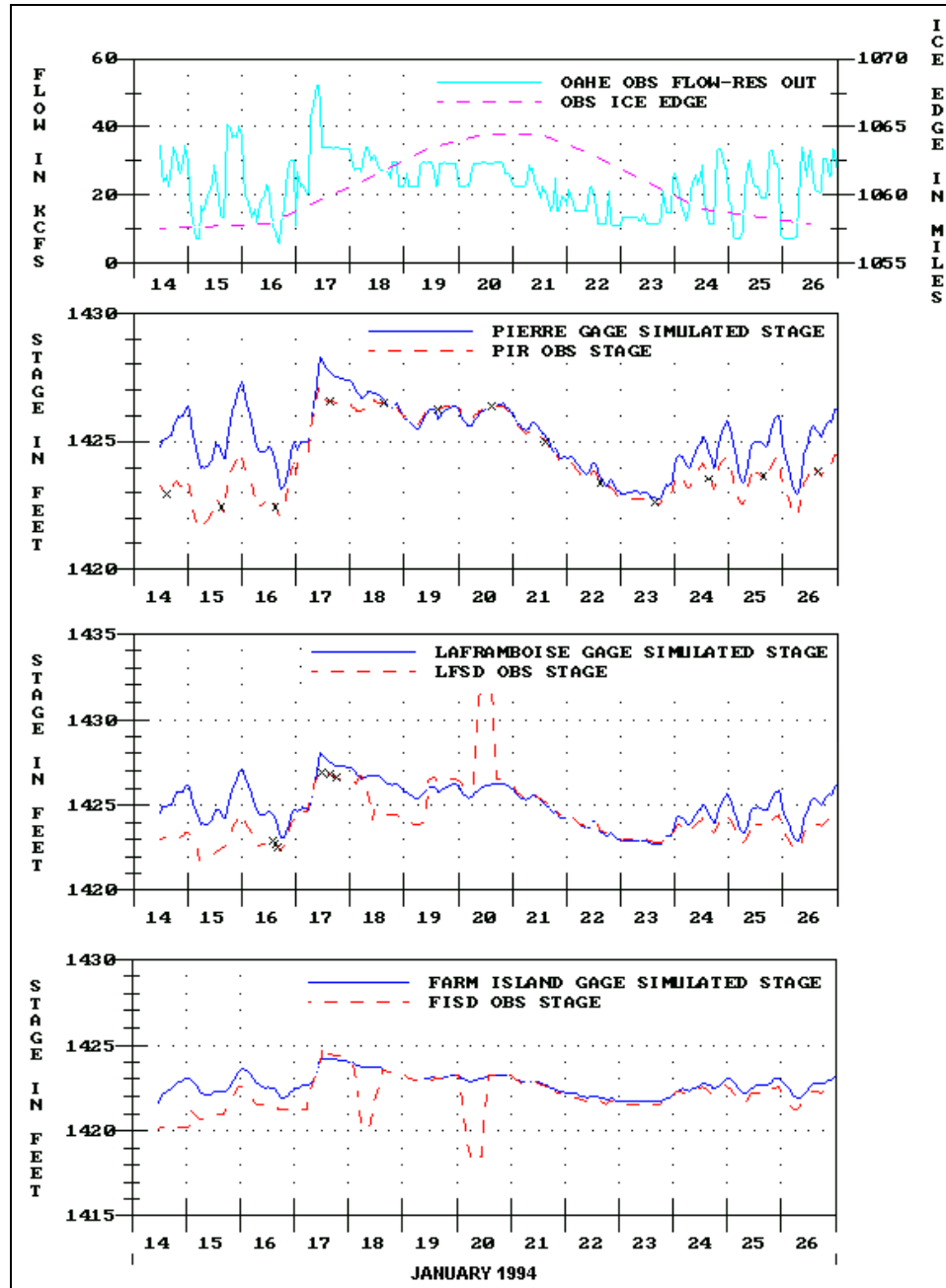


Figure 5. Observed and simulated stages during the ice-affected period of January 1994. (PIR = Pierre; LFSD = LaFramboise; FISD = Farm Island).

Table 4. Summary of data for ice periods.				
Data type	Gage site	Frequency	Quality	Notes
a. 15 December 1996 through January 1997				
Elevation gages	Oahe Tailwater	Hourly	Good	
	Pierre	Hourly	Good	
	LFSD	Hourly	Good	
	FISD	Hourly	Fair	Bad data; missing data period
	Big Bend Dam	Hourly	Good	Downstream b.c.*
Oahe discharge	Oahe Dam	Hourly	Good	Upstream b.c.*
Air temp.	Oahe Dam	Daily Max/Min	Good	
	Pierre Gage	Hourly	Fair	Missing data
Water temp.	Oahe Dam Outflow	Daily	Poor	Upstream b.c.*
	Pierre Gage	Hourly	Very Poor	Bad data
Ice cover obs.		Irregular	Fair	12/19/96 through 1/28/97
Description: Max stages: Jan 10–12. Evidence of smoothing of the ice cover roughness.				
b. 18 January 1996 through 11 February 1996				
Elevation gages	Oahe Tailwater	Hourly	Good	
	Pierre	Hourly	Good	
	LFSD	Hourly	Good	
	FISD	Hourly	Good	
	Big Bend Dam	Hourly	Good	Downstream b.c.*
Oahe discharge	Oahe Dam	Hourly	Good	Upstream b.c.*
Air temp.	Oahe Dam	Daily Max/Min	Good	
	Pierre Gage	Hourly	Missing	
Water temp.	Oahe Dam Outflow	Daily	Poor	Upstream b.c.*
	Pierre Gage	Hourly	Poor	
Ice cover obs.		Irregular	Poor	Missing Data
Description: No ice cover observations after 26 January 1996.				
c. 7 January 1994 through 3 March 1994				
Elevation gages	Oahe Tailwater	Hourly	Poor	Missing Data
	Pierre	Hourly	Fair	
	LFSD	Hourly	Poor	Bad Data
	FISD	Hourly	Poor	Bad Data
	Big Bend Dam	Hourly	Good	Downstream b.c.*
Oahe discharge	Oahe Dam	Hourly	Good	Upstream b.c.*
Air temp.	Oahe Dam	Daily Max/Min	Good	
	Pierre Gage	Hourly	Good	
Water temp.	Oahe Dam Outflow	Daily	Poor	Upstream b.c.*
	Pierre Gage	Hourly	Missing	
Ice cover obs.		Irregular	Fair	

*Boundary condition for simulation model

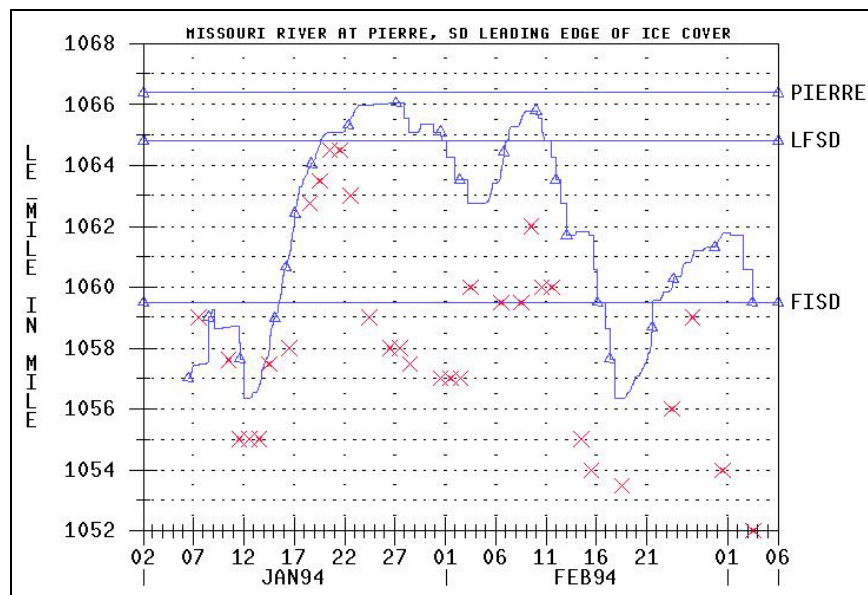
2. *Pan thickness.* This parameter, the initial thickness of ice floes formed by frazil ice in the Missouri River, must be used because there is no theory at this time that can be used to calculate the pan thickness. The value used here was 0.2 ft.

3. *Minimum ice thickness.* The minimum ice thickness at which the stationary ice cover forms is set at 1.5 ft.

4. *Frazil ice river velocity.* The mean rise velocity of the frazil ice crystals transported in suspension is set at 0.008 ft s^{-1} . The rise velocity is a function of the size and shape of the frazil ice crystals (Daly 1984).

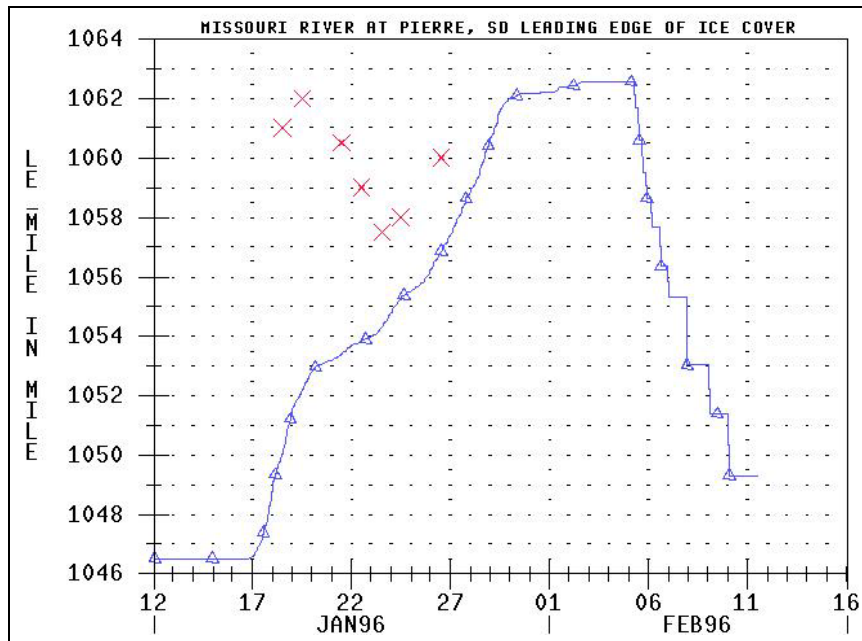
5. *Ice removal factor.* It is assumed that the ice cover is melted out once the ice cover thickness is reduced to a preset fraction of the maximum ice thickness calculated at a section. Numerical experiments indicated that this fraction should be set at 0.98. That is, the ice cover thickness need only be reduced by 2.0% for meltout to occur.

The results of the simulation of the ice cover are compared with the available observations in Figure 6. The model's ability to simulate the extent of the ice cover must be described as encouraging although mediocre at best.

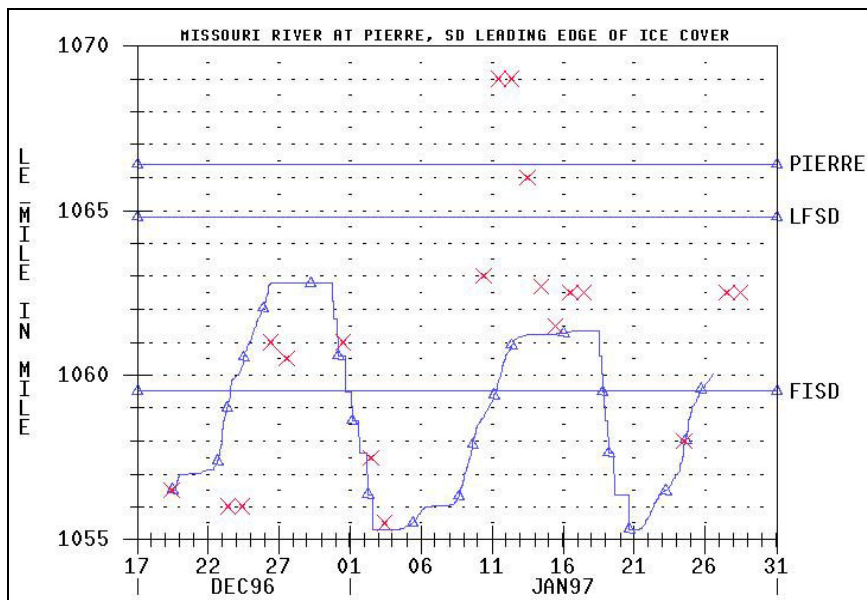


a. January and February 1994.

Figure 6. Observed and simulated ice cover extents.



b. January and February 1996.



c. December 1996 and January 1997.

Figure 6 (cont.). Observed and simulated ice cover extents.

Sources of simulation inaccuracy

The inaccuracies in simulating ice cover progressions can be attributed to several factors, most notably the following:

1. *The highly varied outflow from Oahe Dam.* The outflow of Oahe Dam is highly unsteady, as shown in Figure 3. There is no precedent for simulating ice cover progression in highly unsteady flow. The ice cover progression described earlier implicitly assumes that the flow is steady. The result is that the simulated ice cover advances in a succession of quasi-steady flows. It is difficult to estimate the inaccuracy that this assumption introduces.

2. *The domination of ice cover formation by the juxtaposition.* At the present time there is little basic understanding of the formation and growth of transported pans of ice. The formation of an ice cover by juxtaposition of these pans requires the use of empirical parameters that may vary with time and location.

3. *The use of a one-dimensional ice model.* The growth of shore ice may play an important role in the overall formation of the ice cover in the Missouri River. Photographs often show extensive shore ice that forms, leaving a central open-water expanse that may cover only one half to one third of the channel width. In the simulation the presence of shore ice is not taken into account. Observers generally place the leading edge of the ice cover at the farthest downstream extent of the open-water channel.

4. *The lack of complete outflow water temperature measurements.* The simulation water temperature upstream boundary condition was based on one measurement of the outflow temperature per day. These measurements were linearly interpolated to produce an hourly boundary condition. The water temperature variation throughout a 24-hour period is therefore not taken into account.

5. *The approximation of the water-to-air heat transfer using the temperature difference only.* The heat transfer from the water surface has several components, including long-wave radiation, short-wave radiation, and sensible and latent heat transfer. In addition, the sensible and latent heat transfer rates are influenced by the stability of the atmosphere and the wind velocity. The use of the difference between the air and water temperature is a simplification that is prompted by the difficulty in obtaining observations and forecasting these components. However, this simplification may result in error, especially during periods of high winds.

4.3 Estimation of filter parameters

The main tasks described in this section are estimation of the Kalman filter parameters and development of means to cope with bad or missing observations. Theoretically it is quite straightforward to handle missing data. If an observation

is not available, the updating step of the cycle described above is skipped. Estimation accuracy will suffer from skipping the updating step, but the procedure can be repeated until the next observation is available. A problem arises when some observations are missing and some are available. There are only a few observations of the ice cover extent, for example, and the number of ice cover observations is only a small percentage of the number of hourly stage observations available. This situation presents technical problems in updating, as the vector of observations, \mathbf{z} , and the observation matrix, \mathbf{H} , would need to continually vary with time to adjust to the number of observations that were available. In the approach used here the other source of information on the ice cover extent, the ice cover propagation model, is used to update the model when direct observations of the ice cover extent are missing. In this way the state-space model can be updated on the hourly schedule of the stage measurements and not the irregular schedule of the ice cover observations.

The elements of the system noise covariance, \mathbf{Q} , and the measurement error covariance, \mathbf{R} , were assumed to be a known quantity in the filter equations of Chapter 3. However, in actuality, an *a priori* value of \mathbf{Q} is difficult to describe since it is a function of model errors and natural system variability. The components of \mathbf{R} are, in theory, determined by the measurement instruments and technique and can be independently estimated. In practice, \mathbf{Q} is often adjusted manually until an acceptable level of model performance is achieved. There are also means of estimating \mathbf{Q} through adaptive filtering (Myers and Tapley 1976, Jazwinski 1969, Sage and Husa 1969) in which the components of \mathbf{Q} (and \mathbf{R} , if required) are sequentially estimated, as observations become available, to ensure non-correlation of the innovation sequence.

In the present study the components of \mathbf{Q} were estimated through numerical experiments. In these experiments the model was required to reproduce the recorded observations of ice cover extent and the stage from selected open-water and wintertime historical periods for the Missouri River downstream from Oahe Dam at Pierre, South Dakota. The experiments were designed to estimate the filter parameters that satisfy the following requirements:

1. The model should reproduce the valid observations as closely as possible. A good least-squares criterion for this is the *coefficient of determination of the model* (Assaf and Quick 1991) described in requirement 4 below.

2. The magnitudes of the elements of the covariance matrix, \mathbf{P} , should be reasonable, based on the physics of river hydraulics and knowledge of the possible range of ice extents found in the Missouri River. Satisfying this requirement allows the variance of the model estimates to be reported along with the model

results, so that potential users can judge the reliability of the model results for their particular application.

3. Values recursively estimated for the channel roughness should also be reasonable. This requirement means that negative or unreasonably large values of this parameter are to be largely avoided.

4. The innovation sequence should not be autocorrelated; it should be, in fact, white noise. This last requirement is part of the fundamental conditions under which the Kalman filter was derived. The sample autocorrelation function can be used to assess the degree of correlation of the innovation sequence.

The coefficient of determination, D_j , is the proportion of the initial variance of the measurement of observation j accounted for by the model:

$$D_j = \frac{\bar{F}_j^2 - F_j^2}{\bar{F}_j^2} \quad (166)$$

where

$$\bar{F}_j^2 = \sum_{t=1}^N (z_j^t - \bar{z}_j)^2 \quad (167)$$

$$F_j^2 = \sum_{t=1}^N (z_j^t - x_j^t)^2 \quad (168)$$

where \bar{z}_j = mean of the observations of variable j
 x_j^t = model estimate at time t corresponding to the observation at time t ,
 z_j^t
 N = total number of time steps for which observations and model estimates were available.

The values of x_j^t are the model estimates prior to updating. The value of D is as follows: one, if the model exactly matches the observations; zero, if the model is no better than the mean of the observations at estimating the observed value; and negative, if the model results are worse than using the mean. There is one coefficient of determination for each gage site location. The coefficients can also be combined to arrive at an overall coefficient of determination based on all the observations.

4.3.1 System error covariance for stage and discharge

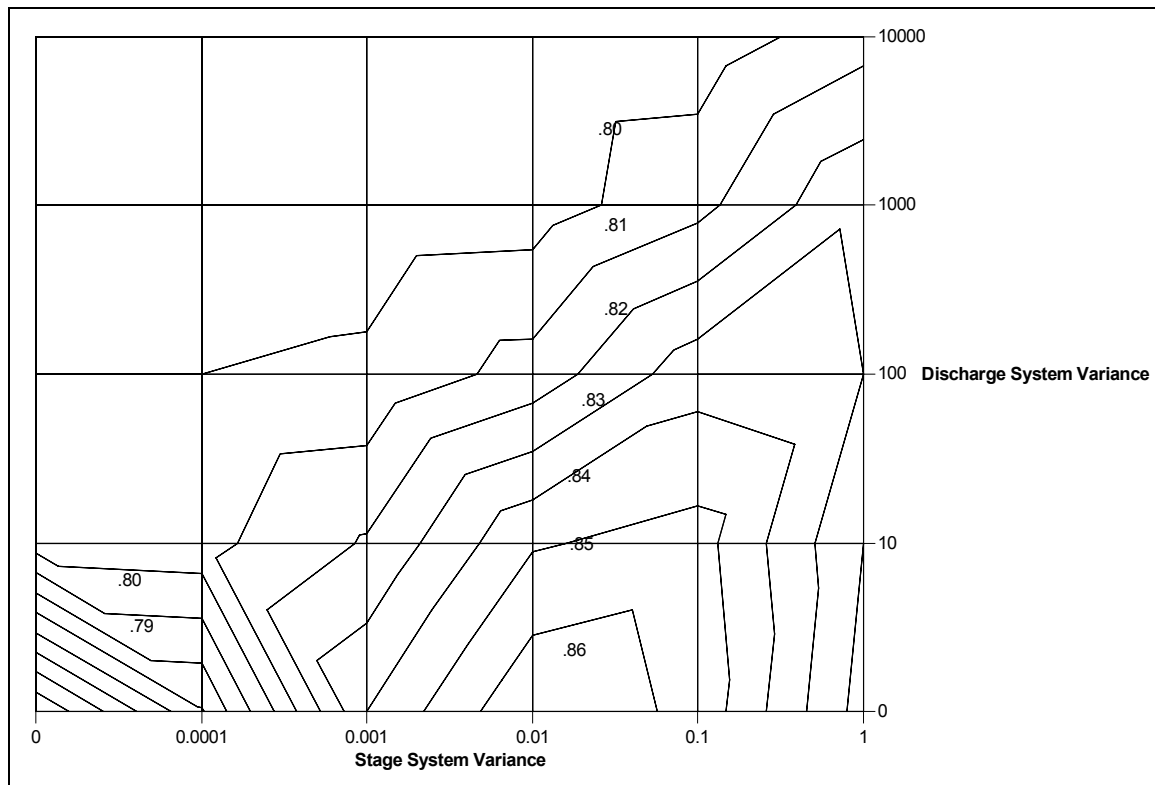
The initial step entailed estimating the system error covariance, often referred to as the system noise, based on the open-water period of June 1998. This step was accomplished through a series of numerical experiments that successively adjusted the system error covariance, as described below. The overall coefficient of determination was used to judge the quality of each result. Similar experiments were conducted for both the calibrated and uncalibrated channel geometry.

Other than the system error covariance, the input data used by the model were similar in each case. The upstream boundary condition applied to the model was the hourly observed outflow of Oahe Dam. The downstream boundary condition was the hourly observed stage at Big Bend Dam. In addition, the observed hourly air temperature at Oahe Dam and the observed outflow water temperature were used for input to the thermal model. However, as ice was not an issue during this time, and there is no accurate observation of water temperature available downstream of Oahe Dam, the temperature results of the model are not considered here. The hourly observed data from the four water stage recorders—the Oahe Tailwater gage, the Pierre gage, the LaFramboise Island gage, and the Farm Island gage—were used to update the model.

In the present study the usual assumption is made that the diagonal elements of Q are zero, because the components of the system error covariance applied to the state–space equation (eq 122) are uncorrelated. In practical terms a wide range of options are available to describe the system error covariance. At one extreme the same system error covariance could be applied to all the sub-equations in the state–space equation. This approach cannot be justified in physical terms, because the state equation describes the propagation of stages, discharges, ice extents, and conveyance adjustments, and it is hardly likely that the same system noise would apply to all. At the other extreme a separate system error covariance could be applied to each component of the state–space equation. In this study, separate system error covariances are applied to each equation, but the identical system noises are applied to each separate physical term. That is, all the system error covariance applied to the equations describing the propagation of stage is set to one value, all the system error covariance applied to the propagation of discharge is set to another value, and so on. This approach reduces the computational burden. The matrix Γ^n , defined in eq 117, becomes the identity matrix and thus does not need to be included in the computation.

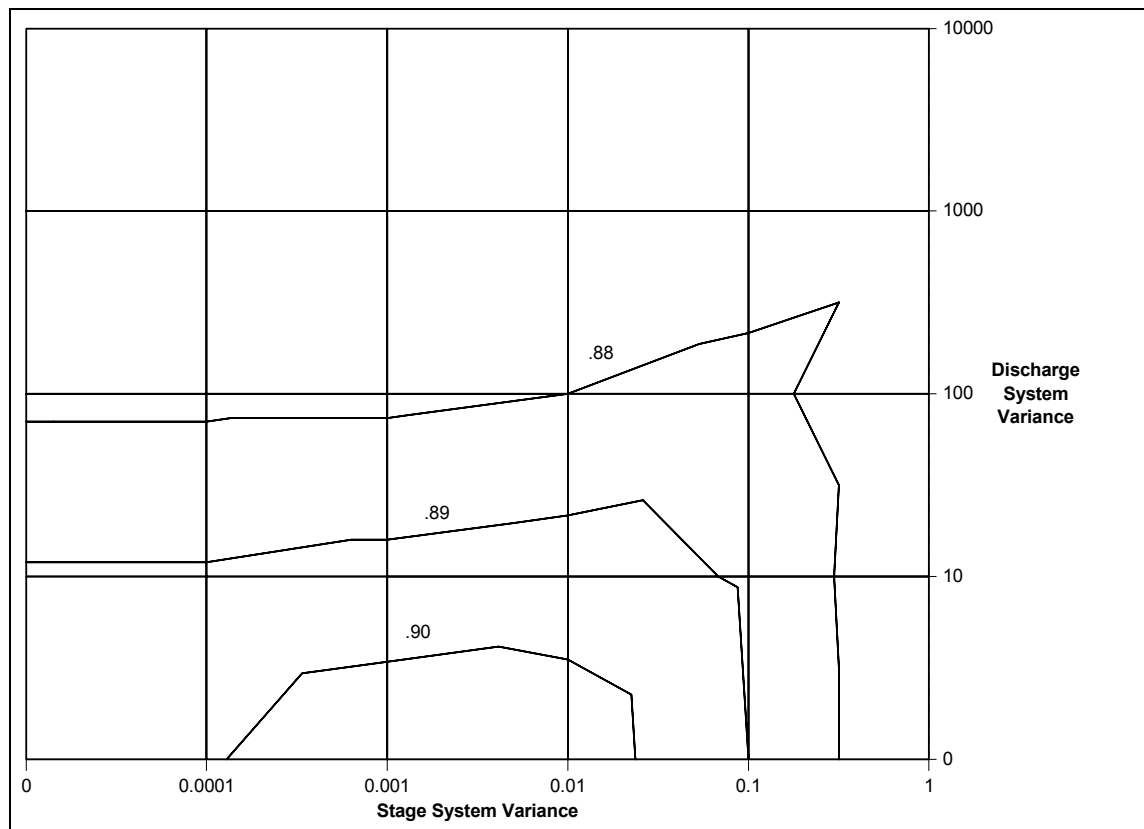
To determine reasonable values for the system error covariance, a series of numerical experiments were conducted in which the system error covariances were estimated for progressively more complete versions of the state–space model. First, the system error covariances were estimated for a model in which

the state vector is composed of only the discharges and the stages. This step allows assimilation of the observed stages. Next, the system error covariance of the conveyance factor was recursively estimated. This increases the size of the state vector to include the channel conveyance factors. The results of the first series of numerical experiments are shown in Figure 7. In these experiments the uncertainty of the measurement of the stages was set at 0.0025 ft^2 (232.25 mm^2). This estimate corresponds to a measurement error of $\pm 0.6 \text{ in.}$ (0.0152 m), which is a reasonable value for measurement error of river gages. The results for both the calibrated and uncalibrated channel geometries are identical. In both cases the overall coefficient of determination was maximized at system error covariance for the stages of 0.01 ft^2 and for the discharges of 0.0 ft^2 . Adjustment of the system error covariance produced the greatest benefits for the uncalibrated model. Some improvement was also seen for the calibrated model, which suggests that



a. Uncalibrated model.

Figure 7. Overall coefficient of determination of the state-space model as a function of assumed system noise for the stage and discharge.



b. Calibrated model.

Figure 7 (cont.). Overall coefficient of determination of the state-space model as a function of assumed system noise for the stage and discharge.

the model calibration could be further improved. The result that the system error covariance for discharge is zero does not mean that the estimated error covariance of the model for discharge is also zero. (Mathematically, the fact that some of the components of \mathbf{Q} are zero does not imply that any of the diagonal terms of \mathbf{P} are also zero.) In fact, because of the strong correlation between the error covariance of the stages and the discharges, the error covariances of the discharge are strongly influenced by the error covariance of the stages. This can be seen in Figure 8, in which the mean discharge and the square root of the model estimated error covariance at each model cross section are shown. The results shown are averages over the entire time period of June 1998. The square root of the model estimated error covariance at each cross section is shown as error bars around the mean discharge. These results were found by averaging the diagonal terms of the \mathbf{P} matrix over the time period of the simulation. The results with respect to stage are shown in Figure 9.

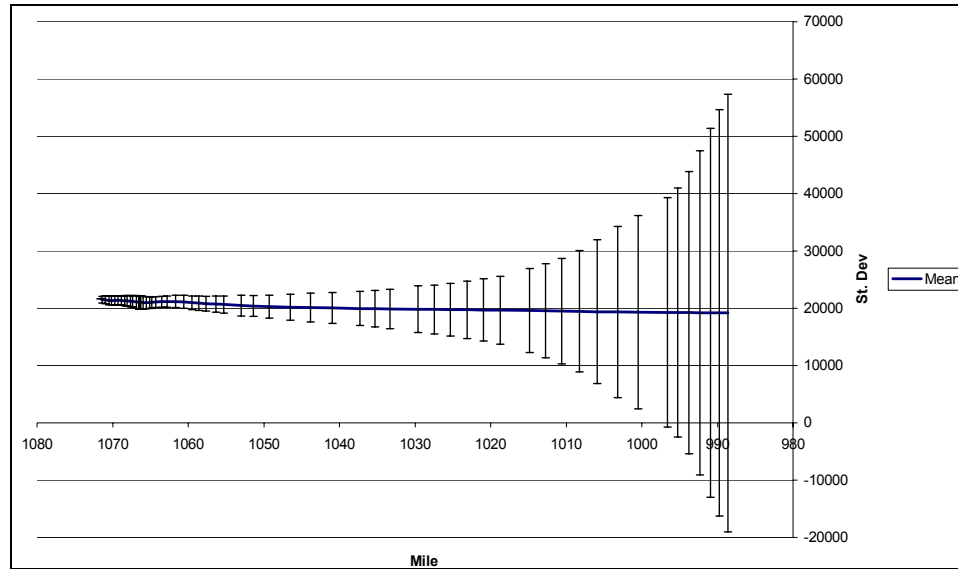


Figure 8. Average model flow with the estimated model uncertainty based on the estimated error covariance.

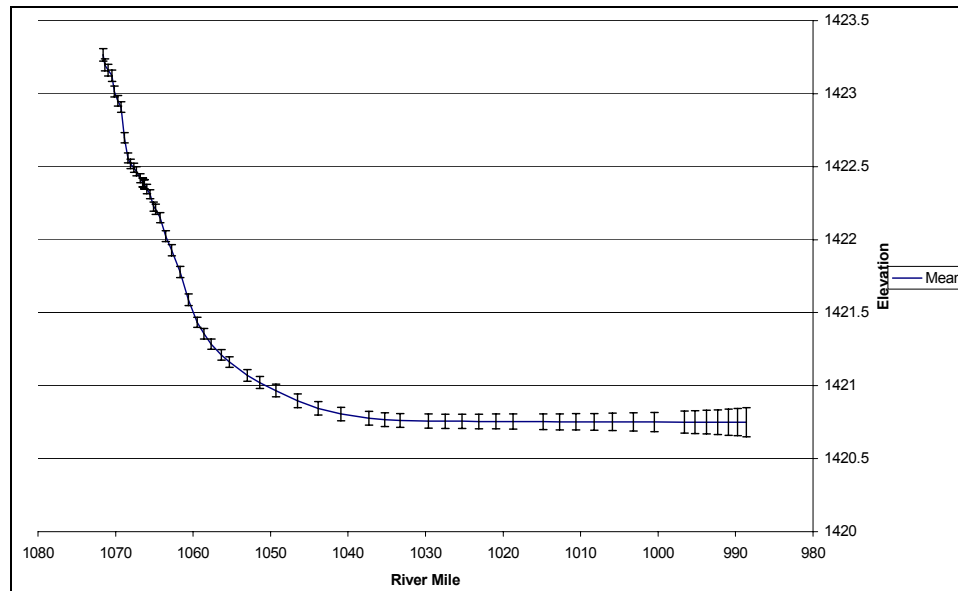
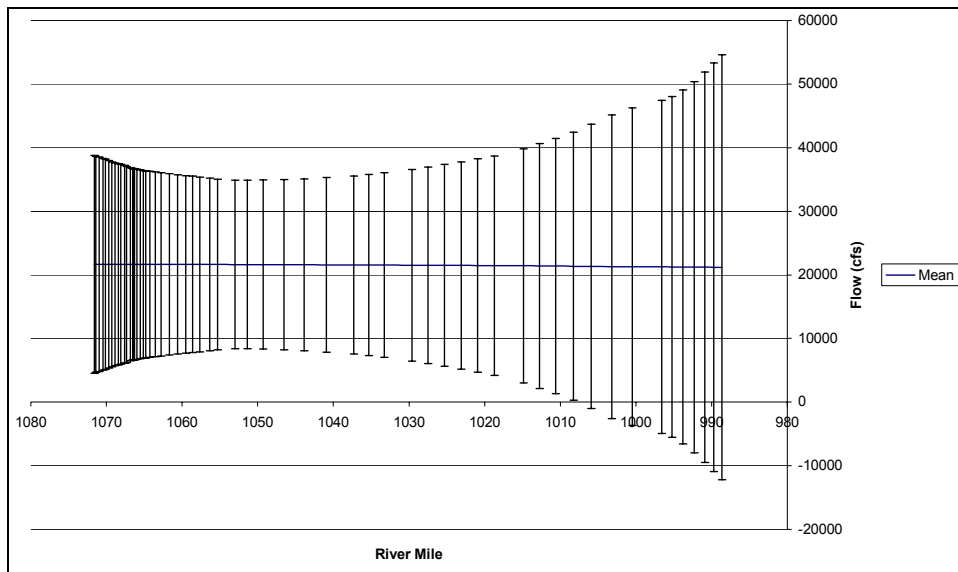


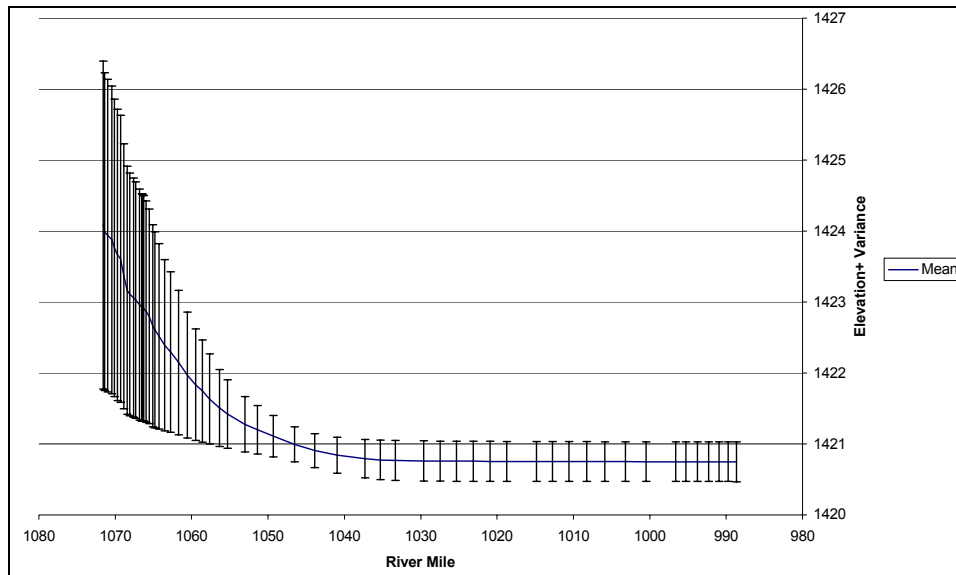
Figure 9. Average model stage with the model uncertainty based on the estimated error covariance.

One method for assessing the reasonableness of the model error covariance is to compare the model error covariance of the stages and discharges with the natural variability of the stages and discharges. The average discharge and average stage for each cross section included in the model are shown in Figure 10 for June 1998. The bars around the average values indicate the standard deviation of the calculated discharges and stages. As can be seen, the variance of discharge increases in the downstream direction, the variance of stage in the upstream direction. The increase in the discharge variance in the downstream direction reflects the difficulty in simulating flows in a reach where the water surface slope is very flat combined with the very large cross-sectional area of the river in the downstream extent of the river reach. The comparison with the model estimated error covariance is shown in Figure 11. Here the standard deviation of the model estimated error covariance of the stages and discharges has been divided by the standard deviations of the stages and discharges and is expressed as a percentage. Over most of the channel length, the estimated error covariance of the stage is less than 20% of the natural variability. The model covariance increases downstream, reaching over 100% at the downstream end of the simulated reach. For the region of Pierre, which is upstream of river mile 1045, the error covariances of the stage and discharge are both less than 20% of the natural variability. As the



a. Average discharge and standard deviation of the discharge.

Figure 10. Average discharge and water surface elevation at each model cross section during June 1998.



b. Average water surface elevation and standard deviation of the elevation.

Figure 10 (cont.).

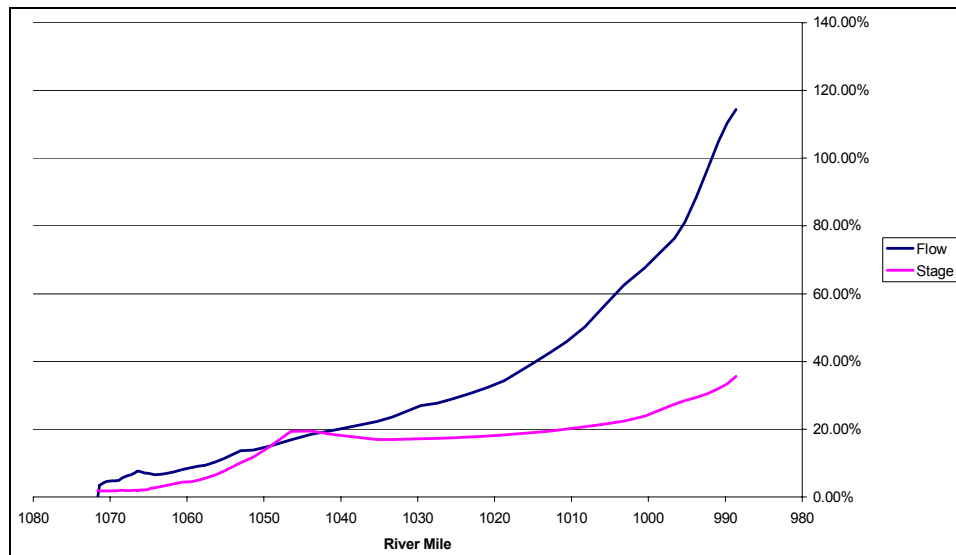


Figure 11. Comparison of the model uncertainty and the variance of the un-updated model results.

estimated model error covariance was reasonably described in the reach of interest, it was decided to not further adjust the system error covariance. However, in further studies, if this downstream reach was of interest, the system error covariance could be further tuned to produce the required distribution of the model error covariance.

4.3.2 System error covariance for conveyance factors

The numerical experiments were extended to include estimation of the system noise of the conveyance factors. It is appropriate at this point to discuss the approach that was used in the application of the conveyance factors into the state-space model.

The fundamental question that must be addressed is the number of conveyance factors. Theoretically the number of conveyance factors could range from the number of cross sections (if a separate conveyance factor was used for each cross section) to one (if a single conveyance factor is applied at all cross sections). The approach used here was to follow a procedure analogous to the standard procedure for calibrating hydraulic model roughness. In that procedure the selection of conveyance factors is controlled by the number of gages along the channel that measure the water surface elevation. A separate conveyance factor can be used for each river reach that has a gage at its upstream and downstream end. In the case of the Missouri River there are five gages for which hourly measurements are available for June 1998. The gages are, from upstream to downstream, the Oahe tailwater gage, the Pierre gage, the LaFramboise gage, the Farm Island Gage, and the Big Bend Dam gage. (The Big Bend Dam gage is the downstream boundary condition for the hydraulic model.) Thus, four conveyance factors can be used. The first would apply to the cross sections in the Oahe–Pierre reach; the second to the Pierre–LaFramboise reach; the third to the LaFramboise–Farm Island reach; and the fourth to the Farm Island–Big Bend reach.

In this series of tests the system error covariance for the stages was set at the values that led to the maximum overall coefficient of determination in the previous tests. The system error covariance of the conveyance factors was systematically varied and the overall coefficient of determination determined. The results are shown in Table 5. The maximum coefficient was found for a system variance of 0.0001. (This system error has no units because the conveyance factor is dimensionless.) The maximum was found at this value for both the calibrated and uncalibrated channel geometry. The coefficient dropped dramatically as the system error was increased beyond the maximum value. In fact, if the system error covariance was increased to 0.01, it was found that the conveyance factor varied widely, which led to inconsistent and numerically unstable results.

Table 5. Coefficient of determination for the June 1998 simulation using various system error covariances.

	Covariance =	0.000001	0.00001	0.0001	0.001	0.01
Uncalibrated		0.914	0.918	0.923	0.911	–
Calibrated		0.916	0.920	0.921	0.904	–

Table 6. Coefficient of determination for the June 1998 simulation with updating.

	Oahe	Pierre	LaFramboise	Farm Island	Overall
No update					
Uncalibrated	0.823	0.758	0.583	–0.010	0.720
Calibrated	0.935	0.944	0.768	0.682	0.894
Stage and discharge update					
Uncalibrated	0.862	0.949	0.818	0.759	0.869
Calibrated	0.919	0.958	0.825	0.821	0.906
Stage, discharge, and conveyance update					
Uncalibrated	0.946	0.960	0.824	0.826	0.921
Calibrated	0.948	0.965	0.819	0.837	0.923

4.3.3 Summary

The overall results with the optimum system error covariances for the open-water period of June 1998 are listed in Table 6. Listed are the coefficients of determination for each of the four gages in the Missouri River downstream of Oahe Dam and the overall value. Shown first are the values for the simulation with no update. The results for the calibrated channel geometry are much better than for the uncalibrated results. The calibrated model shows substantial improvements at each gage and overall. It is interesting to note that the uncalibrated model has the lowest coefficient of determination at the Farm Island gage, which is the most downstream gage and has the smallest water level variation of the four gages. Listed next are the updated model results. The results for the calibrated channel geometry are always slightly better than for the uncalibrated results, but the uncalibrated model results show the largest improvement over the no-update case. This finding suggests that updating may be an alternative to calibration, saving the extensive time and effort calibration requires. The coefficient of determination is only slightly improved by the addition of the conveyance factors for the calibrated channel geometry case. As the channel roughness pre-

sumably was accurately determined during the calibration process, this finding is probably to be expected.

4.4 Hindcasting

Simulation of the Missouri River when river ice is present is now addressed. The system error covariances have now been determined for the stages, discharges, and conveyance factors. The remaining component of the state vector not yet investigated is the system error covariances to apply to the ice cover extents, Σ_{ds} and Σ_{us} , for each cross section. From Chapter 2 it is evident that the values of these variables range from 0 for no ice to 0.05 for a complete ice cover at that section. It was determined that the value for the system error covariances for these variables could be set at 1.0.

Three periods in the recent past were selected for hindcasting by the state-space model. During these times ice was present in the Missouri River and observations are available: 19 December 1996 through 26 January 1997, 18 January 1996 through 11 February 1996, and 7 January 1994 through 3 March 1994. These periods were simulated without updating, with varying success as described in the previous section. As mentioned in the introduction to this chapter, a primary problem that must be dealt with is the lack of observations of ice cover extent. Thirty-two ice observations are available in 1994, eight in 1996, and nineteen in 1996-97. This deficiency must be contrasted with approximately 1296 hourly measurements of stages at each of the four gages in 1994, 600 measurements of stage at each gage in 1996, and 940 measurements in 1996-97. The following procedure was developed to make maximal use of available data and to restrain the computational complexity of the state-space procedure:

1. Recall from the description of the overall solution procedure described in Chapter 2 that the hydraulic model simulates the flow in the channel based on the ice cover extent that is present at the start of a time step. The implicit assumption is that the ice cover extent is constant throughout the time step. However, the ice cover progression model estimates the ice cover extent at the end of the time step. This information is then available to update the model with a better estimate of the ice cover extent at the end of the time step than the assumption that the ice cover extent is constant through this period.

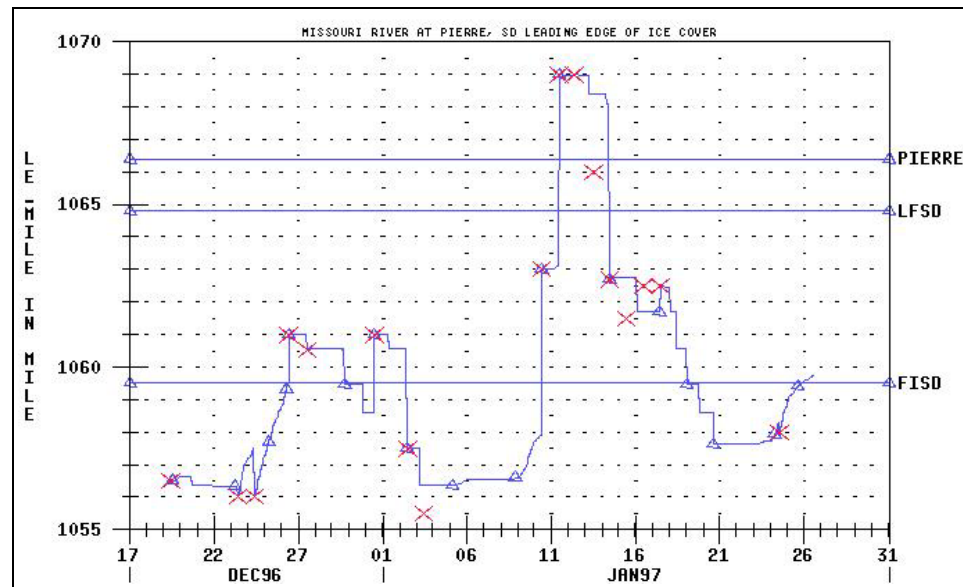
2. If an ice observation was available, the observation was used to update the model. However, if no observation was available, as was most often the case, the state-space model ice cover extent was updated with the estimate of the ice cover extent that was produced by the ice cover progression model.

Useable observations of water temperature downstream of Oahe Dam are not available for the periods under consideration. Observations of ice in transport are also not available for these periods (or any periods of time, for that matter). As a result the thermal and ice transport state-space model is not used in these data assimilation experiments.

As mentioned above, the error covariance of the observation was set at 0.0025 ft^2 , except during the 1993-94 winter period as explain below. However, whenever an observation was greater than 1430 ft (*1929 NGVD*) or less than 1420 ft (*1929 NGVD*), the uncertainty associated with those measurements was set to an arbitrarily large value. As a result the state-space model would essentially ignore those measurements when updating the model.

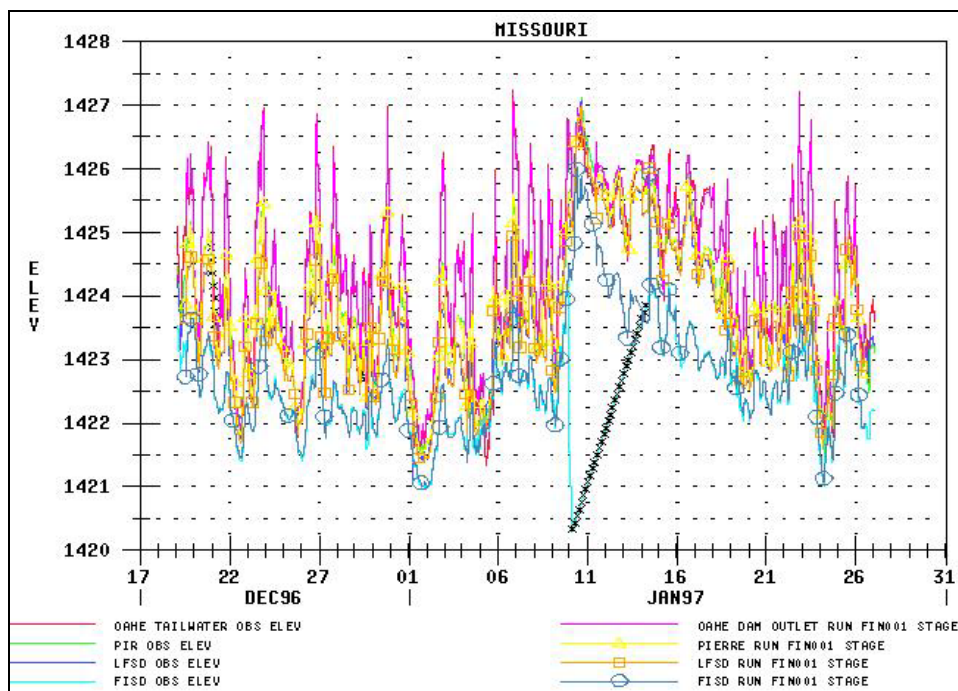
4.4.1 Winter 1996-97

The results of the data assimilation experiment for the period 19 December 1996 through 26 January 1997 are shown in Figure 12. Figure 12a displays the estimated extent of the updated ice cover. The updated results match the observations closely.



a. Updated and observed ice cover extent.

Figure 12. Results of data assimilation experiment for 19 December 1996 through 26 January 1997.

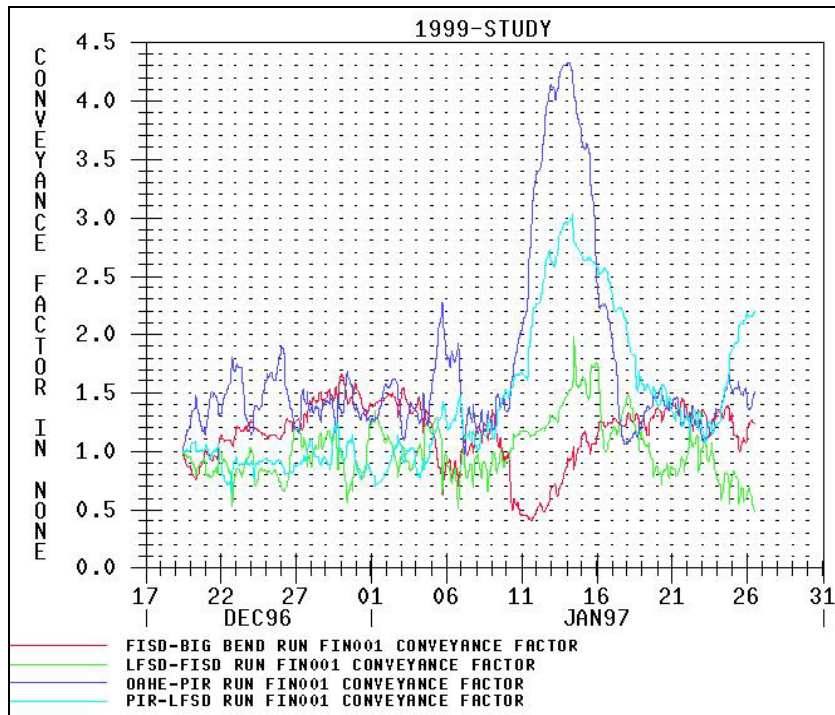


b. Updated and observed water surface elevations. X denotes missing data. Note the missing data for the Farm Island gage for the period 10–14 January.

Figure 12 (cont.). Results of data assimilation experiment for 19 December 1996 through 26 January 1997.

Figure 12b displays the observed and updated stages. The updated stages essentially duplicate the observed stages except during periods when observations are missing or bad, such as 10–14 January for the Farm Island gage. The error covariance of the measurements of the Farm Island gage was set to a large value for the period 10–14 January so that measurements from this gage were ignored for this period.

There were other, subtler problems with the observations during this winter that dramatically affect the estimates of the conveyance factors shown in Figure 12c. The water surface elevations measured at the Oahe tailwater gage, the Pierre gage, and the LaFramboise gage inexplicably nearly coincide during the period 10–14 January. It is not clear what is causing this result. Undoubtedly the cold weather interfered with the proper operation of the gages. The only means the state-space model has for coping with these observations is to assume that the channel upstream of the LaFramboise gage has become much less rough so that the drop in stage between the gages is minimized. As a result the conveyance



c. Estimated conveyance factors.

Figure 12 (cont.).

coefficients increased dramatically during this period for the reach between the Oahe tailwater gage and the Pierre gage and the reach between the Pierre gage and the LaFramboise gage.

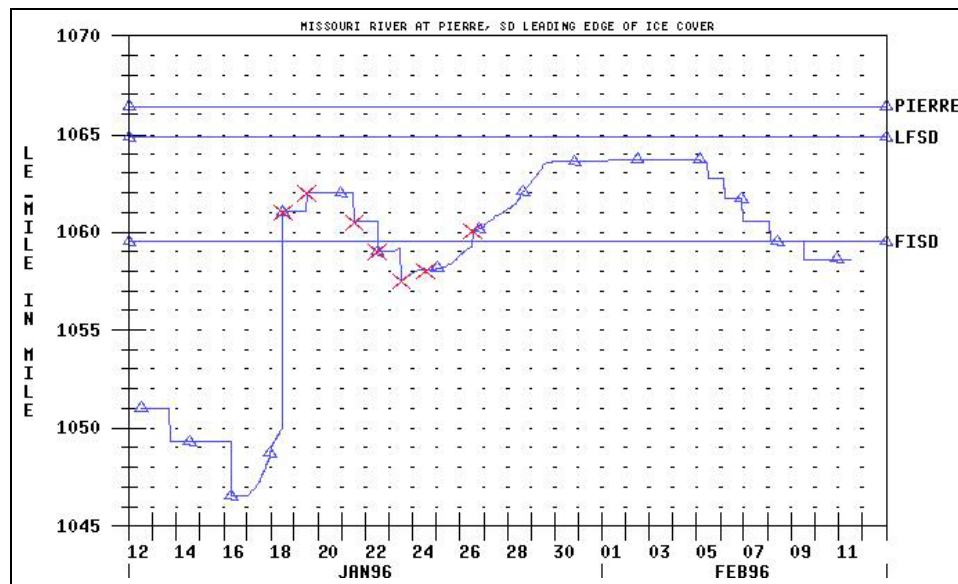
The coefficients of determination for the updated model and the non-updated results are listed in Table 7. The updated results show substantial improvements over the non-updated simulation.

4.4.2 Winter 1995-96

The results of the data assimilation experiment for the period 18 January 1996 through 11 February 1996 are shown in Figure 13. Figure 13a displays the updated ice cover extent result. It can be seen that updated results match the observations closely. However, only a few ice observations are available. Figure 13b displays the observed and updated stages. The updated stages essentially duplicate the observed stages. There are almost no stage data missing during this time period. The large increase in stage that occurred on 18 January coincides with the ice cover progressing quickly upstream.

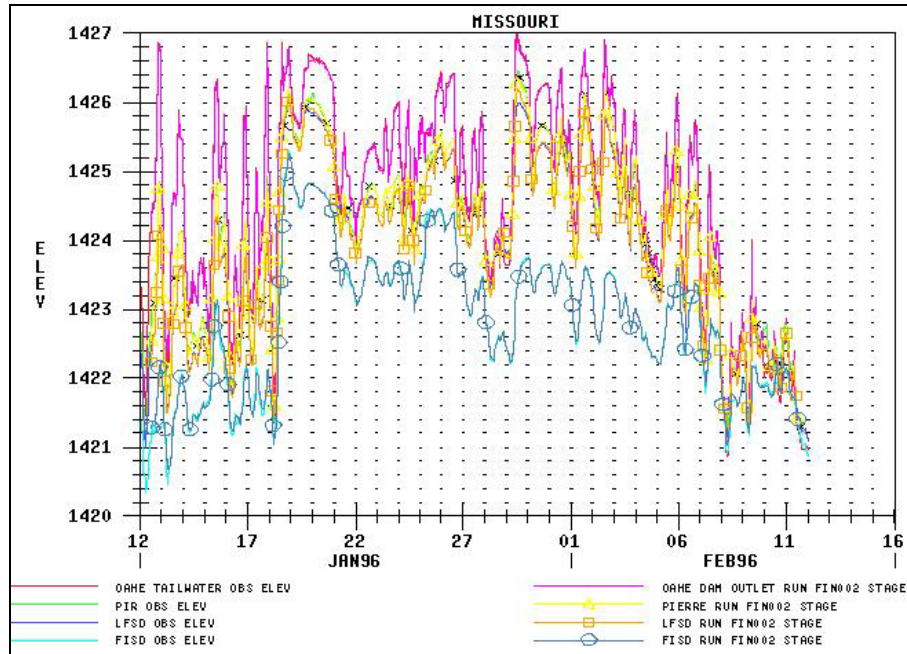
Figure 13c displays the conveyance factors for this period. The conveyance factor for the Farm Island–Big Bend reach drops dramatically when the ice cover progressed upstream. The possible cause for the drop is that the calibrated ice cover roughness underestimated the actual ice cover roughness during this period. The progressive increase in the conveyance factor for this reach may have

Table 7. Coefficient of determination for wintertime simulation.					
	Oahe	Pierre	LaFramboise	Farm Island	Overall
8 January 1994–3 March 1994					
No update	-1.076	-1.243	-0.0500	-0.842	-0.915
Updated	-	0.686	0.735	0.473	0.636
18 January 1996–11 February 1996					
No update	0.737	0.390	0.177	0.053	0.396
Updated	0.978	0.987	0.981	0.986	0.983
19 December 1996–26 January 1997					
No update	0.347	0.168	-0.059	-0.097	0.145
Updated	0.940	0.954	0.874	0.733	0.907

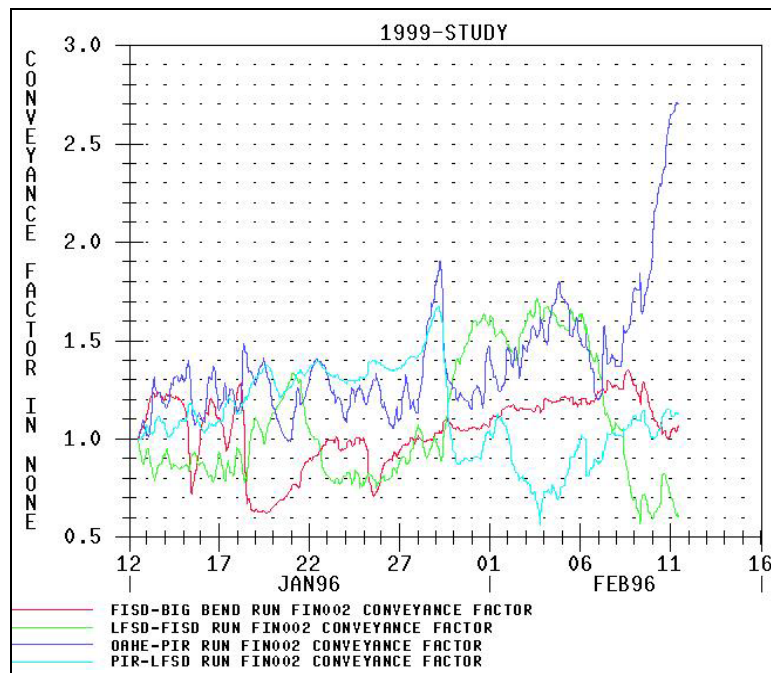


a. Updated and observed ice cover extent.

Figure 13. Results of data assimilation experiment for 18 January 1996 through 11 February 1996.



b. Updated and observed water surface elevations. X denotes missing data.



c. Estimated conveyance factors.

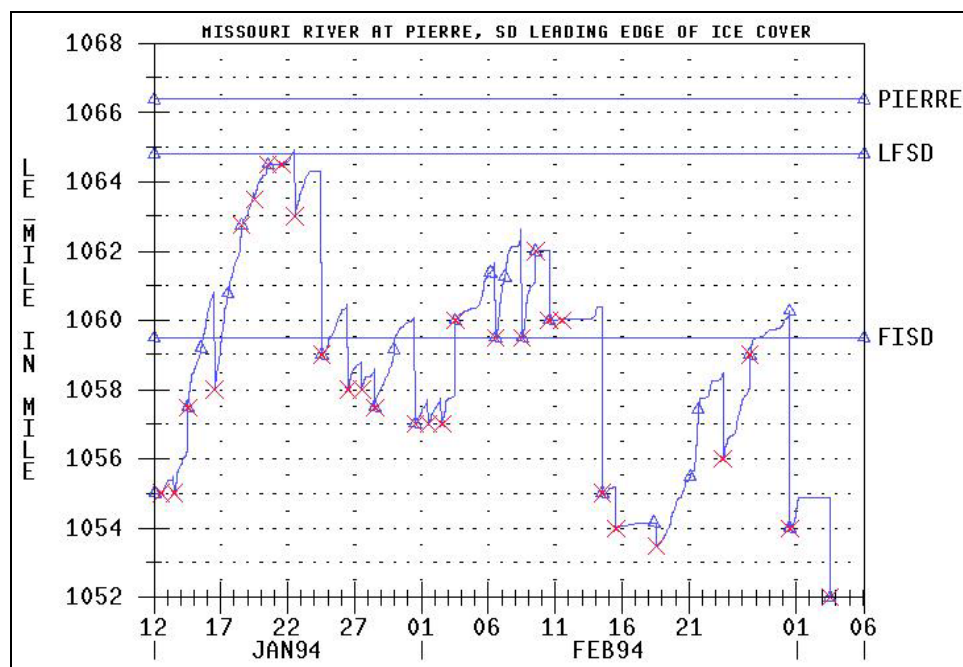
Figure 13 (cont.).

resulted from the progressive smoothing of the ice cover with time. This phenomenon has been reported for other ice-covered rivers (e.g., Ashton 1986). The increase in the conveyance factors at the end of the simulation period probably occurs because the state-space model did not cause the ice cover to retreat fast enough. Unfortunately there are no observations of the ice cover extent to update the model with during this time.

The coefficient of determination for the updated model and the non-updated results are listed in Table 7. For this winter also the updated results show a substantial improvement over the non-updated simulation.

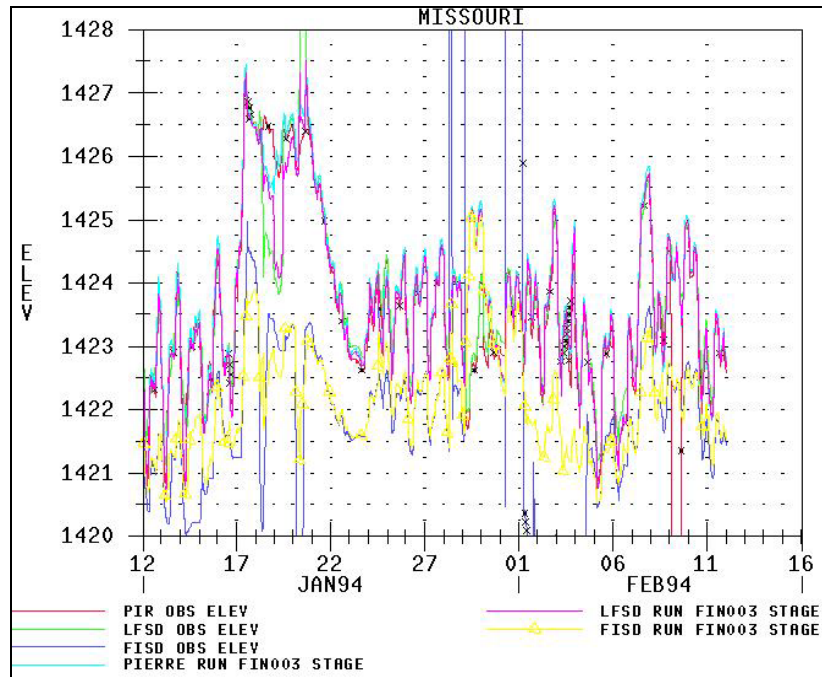
4.4.3 Winter 1993-94

The results of the data assimilation experiment for the period 7 January 1994 through 3 March 1994 are shown in Figure 14. This is the winter of the three presented for which data are worst. The Oahe tailwater gage was missing about 90% of the observations and was removed from the updating procedure. As a result the number of conveyance factors was reduced to three. It was found that if the

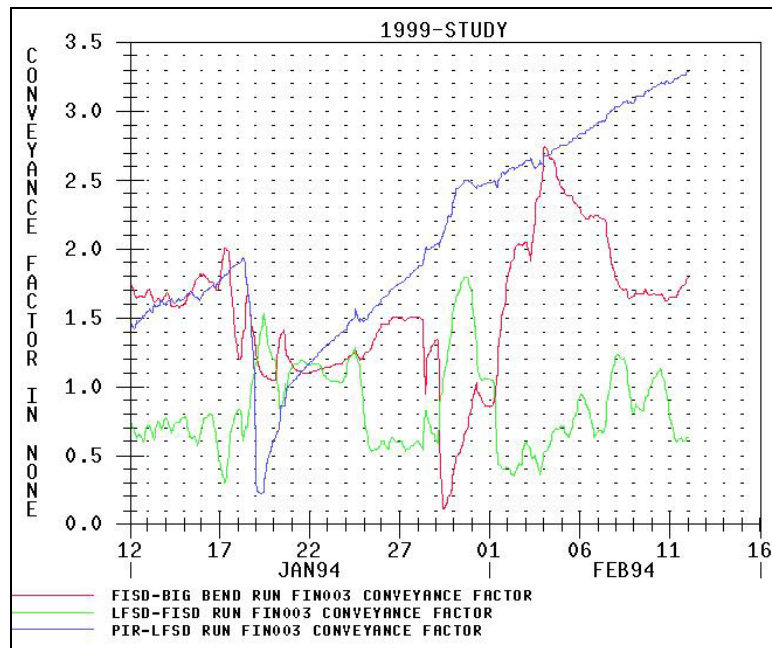


a. Updated and observed ice cover extent.

Figure 14. Results of data assimilation experiment for 7 January 1994 through 3 March 1994.



b. Updated and observed water surface elevations. X denotes missing data.



c. Estimated conveyance factors.

Figure 14 (cont.).

error covariance of the observations was kept at its standard value of 0.0025 ft^2 , then the updating caused the state–space model to become unstable. As a result the error covariance was increased by an order of magnitude to 0.025 ft^2 . Figure 14a displays the updated ice cover extent result. It is evident that updated results match the observed values closely. The stages are shown in Figure 14c. Also, it can be seen that the gages show many spikes during this period. Similarly to the winter of 1996-97, the elevations reported for the Pierre gage and the Oahe gage nearly coincide from 21 January and subsequently. As a result the conveyance factor for this reach increases continuously over that period.

The coefficient of determination for the updated model and the non-updated results are listed in Table 7. The updated results show an improvement over the non-updated simulation. However, given the quality of the observations, the fact that the coefficient of determination is not as great as in the other two simulations should not come as a surprise.

4.4.4. Summary

This section reports the results of the data assimilation experiments. The results show that the state–space model results depend on the quality of the observations used in updating. If all the observations are missing, the state–space model results are no worse than the simulation without updating. If the observations are not missing but are inaccurate, and the inaccuracy is not recognized, the state–space model results can be poor or illogical. The simulations used here apply simple maximum and minimum bounds on observations as one means to estimate their accuracy.

The results also show that more subtle problems occurred with the observations of stage. For instance, the problem became evident when the stages at two gages nearly coincided. The model attempted to cope with such a problem by adjusting the means available to it, i.e., the conveyance factor. Understanding the time-varying accuracy of the observations is important to the application of a state–space model.

4.5 Forecasting

As described in Sections 3.2 and 3.3, the state–space model is operated in a cycle of propagation and updating, repeated throughout the winter, to produce an optimal estimate of the state variables, especially the location of the leading edge of the river ice cover. Forecasts are made at periodic intervals by propagating the state–space river ice model into the future. After a forecast the cycle of propagation and updating is repeated, and a cycle of model propagation, updating, and

forecasting can be repeated throughout the winter season. This section considers the requirements of the river ice state-space model to make unbiased, minimum variance forecasts for the Missouri River downstream of Oahe Dam.

The river ice state-space model inevitably requires predictions of the future values of its boundary conditions to make predictions of the future channel ice cover extent and stages. These boundary conditions are Oahe Dam outflow, Big Bend stage, outflow water temperature, and air temperature. Predictions of future values of these boundary conditions are necessarily outside of the purview of the river ice state-space model itself and are not the focus of this chapter. Rather, the river ice state-space model is operated in the cycle of propagation, updating, and forecasting for the recorded historical winter periods when ice was present in the Missouri River, and the accuracy of the forecasts that are made is assessed. In this case the boundary conditions used to drive the forecasts are the recorded values of Oahe Dam outflow, Big Bend stage, outflow water temperature, and air temperature. Knowledge of the values of these boundary conditions is certainly an advantage, but it is one that allows the focus of the chapter to be on the use of the state-space model for making forecasts. Further work, beyond the scope of this study, is required to determine the best method for estimating future values of the model boundary conditions and their uncertainty.

4.5.1 Procedure

The following procedure was followed in developing forecasts of the river ice and stage conditions in the Missouri River downstream of Oahe Dam:

1. The state-space model was advanced in time, using hourly time steps throughout the winter period. Each hour, the state-space model was updated with the observed stages and the observed ice extent, if that information was available. If an ice cover observation was not available, the state-space model was updated with the estimate developed by the ice cover progression model, as described in the previous section. The values of the Kalman filter parameters determined in the previous section were used.

2. At 1200 hours each day (noon), a data file was created that contained the conveyance factors and the stage, discharge, ice cover extent, water temperature, frazil ice concentration, pan thickness, surface ice concentration, deposited ice thickness, and ice cover thickness at each cross section in the river reach. The data in this file formed the initial conditions for the forecast that would be made. 1200 hours was chosen as the time of day to make the forecast because most observations of ice cover extent were reported prior to this time. This enabled the observation of ice cover extent (if one was available) to be assimilated into the state-space model prior to the forecast.

3. A forecast was made of the river ice conditions and the stages over the next four days (96 hours). The recorded values of the model boundary conditions were used to drive the forecast model.

4. The forecast was not updated with observations. It is obvious that during operational use, observations of future stages and ice cover extents would not be available.

5. This procedure was repeated for each day of the winter period. The result was a series of forecasts, initiated at noon and extending over the next four days. The winters of 1996-97 and 1995-96 were used for forecasting. The winter of 1993-94 was not used because of the poor quality of the data.

The accuracy of the forecasted stages could be quantitatively determined by comparing the forecasted stages with the recorded stages. The mean error of the forecast and the variance of the forecast error were calculated for each hour of the four-day forecast period. Quantitatively estimating the accuracy of the forecasts of the ice cover extents was difficult because of the few observations available. The lack of ice cover observations required that forecast accuracy be based on stage only.

In addition to the procedure described above, the simulation model without updating was also operated each of the winter periods and used to produce initial conditions files each day at noon. These files documenting initial conditions were also used to produce forecasts to compare with the state-space model results. The files did not include conveyance factors, which can only be estimated through updating.

4.5.2 Results

A photo of the ice cover formation is shown in Figure 15. Examples of the forecasts of stage for the winter of 1996-97 are shown in Figure 16. Each solid black line represents the forecasted stage; the blue line marked with circles represents the observed stage at that location. In general, the forecasted and observed stages follow closely, except during periods of rapid ice cover advance, such as 10-12 January, or retreat, such as 14-15 January. The forecasted ice cover extents are shown in Figure 17.

The accuracy of the forecasts was determined by comparing the forecasted model stages with the observed stages. The results by day of forecast are listed in Table 8 and shown graphically by hour of forecast in Figure 18. Based on these results, the following insights emerge:

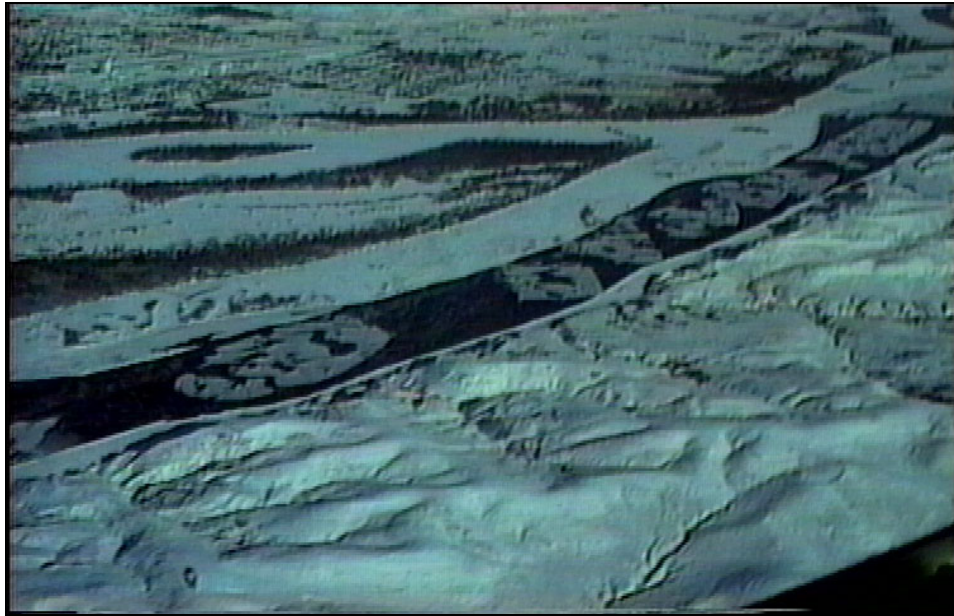
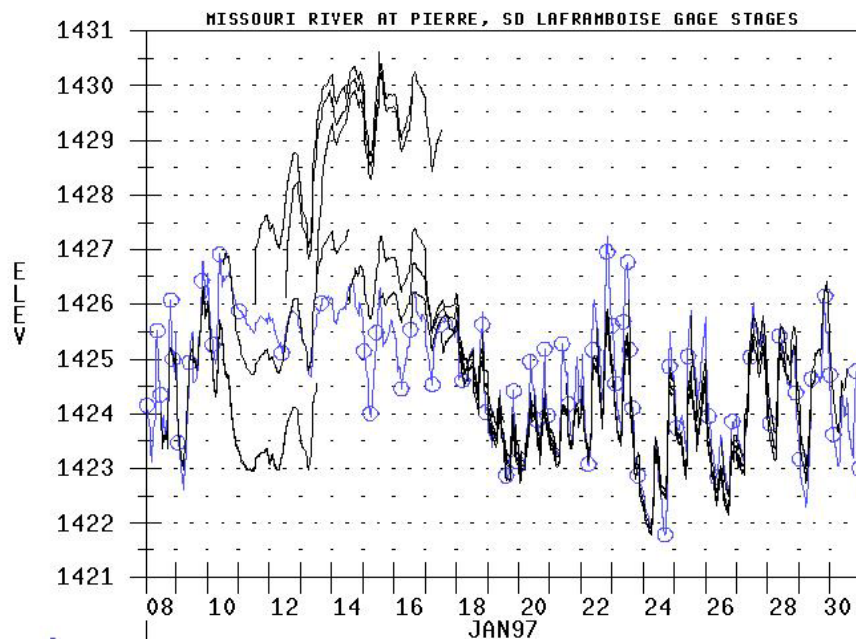
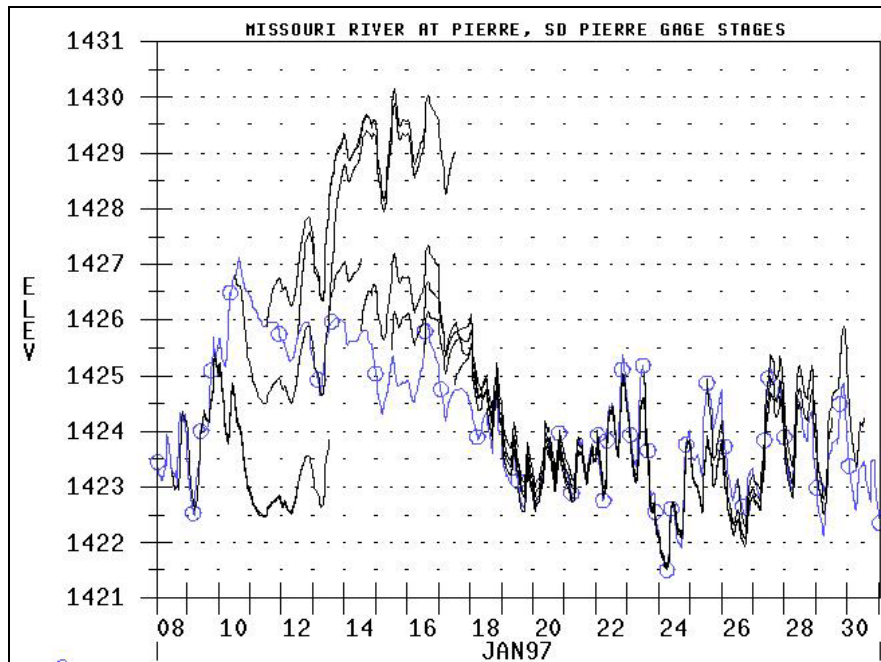


Figure 15. Ice floes moving downstream past LaFramboise Island to the leading edge of the ice cover, which is the top right corner of the view.

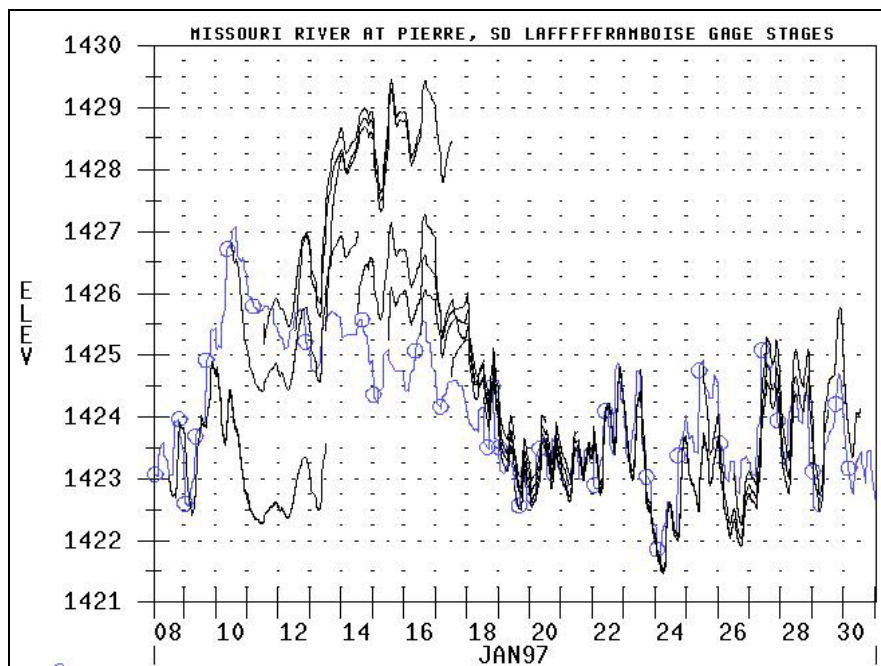


a. Oahe Tailwater gage.

Figure 16. Examples of four-day forecasts of stage for the winter of 1996-97.

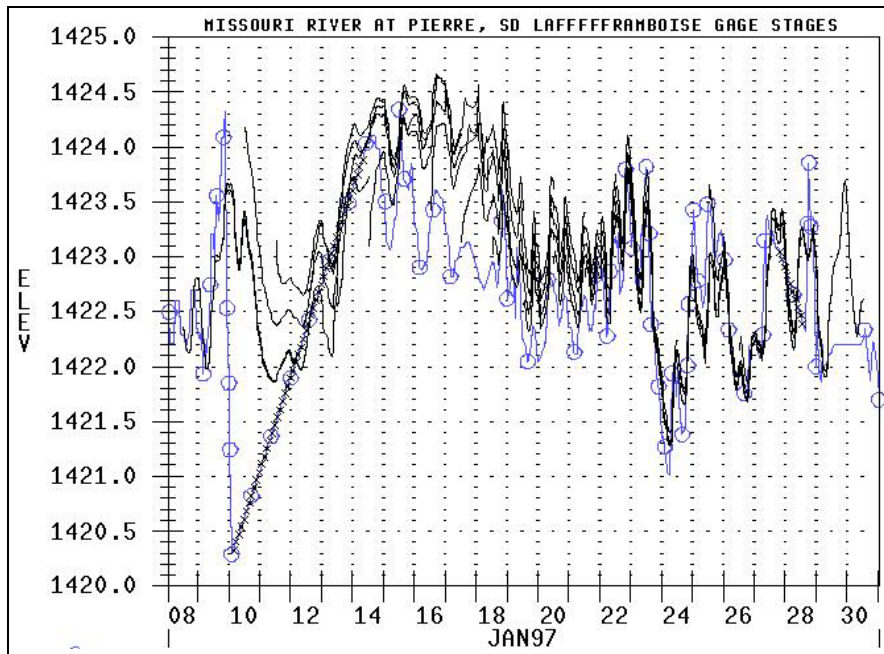


b. Pierre gage.



c. LaFramboise gage.

Figure 16 (cont.). Examples of four-day forecasts of stage for the winter of 1996-97.



d. Farm Island gage.

Figure 16 (cont.).

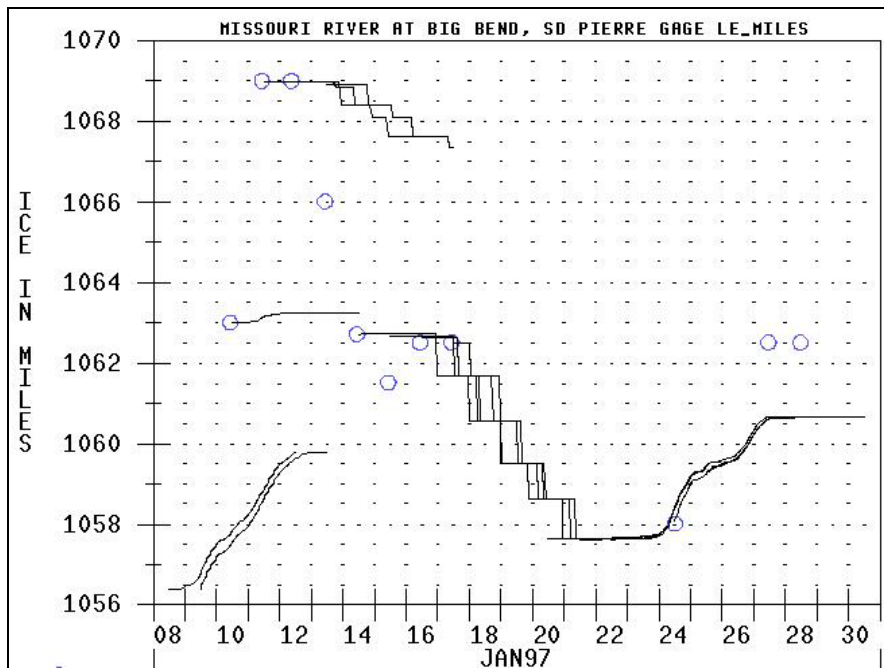
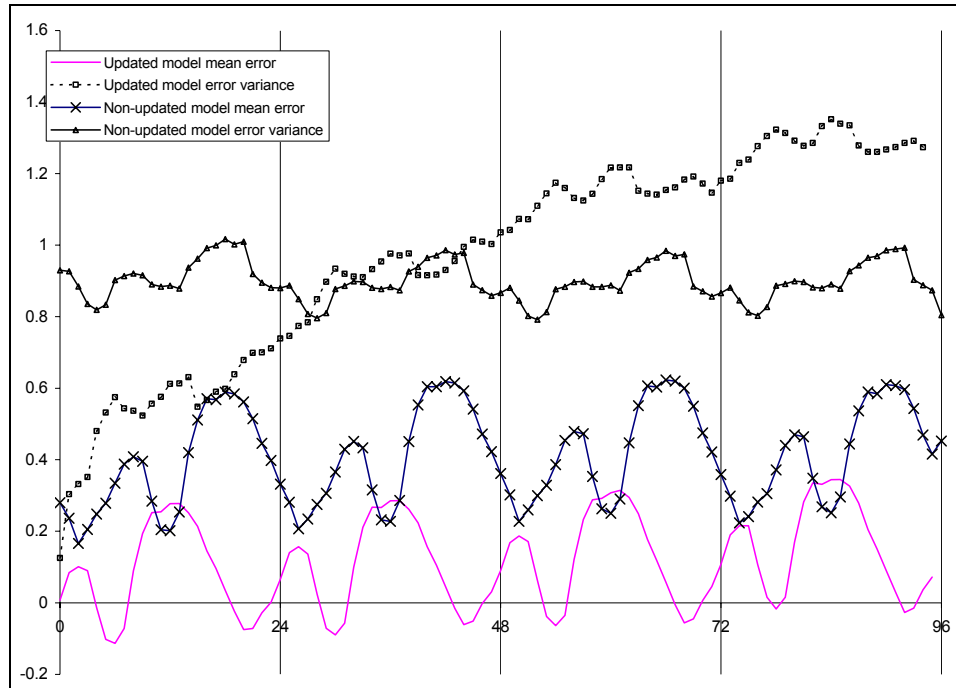
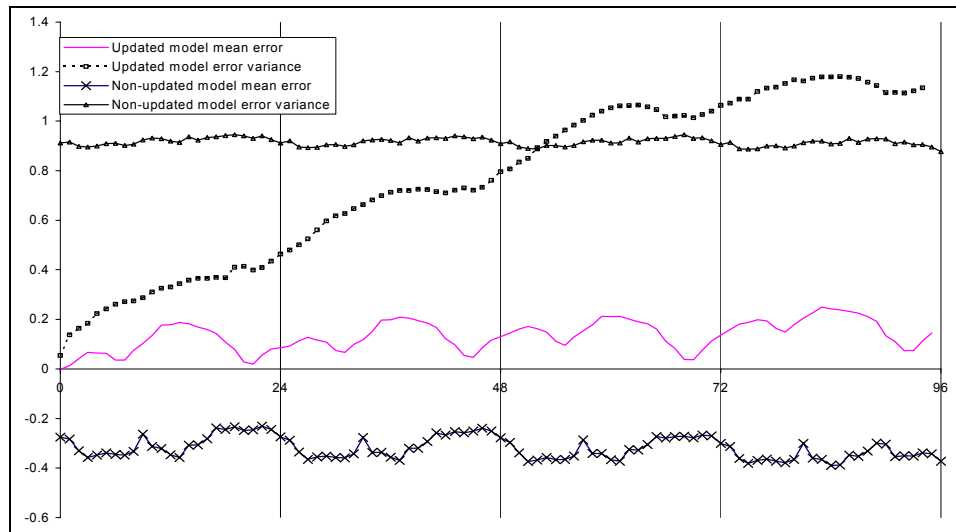


Figure 17. Four-day forecasts of the ice cover extent.

Table 8. Mean error in feet by day of forecast.					
Gage	Day of forecast	No update	System error covariance for conveyance factor		
			0.0001	0.00001	0.000001
a. 1996-97					
Oahe	Day 1	0.636	0.099	0.109	0.196
	Day 2	0.657	0.100	0.111	0.213
	Day 3	0.675	0.103	0.112	0.212
	Day 4	0.668	0.142	0.124	0.196
	Four Days	0.659	0.111	0.114	0.204
Pierre	Day 1	0.195	0.094	0.074	0.134
	Day 2	0.231	0.102	0.083	0.159
	Day 3	0.249	0.111	0.092	0.170
	Day 4	0.246	0.167	0.123	0.178
	Four Days	0.230	0.119	0.093	0.160
LaFramboise	Day 1	0.236	0.096	0.066	0.096
	Day 2	0.268	0.090	0.065	0.115
	Day 3	0.279	0.094	0.068	0.117
	Day 4	0.261	0.151	0.094	0.120
	Four Days	0.261	0.108	0.073	0.112
Farm Island	Day 1	0.446	0.099	0.062	0.135
	Day 2	0.492	0.192	0.142	0.233
	Day 3	0.509	0.314	0.233	0.291
	Day 4	0.504	0.459	0.314	0.338
	Four Days	0.488	0.266	0.189	0.249
b. 1995-96					
Oahe	Day 1	0.066	0.112	0.112	0.228
	Day 2	0.060	0.175	0.173	0.317
	Day 3	0.057	0.215	0.213	0.345
	Day 4	0.036	0.269	0.266	0.385
	Four Days	0.055	0.193	0.192	0.319
Pierre	Day 1	-0.450	0.085	0.067	0.163
	Day 2	-0.457	0.135	0.117	0.241
	Day 3	-0.469	0.164	0.148	0.255
	Day 4	-0.502	0.217	0.197	0.284
	Four Days	-0.470	0.151	0.133	0.237
LaFramboise	Day 1	0.474	0.102	0.081	0.181
	Day 2	-0.486	0.146	0.124	0.256
	Day 3	-0.498	0.173	0.151	0.267
	Day 4	-0.527	0.223	0.202	0.299
	Four Days	-0.497	0.162	0.140	0.252
Farm Island	Day 1	-0.348	0.066	0.034	0.182
	Day 2	-0.365	0.048	0.009	0.258
	Day 3	-0.379	0.018	-0.017	0.267
	Day 4	-0.410	-0.005	-0.035	0.301
	Four Days	-0.375	0.032	-0.002	0.252



a. Winter 1996-97.



b. Winter 1995-96.

Figure 18. Error statistics (in ft) for the forecasts. Shown is the error for each hour from the time of the forecast.

1. The mean error produced by the river ice state–space model with updating is substantially less than the simulation model with updating. The mean error is reduced for all days of the forecast.

2. The mean error of the simulation model without updating is essentially constant with time, as can be easily seen in Figure 18. The mean error of the forecast made using the state–space model shows a small increase with time. In general, the farther into the future the forecast, the larger the mean error.

3. Through numerical experiment it was determined that the forecasts could be improved if the system error covariance of the conveyance factors was reduced over the value determined in the previous section. This can be seen in Table 8, where the mean errors are listed for the winters of 1996-97 and 1995-96. Reducing the system error covariance of the conveyance factors was found to improve the forecast results slightly. Reducing the system error covariance applied to the conveyance factors has the effect of reducing the variation in the factors.

4. The overall results for the winter of 1996-97 are presented graphically in Figure 18a. The mean error and the standard deviation of the error are shown both for the state–space model and the simulation model without updating. The mean error of the state–space model is always less than that of the simulation model without updating. The daily cycling of the release outflow of Oahe Dam, which is quite regular, apparently causes the cyclic nature of the errors. The variance of the forecast errors increases with time. The variance of the forecast error is equal to the variance of the non-updated simulation forecasts after about 30 hours. Throughout much of the winter of 1996-97 there was a problem with the inaccurate gage reading, which led to the high estimate of the conveyance factors in the upstream portions of the Missouri River (as discussed in section 4.3.2). The inaccurate data most likely also contributed to the lack of accuracy during the winter of 1996-97.

5. The overall results for the winter of 1995-96 are presented graphically in Figure 18b. It can be seen that the mean error of the state–space model is always less than that of the simulation model without updating. It also is evident that the variance of the forecast error increases with time. In this case the variance of the forecast error is equal to the variance of the non-updated simulation forecasts after about 50 hours. The better results for the winter of 1995-96 partially reflect the fact that there were few data missing for this winter period than for 1996-97.

4.6 Summary

In this chapter the state-space river ice model derived in the previous two chapters was applied to the Missouri River. The benefits and some of the problems in using a state-space model to simulate river ice conditions were demonstrated. The benefits derive from the ability to update the state-space model with observations of stage and river ice conditions. It was shown that hindcasts of river ice conditions with the state-space model dramatically improve hindcast accuracy compared to the deterministic river ice model.

Bad and missing data present a challenge for the state-space model. A scheme for coping with the small number of observations of ice conditions compared to the many observations of stage was presented. Bad data can cause the state-space model to produce poor or illogical results if the inaccuracy is not recognized. Simple maximum and minimum bounds on observations were presented as one means to estimating the accuracy of observations. However, more subtle problems with the observations were also encountered, as described in this chapter. Forecasts made with the state-space model also show a dramatic improvement compared with the deterministic model, but the improvements lessen the farther the forecast is extended into the future, and the state-space model is about as accurate as the deterministic model for forecasts beyond roughly 48 hours. Reducing the system error covariance for the conveyance factor, compared to the optimal value found for open water, was determined to improve the forecast accuracy slightly. This result from the model reflects the rapid rate of change of the ice extent and hydraulic roughness in the Missouri River.

5 CONCLUSIONS AND RECOMMENDATIONS

5.1 Summary

This study evaluates the utility of a state–space model for forecasting the progression of a river ice cover. The model incorporates a hydraulic component, a thermal and ice transport component, and an ice cover progression component. In particular the study focuses on the use of the Kalman filter technique as a means of enhancing forecast accuracy. The technique updates the model by applying the Kalman filter procedure using observed stages and the observed position of the upstream leading edge of the ice cover to arrive at an efficient and optimal estimate of the river ice and hydraulic conditions. The model can also account for changes in the effective hydraulic roughness produced by smoothing of the underside of the river ice cover and other effects. It does so by recursively estimating a conveyance factor using the augmented Kalman filter procedure.

The state–space model was applied to the Missouri River downstream of the Oahe Dam, a peaking hydropower plant located in Pierre, South Dakota. The outflow of the dam can vary between 0 and 55,000 cfs in a matter of minutes to meet the demands of the power grid. This large variation in flow makes the Missouri River downstream of Oahe Dam a significant location to examine the utility of using the Kalman filter technique.

The system error covariance of the model was adjusted to produce the optimal results in simulating the river stages downstream of Oahe Dam based on least-squares criteria. Forecasts of the downstream stages and river ice conditions are presented. The state–space model forecast accuracy is assessed as applied to a series of past winters in which ice conditions were severe. The updated model results show substantial improvements in the forecasts compared to those of non-updated models.

5.2 Conclusions and recommendations

The following conclusions and recommendations are drawn from the study:

1. A state–space model reduces the mean error of forecasts of river stage compared to estimates made using a simulation model without updating.
2. It is possible to reduce the variance of error of forecasts of river stage for time periods that range from 30 to 50 hours through the use of a state–space model compared to the use of a simulation model without updating. Beyond this range the variance of the forecast errors of the state–space model is equal to or slightly larger than the model without updating.

3. In the case of the conveyance factor the Kalman filter parameter that produced the best result for data assimilation as measured by the coefficient of determination did not produce the best result as measured by the forecast accuracy. The forecast results were improved by reducing the variation of the conveyance factor with time.

4. The benefits of the river ice state-space model depend on the accuracy and availability of observations. If no observations are available, the state-space model will do no better than a simulation model with no updating. If observations are available but are inaccurate, the integrity of the state-space model depends on recognition of the accuracy of the observations that are used. This is an important issue in the present study, because the intense cold conditions of winter can have a sudden, deleterious effect on the accuracy of river gages. If the inaccuracy of the gage is recognized, the state-space model can be instructed to reduce its influence and to proceed forward in time.

5. The number of observations of the river ice conditions is far less than the number of observations of stage. Increasing the number of observations of river ice extent would improve the state-space model results.

6. Improvements in the simulation of the river ice progression and retreat would benefit the present results. There are three areas in which the simulation of the ice cover progression and retreat could be improved:

a) Develop a more physically based representation of the heat transfer from the water surface to the atmosphere. In the present study the heat transfer was assumed to be a constant linear function of the difference between the air and water temperature. The simulation could be improved through including the effects of wind speed, evaporation, and long-wave and short-wave radiation.

b) Develop a more physically based representation of the formation of river ice floes. Unfortunately there is little theory to guide this development. The ice cover in the Missouri River downstream of Pierre is largely formed from such floes.

c) Expand the data collection program at Oahe Dam to include hourly measurements of the release water temperature and develop accurate measurements of the water temperature at the gage locations downstream of Oahe Dam.

7. Application of the state-space model requires procedures to forecast the boundary conditions of the state-space model. For the river reach examined in this study, such boundary conditions are the Oahe Dam outflow, the downstream stage at Big Bend Dam, the release water temperature, and the air temperature. Each of these boundary conditions requires a separate procedure. Development of such procedures comprises an important area for future work.

LITERATURE CITED

- Andreasson, P., L. Hammer, and H.T. Shen** (1998) The influence of surface turbulence on the formation of ice pans. In *Ice in Surface Waters* (H.T. Shen, ed.), *Proceedings of the International Association of Hydraulic Research 14th Ice Symposium, Potsdam, New York, July 27–31, 1998*, Vol. I, p. 69–76.
- Ashton, G.** (1986) *River and Lake Ice Engineering*. Littleton, Colorado: Water Resources Publications.
- Assaf, H., and M.C. Quick** (1991) Updating hydrologic forecast models. *Canadian Journal of Civil Engineering*, **18**: 673–674.
- Beltaos, S. (ed.)** (1995) *River Ice Jams*. Littleton, Colorado: Water Resources Publications.
- Bravo, H.R., W.F. Krajewski, and F.M. Holly** (1993) State space model for river temperature prediction. *Water Resources Research*, **29**(5): 1457–1466.
- Budgell, W.P.** (1981) A stochastic-deterministic model for estimating tides in branched estuaries. Ph.D. Thesis, University of Waterloo, Waterloo, Ontario, Canada.
- Chiu, C.L. (ed.)** (1978) Applications of the kalman filter to hydrology, hydraulics, and water resources. *Proceedings of the American Geophysical Union Chapman Conference, May 22–24, 1978*, Department of Civil Engineering, University of Pittsburgh, Pittsburgh, Pennsylvania.
- Chiu, C.L., and E.O. Isu** (1978) Kalman filter in open channel flow estimation. *American Society of Civil Engineers Journal of Hydraulic Engineering*, **104**(HY8): 1137–1152.
- Corps of Engineers** (1990) HEC-2 water surface profiles user's manual. U.S. Army Corps of Engineers Hydrologic Engineering Center, Davis, California.
- Corps of Engineers** (1995) HEC-DSS user's guide and utility manuals. U.S. Army Corps of Engineers Hydrologic Engineering Center, Davis, California.
- Corps of Engineers** (1997) UNET one-dimensional unsteady flow through a full network of open channels, User's manual. U.S. Army Corps of Engineers Hydrologic Engineering Center, Davis, California.
- Crissman, R.D., C-L Chiu, W. Yu, K. Mizumura, and I. Corbu** (1993) Uncertainties in flow modeling and forecasting for the Niagara River. *American Society of Civil Engineers Journal of Hydraulic Engineering*, **119**(11): 1231–1250.

Cunge, J., F.M. Holly, and A. Verway (1980) Practical aspects of computational river hydraulics. Institute of Hydraulic Research, University of Iowa, Iowa City, Iowa.

Daly, S.F. (1984) Frazil ice dynamics. Monograph 84-1, U.S. Army Corps of Engineers Cold Regions Research and Engineering Laboratory, Hanover, New Hampshire.

Daly, S.F. (ed.) (1994) International Association for Hydraulic Research Working Group on Thermal Regimes: Report on frazil ice. Special Report 94-23, U.S. Army Corps of Engineers Cold Regions Research and Engineering Laboratory, Hanover, New Hampshire.

Daly, S.F. (1995) Fracture of river ice covers by river waves. *American Society of Civil Engineers Journal of Cold Regions Engineering*, **9**(1): 41–52.

Fischer, H.B., J.L. List, R.C.Y. Koh, J. Imberger, and N.S. Brooks (1979) *Mixing in Inland and Coastal Waters*. New York: Academic Press.

Fread, D.L. (1974) Numerical properties of implicit four-point finite difference equations of unsteady flow. NOAA Technical Memorandum NWS HYDRO-18, National Weather Service, NOAA, U.S. Department of Commerce, Silver Spring, Maryland.

Fread, D.L., and M. Jin (1993) Real-time dynamic flood routing with NWS FLDWAV model using Kalman filter updating. *Proceedings, Engineering Hydrology: Proceedings of the Symposium, July 25–30, 1993, San Francisco, California* (C.Y. Kuo, ed.), New York: American Society of Civil Engineers, p. 946–951.

Gelb, A. (ed.) (1992) *Applied Optimal Estimation*. Cambridge, Massachusetts: The MIT Press.

Georgakakos, K.P., and W.F. Krajewski (1985) A simulation study of recursive parameter estimation techniques for a stochastic-dynamic flood routing model. *Proceedings of the IFAC Conference, Lisbon, Portugal, 2–4 October 1985*, p. 27–33.

Grewal, M.S., and A.P. Andrews (1993) *Kalman Filtering: Theory and Practice*. Englewood Cliffs, New Jersey: Prentice Hall, Inc.

Hammar, L., and H.T. Shen (1995) Frazil evolution in channels. *Journal of Hydraulic Research*, **33**(3): 291–306.

Holly, F.M. (1984) Dispersion in rivers and coastal waters—1. Physical principles and dispersion equations. In *Developments in Hydraulic Engineering 3* (P. Novak, ed.). New York: Elsevier Applied Science Publishers, p. 1–38.

- Hsieh, B.** (1987) A tidal hydraulic model of the C&D Canal. *Hydraulic Engineering, Proceedings of the 1987 National Conference on Hydraulic Engineering, Williamsburg, Virginia, 3–7 August 1987*, p. 183–188.
- Jazwinski, A.H.** (1969) Adaptive filtering. *Automatica*, **5**: 475–485.
- Kailath, T.** (1980) *Linear Systems*. Englewood Cliffs, New Jersey: Prentice-Hall.
- Kalman, R.E.** (1960) A new approach to linear filtering and prediction problems. *Transactions, American Society of Mechanical Engineering, Journal of Basic Engineering, Series 82D*, p. 35–45.
- Kalman, R.E., and R.S. Bucy** (1961) New results in linear filtering and prediction theory. *Transactions, American Society of Mechanical Engineering, Journal of Basic Engineering, Series 83D*, p. 95–108.
- Kitanidis, P.K., and R.L. Bras** (1980) Real-time forecasting with a conceptual hydrologic model. 1. Analysis of uncertainty. *Water Resources Research*, **16**(6): 1025–1033.
- Lal, A.M.W., and H.T. Shen** (1992) Numerical simulation of river ice dynamics. *Proceedings of the Third International Conference on Ice Technology, Massachusetts Institute of Technology, Cambridge, Massachusetts, 11–13 August, 1992*.
- Lal, A.M.W., and H.T. Shen** (1993) A mathematical model for river ice processes. CRREL Report 93-4, U.S. Army Corps of Engineers Cold Regions Research and Engineering Laboratory, Hanover, New Hampshire.
- Lee, Y.H., and V.P. Singh** (1999) Tank model using Kalman filter. *American Society of Civil Engineers, Journal of Hydrologic Engineering*, **4**(4): 344–349.
- Matousek, V.** (1984) Types of ice run and conditions for their formation. *Proceedings of the 7th International Association of Hydraulic Research Symposium on Ice, Hamburg, Germany, vol. 1*, p. 315–327.
- Mizumura, K., and C.-L. Chiu** (1985) Prediction of combined snowmelt and rainfall runoff. *American Society of Civil Engineers, Journal of Hydraulic Engineering*, **111**(2): 179–193.
- Myers, K.A., and B. Tapley** (1976) Adaptive sequential estimation with unknown noise statistics. *IEEE Transactions on Automatic Control*, 520–523.
- Sage, A.P., and G. Husa** (1976) Adaptive filtering with unknown prior statistics. *Proceedings of the Joint Automatic Control Conference*, p. 760–769.

- Sauvaget, P.** (1984) Dispersion in rivers and coastal waters—2. Numerical computation of dispersion. *Developments in Hydraulic Engineering 3* (P. Novak, ed.), New York: Elsevier Applied Science Publishers, p. 39–78.
- Shen, H.T.** (1996) River ice processes—State of research. *Proceedings of the International Association of Hydraulic Research, 13th Ice Symposium, Beijing, China*.
- Shen, H.T., and P.D. Yapa** (1986) Flow resistance of river ice cover. *Journal of Hydraulic Engineering*, **112**(2): 142–156.
- Shen, H.T., G. Bjedov, S.F. Daly, and A.M.W. Lal** (1991) Numerical model for forecasting ice conditions on the Ohio River. CRREL Report 91-16, U.S. Army Corps of Engineers Cold Regions Research and Engineering Laboratory, Hanover, New Hampshire.
- Shen, H.T., D.S. Wang, and A.M.W. Lal** (1995) Numerical simulation of river ice processes. *American Society of Civil Engineers Journal of Cold Regions Engineering*, **9**(3): 107–118.
- Sorenson, H.W. (ed.)** (1985) *Kalman Filtering: Theory and Application*. New York: IEEE Press.
- Wang, D.S., H.T. Shen, and R.D. Crissman** (1995) Simulation and analysis of Upper Niagara River ice-jam conditions. *American Society of Civil Engineers Journal of Cold Regions Engineering*, **9**(3): 119–134.

